PhD thesis

Anders Ettrup

Serotonin receptor studies in the pig brain:

pharmacological intervention and positron emission tomography tracer development

Academic advisor: Gitte Moos Knudsen

Submitted: 01/07/10

Defended: 15/10/10

Preface

The present PhD thesis is the result of a 3½-year integrated Master's/PhD programme in Human Biology at The Faculty of Health Sciences, University of Copenhagen. The work was carried out from February 2007 to July 2010 primarily at the Neurobiology Research Unit, Copenhagen University Hospital, Rigshospitalet.

This thesis is based on the following manuscripts which in the text are referred to by their Roman numerals:

   I. **Ettrup A**, Kornum BR, Weikop P, Knudsen GM. An Approach for Serotonin Depletion in Pigs: Effects on Serotonin Receptor Binding. *Synapse. 2010 Jun 16. (Epub ahead of print)*

  II. **Ettrup A**, Palner M, Gillings N, Santini MA, Hansen M, Kornum BR, Rasmussen LK, Någren K, Madsen J, Begtrup M, Knudsen GM. Radiosynthesis and evaluation of ^{11}C-CIMBI-5 as a high affinity 5-HT$_{2A}$ receptor agonist radioligand for PET. *Journal of Nuclear Medicine. 2010 Nov. (article proofs)*

 III. **Ettrup A**, Hansen M, Santini MA, Paine J, Gillings N, Palner M, Lehel S, Madsen J, Begtrup M, Knudsen GM. In vivo evaluation of a series of substituted ^{11}C-phenethylamines as 5-HT$_{2A}$ agonist PET tracers. *Manuscript*

The following publications are related to the work described in the thesis, and are referred to as regular references:

 1. Holm P*, **Ettrup A***, Klein AB, Santini MA, El-Sayed M, Elvang AB, Stensbøl TB, Mikkelsen JD. Knudsen GM, Aznar S. Plaque Deposition Dependent Decrease in 5-HT$_{2A}$ Serotonin Receptor in AβPPswe/PS1dE9 Amyloid Overexpressing Mice. *Journal of Alzheimer's Disease 2010;20(4):1201-13.*

 2. Kornum BR*, Stott SR*, Mattsson B, Wisman L, **Ettrup A**, Hermening S, Knudsen GM, Kirik D. Adeno-associated viral vector serotypes 1 and 5 targeted to the neonatal rat and pig striatum induce widespread transgene expression in the forebrain. *Experimental Neurology 2010 Mar;222(1):70-85.*

*equal contributions by the two authors

Table of Contents

Acknowledgements

Summary in English

Serotonin (5-HT) is an important neurotransmitter that modulates significant behavioural effects such as mood, anxiety, appetite, and sleep. Accordingly, dysfunction in the serotonergic system has been implicated in the pathophysiology of a wide range of neuropsychiatric disorders. The 5-HT_{2A} receptor is the most abundant excitatory 5-HT receptor in the human brain, it mediates the hallucinogenic effects of several recreational drugs and is the target of atypical antipsychotics. Positron emission tomography (PET) is a powerful technique to map and quantify receptors in the living brain, and PET scanning is widely used to investigate 5-HT receptors in both human and animal studies. For 5-HT_{2A} receptor imaging with PET, only antagonist PET tracers are currently in use, however, agonist PET tracers hold promise to image receptors in the high-affinity state selectively and thereby to serve as a more functional measure of 5-HT_{2A} receptor function. Furthermore, agonist PET tracers are potentially more sensitive to changes in neurotransmitter levels than antagonist tracers. Novel PET tracers can be evaluated in the pig, because of its relatively large brain and its neuroanatomical resemblance to the human brain. However, manipulations of the 5-HT system in the pig brain have not been thoroughly validated.

The aims of this PhD thesis were: 1) To develop and validate a porcine model of serotonin depletion and use this to investigate the effect of decreased levels of 5-HT on selected serotonergic markers. 2) To develop a range of 5-HT_{2A} receptor agonist PET tracers and validate their in vivo properties in the pig brain.

We found that inhibition of synthesis effectively decreased 5-HT levels in the pig brain, as evaluated by immunostaining and HPLC analysis. Thus, this provides an approach for decreasing serotonergic neurotransmission in a large animal species that subsequently could be used in imaging studies. In this porcine model of serotonin depletion, the 5-HT_4 receptor binding was consistently up-regulated, suggesting that this receptor is more sensitive to changes in 5-HT levels in comparison to 5-HT_{1A} and 5-HT_{2A} receptors. Our development of PET tracers showed that the ^{11}C-labelled high-affinity 5-HT_{2A} receptor agonist [^{11}C]Cimbi-5 could be used for in vivo 5-HT_{2A} receptor imaging in the pig brain. The cortical binding of [^{11}C]Cimbi-5 was blocked by ketanserin treatment, and in the pig brain, non-displaceable binding potential (BP_{ND}) in the cortex was comparable to [^{18}F]altanserin. To further optimize the target-to-background ratio, we modified the chemical structure of [^{11}C]Cimbi-5 and tested a total of nine high-affinity 5-HT_{2A} receptor agonist PET tracers in the pig brain. Of these nine compounds, [^{11}C]Cimbi-36 showed both better brain uptake and higher target-to-background ratio than [^{11}C]Cimbi-5. The cortical BP_{ND} of [^{11}C]Cimbi-

36 decreased by ketanserin treatment, indicating that the cortical binding is specific for 5-HT_{2A} receptors. Thus, for in vivo imaging of 5-HT_{2A} receptors in their high-affinity state [^{11}C]Cimbi-36 is identified as our primary candidate for further human studies.

In conclusion, the work in this thesis validated a method for decreasing serotonergic neurotransmission in the pig brain. Secondly, our PET tracer development generated several possible candidates for imaging of high-affinity 5-HT_{2A} receptors that may show sensitivity towards changes in levels of endogenous 5-HT thus serving to measure serotonergic tone in the living brain.

Resumé på dansk

Serotonin (5-HT) er en vigtig neurotransmitter, der regulerer væsentlige typer af adfærd såsom humør, appetit, angst og søvn. Dysfunktion af det serotonerge system er endvidere af patofysiologisk betydning ved en række neuropsykiatriske sygdomme. 5-HT$_{2A}$ receptoren er den mest udbredte excitatoriske 5-HT receptor i menneskets hjerne, den er ansvarlig for de hallucinogene virkninger af flere psykoaktive stoffer, og den blokeres af atypiske antipsykotika. Med positronemissionstomografi (PET) kan man kortlægge og måle bl.a. 5-HT$_{2A}$ receptorer hos levende mennesker og forsøgsdyr, men til billeddannelse af 5-HT$_{2A}$ receptoren har man hidtil kun haft antagonistsporstoffer til rådighed. PET agonistsporstoffer formodes derimod at binde sig selektivt til receptorer i højaffinitetstilstanden, og de vil dermed muliggøre en mere funktionel måling af 5-HT$_{2A}$ receptoren. PET agonistsporstoffer er endvidere mere tilbøjelige end antagonistsporstoffer til at blive displaceret ved endogen konkurrence med den den pågældende neurotrasmitter. Nye PET sporstoffer kan med rette evalueres i grisen grundet dens relativt store hjerne samt neuroanatomiske lighed med menneskets hjerne. Dog er manipulationer af 5-HT systemet i grisehjernen endnu ikke valideret.

Formålene med denne ph.d.-afhandling var 1) at udvikle og validere en grisemodel for serotonindepletering og at anvende dette til at undersøge virkningen af formindskede 5-HT niveauer på udvalgte 5-HT markører, 2) at udvikle PET agonistsporstoffer til måling af 5-HT$_{2A}$ receptoren og at validere deres egenskaber i grisehjernen.

Vores resultater viste, at farmakologisk hæmning af serotoninsyntesen effektivt mindskede 5-HT niveauerne i grisehjernen. Denne metode kan således bruges til at mindske serotoninniveauet i en større dyreart, og modellen kan samtidig anvendes i billeddannende studier. Hos den serotonindepleterede gris fandtes 5-HT$_4$ receptorbindingen opreguleret, hvilket tyder på, at denne receptor er mere følsom for ændringer i 5-HT niveauet end 5-HT$_{1A}$ og 5-HT$_{2A}$ receptorerne. Vores udvikling af PET sporstoffer viste, at den ^{11}C-mærkede, højaffinitets 5-HT$_{2A}$ receptoragonist [11]C[Cimbi-5 kunne anvendes til in vivo billeddannelse af 5-HT$_{2A}$ receptoren i grisehjernen. Den kortikale binding af [11]C[Cimbi-5 blev blokeret ved forbehandling med ketanserin, og i grisehjernen fandtes det ikke-displacérbare bindingspotentiale (BP$_{ND}$) i cortex sammenligneligt med bindingspotentialet for [18]F[altanserin. For yderligere at optimere dets target-to-background-ratio modificerede vi den kemiske struktur af [11]C[Cimbi-5 og testede i alt ni PET sporstoffer, der alle var højaffine 5-HT$_{2A}$ receptoragonister. Ud af disse ni viste [11]C[Cimbi-36 højere optag i hjernen samt forbedret target-to-background-ratio i forhold til [11]C[Cimbi-5. Det kortikale BP$_{ND}$ af

[^{11}C]Cimbi-36 kunne blokeres med ketanserin behandling, hvilket bekræfter, at den kortikale binding er specifik for 5-HT$_{2A}$ receptorerne. Til in vivo billeddannelse af 5-HT$_{2A}$ receptorer i deres højaffinitetstilstand er [^{11}C]Cimbi-36 således identificeret som vores primære kandidat til fremtidige studier i mennesker.

Denne afhandling beskriver således en metode til at mindske den serotonerge neurotransmission i grisehjernen. Derudover udviklingde og testede vi flere mulige PET sporstoffer til billeddannelse af 5-HT$_{2A}$ receptorer i højaffinitetstilstanden. Disse vil siden kunne testes med henblik på deres sensitivitet over for ændringer i niveauet af endogen 5-HT, og hvis dette kan påvises vil man have en metode til in vivo monitorering af det serotonerge niveau i den levende hjerne.

Abbreviations

5,7-DHT	5,7-dihydroxytryptamine	IPR	imaging plate reader
5-HIAA	5-hydroxyindoleacetic acid	K_D	equilibrium dissociation constant
5-HT	5-hydroxytryptamine, serotonin	LSD	lysergic acid diethylamide
AC	adenylate cyclase	MAO	monoamine oxidase
AD	Alzheimer's disease	MDMA	methylenedioxymethamphetamine
ANOVA	analysis of variance	MRI	magnetic resonance imaging
APP	amyloid precursor protein	MRN	median raphe nucleus
ATD	acute tryptophan depletion	NRU	Neurobiology Research Unit
AUC	area under curve	NSB	non-specific binding
BBB	blood-brain barrier	pCPA	para-chlorophenylalanine
B_{max}	maximal concentration of binding sites	PD	Parkinson's disease
		PET	positron emission tomography
BP_{ND}	non-displaceable binding potential	P-gp	P-glycoprotein
cAMP	cyclic adenosine monophosphate	PLC	phospholipase C
CNS	central nervous system	PSL	photostimulated luminescence
CSF	cerebrospinal fluid	rAAV	recombinant adeno associated viral vector
CTD	chronic tryptophan depletion		
DAG	diacylglycerol	RP-HPLC	reversed phase high-performance liquid chromatography
DOI	2,5-dimethoxy-4-iodoamphetamine		
DRN	dorsal raphe nucleus	ROI	region of interest
GABA	γ-aminobuturic acid	SB	specific binding
GPCR	G-protein coupled receptor	SERT	serotonin transporter
HPLC	high performance liquid chromatography	SRTM	simplified reference tissue model
		SSRI	selective serotonin reuptake inhibitor
HRRT	high resolution research tomography		
		SUV	standardized uptake value
HTR	head-twitch response	TB	total binding
icv	intra-cerebroventricular	TE	tissue equivalent
i.m.	intra-muscular	TPH	tryptophan hydroxylase
i.p.	intra-peritoneal	TR-IP	tritium radiation-sensitive IP
IP	imaging plate	VOI	volume of interest
IP_3	inositol trisphosphate		

Introduction

The serotonin system

Serotonin (5-hydroxytryptamine, 5-HT) was first found in *serum* as a substance that affected vascular *tone*. Hence, it was given the name serotonin. Later, the molecule was biochemically characterised and found to possess other functions both peripherally and in the central nervous system (CNS). Now, the designations 5-HT and serotonin are used interchangeably. 5-HT is a monoamine and functions in the CNS as a neurotransmitter, i.e. upon neuronal firing, 5-HT is released from secretory vesicles in pre-synaptic neurons into the synaptic cleft of serotonergic synapses from where it diffuses to the post-synaptic neuron and binds to 5-HT receptors (figure 1). The degradation of monoamine neurotransmitters and thus termination of their neurotransmission is catalysed by monoamine oxidase (MAO), and the main metabolite from the degradation of 5-HT is 5-hydroxyindoleacetic acid (5-HIAA). Serotonergic neurotransmission is also readily attenuated by rapid reuptake into the pre-synaptic neuron by the serotonin transporter (SERT) decreasing synaptic concentrations of 5-HT. After reuptake, 5-HT is either re-packaged into secretory vesicles or degraded by MAO located in the outer mitochondrial membrane. Both in the periphery and in the CNS, 5-HT is synthesised from the essential amino acid tryptophan in a two step process catalysed by the enzymes tryptophan hydroxylase (TPH) and the relatively non-specific aromatic amino acid decarboxylase. In the biosynthesis, TPH is the rate-limiting enzyme for the formation of 5-HT allowing for decreased synthesis rate of 5-HT by inhibition of TPH or depleting levels of its substrate, tryptophan.

The vast majority of the serotonergic innervations in the brain are derived from neurons in the dorsal raphe nucleus (DRN) and median raphe nucleus (MRN) in the brainstem. The raphe nuclei send projections to most of the cerebrum including cortical areas, basal ganglia, and limbic system, whereas the cerebellum is only sparsely innervated by serotonergic neurons. In classical (or hard-wired) neurotransmission, the release and action of neurotransmitters is restricted to the synaptic cleft. Furthermore, neurotransmitters may diffuse to more remote receptor sites referred to as diffuse, paracrine, or volume neurotransmission (Hensler, 2006). Important factors to determine the type of neurotransmission include location of the receptors relative to the release site, rate of diffusion away from the release site, and removal or reuptake by the transporter. The serotonin system utilizes both hard-wired synaptic and paracrine extrasynaptic neurotransmission (De-Miguel and Trueta, 2005). This duality of the serotonergic system has been observed in the DRN of cats using a combination of immunohistochemistry and electron microscopy finding both synaptic and extrasynaptic release sites (Chazal and Ralston, 1987). In this study, 5-HT-containing vesicles were observed in pre-synaptic terminal axons of hard-wired synapses and along the dendritic shafts of serotonergic neurons releasing 5-HT via diffusively located extrasynaptic varicosities. Also, activation of serotonergic neurons has shown to increase concentrations of 5-HT in the extracellular

fluid (De-Miguel and Trueta, 2005). The modulating effects of 5-HT are diverse and may vary among brain areas depending on the type of 5-HT receptor in question (Barnes and Sharp, 1999;Gu, 2002).
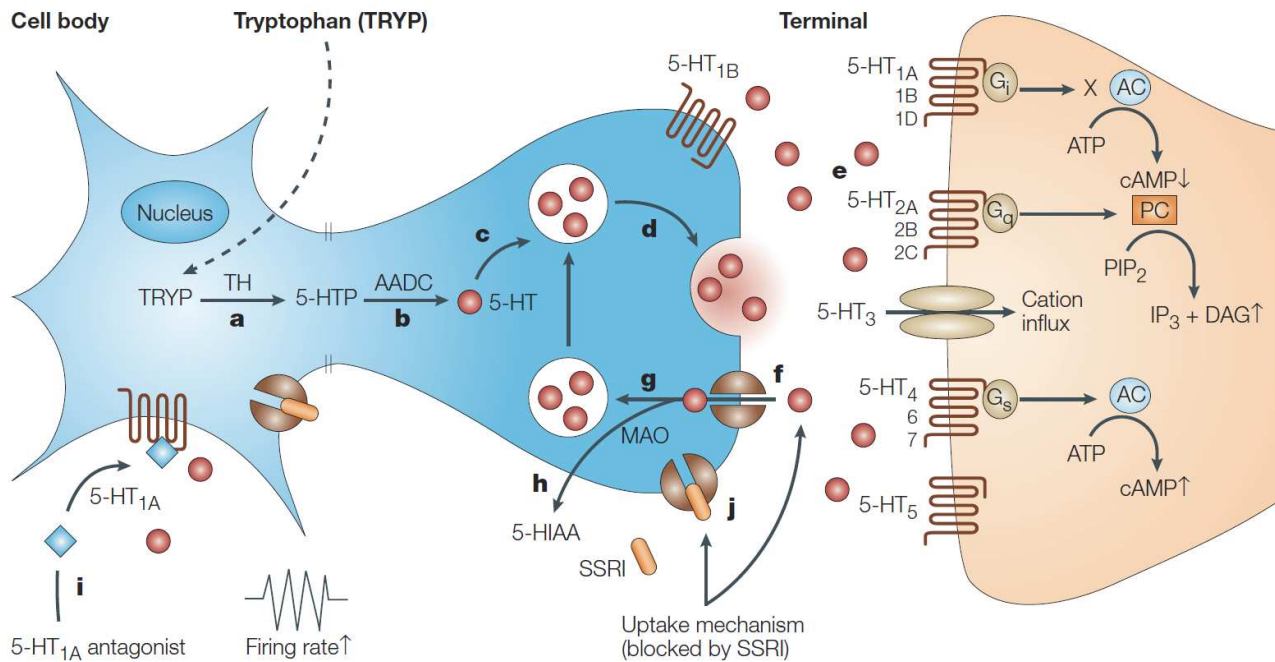
Figure 1 Diagram of the serotonergic neurotransmission. **a** Tryptophan hydroxylase (TH) catalyses the conversion of tryptophan (TRYP) to 5-hydroxytryptophan (5-HTP) in the pre-synaptic neuron. **b** Aromatic aminoacid decarboxylase (AADC) catalyses the conversion of 5-HTP to 5-hydroxytryptamine (5-HT, serotonin). **c** 5-HT is taken up into storage vesicles. **d** 5-HT is released from storage vesicles into the synaptic cleft upon neuronal activation. **e** 5-HT can activate subtypes of the seven existing 5-HT receptor families, which couple with their respective system of signal transduction inside the post-synaptic neuron. **f** 5-HT is taken up into the pre-synaptic 5-HT terminals by the 5-HT transporter (SERT). **g,h** Within the pre-synaptic 5-HT terminals, 5-HT would either be taken up by the storage vesicles or degraded by monoamine oxidase (MAO). **i** 5-HT activates the pre-synaptic somatodendritic 5-HT_{1A} autoreceptor, which can be blocked by selective 5-HT_{1A} antagonists. **j** Selective serotonin reuptake inhibitors (SSRIs) inhibit the 5-HT transporter. 5-HIAA, 5-hydroxyindolacetic acid; AC, adenylate cyclase; DAG, diacylglycerol; IP_3, inositol-1,4,5-trisphosphate; PIP_2, phosphatidylinositol-4,5-bisphosphate. Figure adapted from Wong et al., 2005.

5-HT receptors

5-HT is the neurotransmitter for which the greatest number of receptor types exists. In humans, 15 genes encoding functional 5-HT receptors are currently identified, and the diversity of these receptors is further increased by post-genomic modifications, such as alternative splicing and RNA editing (Bockaert et al., 2006). The human 5-HT receptors comprise 7 families designated 5-HT_1 through 5-HT_7; all of them have been cloned and characterized (Barnes and Sharp, 1999). Except for 5-HT_3, which functions as an ionotropic ligand-gated cation channel, all 5-HT receptors are metabotropic G-protein coupled receptors (GPCR) with seven transmembrane domains (Bockaert et al., 2006). Thus, 5-HT is one of the neurotransmitters, like acetylcholine, glutamate, and γ-aminobuturic acid (GABA) that relies on both ionotropic and metabotropic

signalling adding to the complexity of the serotonin system. Furthermore, metabotropic GPCR 5-HT receptors vary in their distribution, coupling to G-proteins, and secondary signalling pathways excising differential effects upon activation. Generally, the metabotropic 5-HT receptors are grouped according to their main second messenger system: $5\text{-}HT_1$ receptors are coupled to $G\alpha_i/G\alpha_o$ inhibiting the formation of cyclic adenosine monophosphate (cAMP) by adenylate cyclase (AC); $5\text{-}HT_2$ receptors are coupled to $G\alpha_q$ stimulating phospholipase C (PLC) and increasing cellular levels of inositol trisphosphate (IP_3) and diacylglycerol (DAG); and $5\text{-}HT_4$, $5\text{-}HT_6$, $5\text{-}HT_7$ are all coupled to G_s protein increasing cellular levels of cAMP (Raymond et al., 2001). In the Paper I, representatives from these three groups are quantified, viz. the $5\text{-}HT_{1A}$, $5\text{-}HT_{2A}$, and $5\text{-}HT_4$. These receptors are the focus of extensive ongoing research and are involved in important biological functions ranging from modulation of neuronal activity and transmitter release to behavioural change (Barnes and Sharp, 1999). Furthermore, the $5\text{-}HT_{2A}$ receptor is the focus of Paper II and III, and the more specific function, signalling, localization of this receptor and its ligands are presented below.

Effects of 5-HT$_{2A}$ activation

The $5\text{-}HT_{2A}$ receptor is the most abundant excitatory post-synaptic 5-HT receptor in the human CNS, and cellular effects after activation of neurons include signalling through PLC promoting the release of DAG and IP_3 which in turn stimulates protein kinase C activity and increase intracellular Ca^{2+} (Bockaert et al., 2006). This signalling cascade provides the basis for activation of $5\text{-}HT_{2A}$ receptors yielding both neuronal activation and regulation of gene transcription. $5\text{-}HT_{2A}$ receptors are widely distributed at varying densities throughout the brain but are particularly abundant in the telencephalic areas such as cerebral cortex, olfactory system, and pre-frontal cortex (Leysen, 2004). The cellular localization of $5\text{-}HT_{2A}$ receptors is mainly somatodendritic, and they are predominantly present on non-serotonergic neurons, e.g. GABAergic interneurons and glutamatergic pyramidal neurons (Bockaert et al., 2006). Neuronal activation and glutamatergic neurotransmission is necessary for this $5\text{-}HT_{2A}$-mediated induction of downstream gene expression factors and effectors such as Arc (Pei et al., 2004).

Selective activation of $5\text{-}HT_{2A}$ receptors can be achieved in vitro and in vivo with agonists. In relation to the chemical structure, $5\text{-}HT_{2A}$ receptor agonists fall into three classes: tryptamines (e.g. as the endogenous ligand 5-HT and the mushroom-derived psilocybin), ergolines (such as lysergic acid diethylamide (LSD)), and phenetylamines (such as 2,5-dimethoxy-4-iodoamphetamine (DOI) and other amphetamine-derived compounds like the peyote cactus-derived mescaline) (Nichols, 2004). The most well-described and spectacular pharmacological property of these compounds is their potential to exert hallucinogenic or psychedelic effects when administered to humans. Hallucinogens alter perception, cognition, and mood, often in dramatic ways, and the use of naturally occurring compounds within these

drug classes, e.g. in relation to religious ceremonies, dates back more than 2000 years (Nichols, 2004). The mediator of hallucinogenic effect is the 5-HT$_{2A}$ receptor activation, and 5-HT$_{2A}$ receptor knock-out mice display no head-twitch response (HTR), a measure of hallucinogenic effects in rodents, following administration of hallucinogens (Gonzalez-Maeso et al., 2007). Also, HTR in rodents following DOI administration can be blocked by pre-treatment with a 5-HT$_{2A}$ receptor antagonist, indicating that this receptor is necessary for the hallucinogenic effect. These data imply that 5-HT$_{2A}$ receptors are directly involved in perception and sensory processing. Interestingly, not all 5-HT$_{2A}$ receptor agonists possess hallucinogenic properties. This is attributed to differential intracellular signalling by cortical 5-HT$_{2A}$ receptors dependent on the agonist, and only 5-HT$_{2A}$ receptor agonists that activate the *egr-1* and *egr-2* pathways are hallucinogenic in vivo (Gonzalez-Maeso et al., 2007).

Significant overlap exists between the behavioural effects elicited by hallucinogenic 5-HT$_{2A}$ receptor agonists and the positive symptoms of schizophrenia patients which comprise delusions, auditory hallucinations, and thought disorder (Gonzalez-Maeso and Sealfon, 2009). In line with this, the newer clinically used atypical antipsychotic therapeutics, such as clozapine and olanzapine, are antagonists at the 5-HT$_{2A}$ receptors. Further, the widely used animal model of schizophrenia using phencyclidine-induced psychosis also display HTR that is reversible by 5-HT$_{2A}$ receptor antagonists (Gonzalez-Maeso and Sealfon, 2009). Taken together, these data suggest a role for the 5-HT$_{2A}$ receptor in the pathophysiology of schizophrenia. However, adding to the complexity of 5-HT$_{2A}$ receptor function and its relevance in human disease states is that the 5-HT$_{2A}$ receptor exists in multiple affinity states which are affected differently by exposure to agonists.

High- and low-affinity states of 5-HT$_{2A}$ receptors

The most widely accepted pharmacological model for 5-HT$_{2A}$ receptor-agonist interaction is the ternary complex model. This model predicts that the GPCR is in dynamic equilibrium between two conformational states, i.e., an inactive and an active state. While agonist ligands display higher affinity for the active state of receptors and also stabilize this conformational state shifting the equilibrium towards this state, antagonist ligands bind the active and inactive state of receptors with the same affinity. Thus, the agonist-mediated activation of receptors is thought to involve stabilization of the agonist/receptor/G-protein complex which then activates signalling and cellular response through second messengers. Several lines of evidence support the existence of multiple affinity states of GPCRs. For dopamine receptors, the existence of such interconvertible affinity states is well-established (Sibley et al., 1982), and here the high affinity state is regarded as the functional state due to the G-protein coupling. For 5-HT$_{2A}$ receptors, the classic demonstration of two affinity states for the 5-HT$_{2A}$ receptor comes from in vitro binding experiments where radiolabelled [^{125}I]DOI agonist binding is best fitted by two-site model (Lopez-Gimenez et al., 2001). By contrast, 5-HT$_{2A}$ receptor antagonist radioligand binding data is best fitted by a one-site model indicating that

antagonists do not discriminate between high- and low-affinity states of 5-HT$_{2A}$ receptors (Roth et al., 1997). Further, the two-site agonist binding is reduced to a one-site by pre-treatment with Gpp(NH)p which is a non-hydrolysable GTP analogue that uncouples the G-protein from the GPCR. These studies typically find that approximately 20% of 5-HT$_{2A}$ receptors are in the high-affinity state when examined by in vitro autoradiography (Lopez-Gimenez et al., 2001) or binding assays (Roth et al., 1997). Taken together, these results indicate that 5-HT$_{2A}$ receptor agonists preferentially bind the receptors in their high-affinity state whereas antagonists bind to the total pool of receptors with equal affinity.

The ternary complex model for 5-HT$_{2A}$ receptor agonist activation is generally accepted as far as the existence of multiple affinity states of the receptor. However, some studies then find a proportional relationship between intrinsic activity for various 5-HT$_{2A}$ receptor agonists and the ratio between affinities for the high- and low-affinity states of the 5-HT$_{2A}$ receptor supporting the two-state model of agonist action (Fitzgerald et al., 1999). By contrast, other studies find more complex relationship between agonist activities and high versus low affinity ratios suggesting that the ternary complex model should be extended to include additional affinity states (Egan et al., 2000;Roth et al., 1997). The existence of more than one high-affinity state of 5-HT$_{2A}$ receptors is also supported by different agonists being able to stabilize different high-affinity states of receptors, which in turn activate different down-stream signalling pathways (Gonzalez-Maeso et al., 2007).

Besides from the co-existence of the multiple affinity states, 5-HT$_{2A}$ receptors can also be localized in separate cellular compartments, i.e. in intracellular vesicles or in the plasma membrane. Interestingly, the largest fraction of 5-HT$_{2A}$ receptors are found in intracellular vesicles compared to the plasma membrane (Cornea-Hebert et al., 2002), while receptors in the plasma membrane are thought to be G-protein coupled and functional as opposed to the internalized receptor. The large intracellular pool of receptors probably serve as a reserve ready for trafficking to the plasma membrane, and factors that affect trafficking to the plasma membrane thus adds another mechanism at which 5-HT$_{2A}$ receptor signalling can be regulated (Magalhaes et al., 2010). One effect of 5-HT$_{2A}$ receptor interaction with a ligand (agonist or antagonist) is increased receptor internalization and thus increased degradation. This results in a curious receptor regulation where the 5-HT$_{2A}$ receptor down-regulated in vivo following chronic antagonistic blockade (Van Oekelen et al., 2003). However, the implications for the multiple affinity states and the differential cellular localization of 5-HT$_{2A}$ receptor and consequences for the function of the serotonergic system in human disease remain to be elucidated.

The serotonin system in human disease

The serotonin system has an important influence on several different biological functions including affective states, cognition, motor function, circadian rhythm, sleep, pain, and sexual behaviour (Mann, 1999). The diversity in the effects excised by the serotonin system lies among other factors in the number, complexity,

and diversity of 5-HT receptor subtypes as mentioned above. Furthermore, dysfunction in the serotonin system is related to a variety of human diseases such as depression, schizophrenia, and Alzheimer's disease (AD), and the serotonin system has been associated with a wide range of neuropsychiatric conditions, including anxiety, suicidal behaviour, obsessive-compulsive disorder, mania, eating disorders, and alcoholism (reviewed in Mann, 1999). A serotonergic vulnerability, i.e., a tendency to hypofunction when exposed to certain environmental factors, e.g. stress, is currently viewed as a risk factor for depression in humans (Jans et al., 2007). Moreover, dysfunction of the serotonin system is also involved in other non-psychiatric diseases. In AD, a specific degeneration of serotonergic neurons (Lanctot et al., 2001) is observed along with decreased post-mortem tissue concentrations of 5-HT and 5-HIAA (Nazarali and Reynolds, 1992). Furthermore, the 5-HT_{2A} receptor has been associated with AD in several PET studies finding decreased 5-HT_{2A} receptor binding in both AD patients (Blin et al., 1993;Marner et al., 2010a;Meltzer et al., 1999;Santhosh et al., 2009;Versijpt et al., 2003) and in patients with mild cognitive impairment, a prodromal stage to AD (Hasselbalch et al., 2008). Also in the murine model of AD displaying accelerated amyloid plaque deposition, defects in the serotonin system have been reported. Double transgenic mice owning the human mutated versions of the amyloid precursor protein (APP) and presenilin 1 (PS1) genes display loss of serotonergic fibres (Liu et al., 2008). Further, in our lab we found that these same mice showed decreased levels and functionality of the 5-HT_{2A} receptor, and these changes were specific for the 5-HT_{2A} receptor and not accompanied by changes in SERT levels (Holm et al., 2010). Taken together, these observations relate dysfunction of the serotonin system to the pathophysiology of AD and suggest that decreased 5-HT_{2A} receptor levels and functionality may be important for AD symptomatology.

Serotonin depletion

An important tool for discovering effects of the serotonin system has been pharmacological manipulation of 5-HT levels. Experimentally induced serotonin depletion provides means to study interactions between the serotonin system and other neurotransmitter systems and to investigate effects of reduced 5-HT availability on behaviour, receptor regulation, and gene expression. Different experimental serotonin depletion regimes are used in rats, monkeys, and humans, including specific lesioning of serotonergic neurons, depletion of the 5-HT precursor, tryptophan, sustained 5-HT release, and inhibition of 5-HT synthesis as described in the next sections.

Selective degradation of serotonergic neurons in the raphe nucleus causes serotonin depletion, and neurotoxins may affect serotonergic neurons selectively if, for example, they are taken up specifically in serotonergic neurons as is the case for 5,7-dihydroxytryptamine (5,7-DHT). 5,7-DHT and similar substituted indoleamines are taken up in serotonergic neurons by SERT and converted to quinone-like metabolites that show cytotoxic effects. Selective neurotoxins provide a nearly complete and irreversible serotonin depletion (Baumgarten and Björklund, 1976) when administered either by intracerebroventricular (icv) or by intra-

raphe injections, however, application of the neurotoxin does not only deplete stores of 5-HT but also deteriorate serotonergic projections.

Increased 5-HT levels can acutely be obtained by administration of compounds that disrupt vesicular storage and release 5-HT such as the amphetamine analogue fenfluramine. Blockade, or even reversion, of the SERT-mediated 5-HT reuptake by administration of e.g. cocaine or methylenedioxymethamphetamine (MDMA, "ecstasy"), also raises the levels of 5-HT acutely in the extracellular space. However, since 5-HT is more susceptible to degradation in the extracellular space compared to 5-HT stored intracellulary, serotonin depletion can also be obtained following administration of these agents that acutely increase synaptic concentrations of 5-HT. One single dose of MDMA in rats has been reported to decrease 5-HT tissue levels in a time dependent manner: Approximately 30% after 6 hours, 50% after 3 days, and 90% at 30 days after treatment (Reneman et al., 2002). Similarly, four consecutive daily treatments with fenfluramine in rats resulted in a 70% decrease in 5-HT tissue levels after 5 days (Kornum et al., 2006).

Yet another method for obtaining serotonin depletion in an experimental setting is acute tryptophan depletion (ATD). Biosynthesis of 5-HT is strongly affected by the availability of its precursor tryptophan, and the rationale underlying acute tryptophan depletion is to reduce 5-HT biosynthesis by depleting its precursor. Under normal circumstances, tryptophan is transported in plasma from where it is actively transported into the brain by a carrier system in competition with other amino acids (Neumeister, 2003). After providing a drink or pellet depleted of tryptophan, the plasma levels rapidly decrease hence lowering the plasma tryptophan levels, which in turn decrease transport of tryptophan to the brain, and the lowered brain tryptophan levels cause some depletion of 5-HT. The great advantage of applying tryptophan depletion as a method for obtaining serotonin depletion is its physiological nature, which also makes tryptophan depletion applicable in clinical studies. Also, absence of overt neurotoxicity makes ATD a gentle method for serotonin depletion, however, therefore ATD is also limited in its efficiency yielding a serotonin depletion of around 40% (Cahir et al., 2007).

Finally, a very prominent method to cause experimental serotonin depletion is inhibition of the rate-limiting enzyme in the 5-HT biosynthesis, tryptophan hydroxylase (TPH). Several substances are known to inhibit TPH activity, but few are specific and selective. One of them is para-chlorophenylalanine (pCPA), an irreversible and specific inhibitor of TPH (Koe and Weissman, 1966). A single injection pCPA in rats was found to rapidly reduce in vitro enzyme activity of TPH by 90% in raphe nucleus with a gradual recovery to baseline after 7 days (Park et al., 1994). Thus, serotonin depletion achieved using pCPA is a transient and non-neurotoxic state of decreased serotonergic neurotransmission. Four consecutive daily injections of pCPA have been reported to very efficiently deplete rat brain 5-HT levels by 95% (Kornum et al., 2006). Furthermore, serotonin depletion using pCPA was reported to be quantitatively more effective compared to regimens based on sustained release alone. Normally, pCPA is used in doses that almost

completely deplete tissue 5-HT in rats, however, this nearly complete serotonin depletion must be regarded as unphysiological in comparison to serotonergic dysfunction in humans diseases. In Paper I, we administered 50-100 mg/kg pCPA by i.m. injections in pigs to obtain serotonin depletion. These doses were based on previous studies administering pCPA to monkeys and reporting effects attributable to effective serotonin depletion (Gradwell et al., 1975;Raleigh et al., 1980). Similar doses of pCPA were also administered in clinical trials in cancer patients prior to chemotherapeutic intervention and found to antagonize the emetic response and decrease the urinary excretion of 5-HIAA (Alfieri and Cubeddu, 1995). However, the doses given to the pigs were lower as compared to the 250 mg/kg used to obtain nearly complete serotonin depletion in rats (Kornum et al., 2006;Licht et al., 2009).

Serotonin depletion has been shown to cause robust behavioural effects, both in experimental and clinical studies. In rats, serotonin depletion is well-established to increase aggressiveness in rats indicated by increased levels of muricide suggesting an inverse relationship between 5-HT and aggression (Paxinos et al., 1977). Contrasting this, many discrepant data in the literature reports how serotonin depletion effects most other behavioural outcomes including anxiety (Griebel, 1995) and affective behaviour (Blokland et al., 2002;Lieben et al., 2006). The variable results found in animal models of anxiety and depression following serotonin depletion underline the complexity of behavioural phenotypes, and several factors may impact the results (or lack of same) including severity of serotonin depletion, method used to obtain depletion, time course of treatment, type of behavioural model, time of testing relative to treatment, and strain of the tested animals. Therefore, no unambiguous answer can be given to how serotonin depletion affects depressive and anxiety-related behaviour. Furthermore, experimental serotonin depletion is also used to attenuate behavioural effect mediated by 5-HT, i.e. if a behavioural phenotype is normalized following serotonin depletion, the effect is concluded to be mediated by 5-HT. In mice, the antidepressant effects of fluoxetine and citalopram (SSRIs) in the tail-suspension test are attenuated by serotonin-depleting pre-treatment indicating that 5-HT mediates the antidepressant effects of these compounds (O'Leary et al., 2007).

In clinical studies, the most solid evidence of the involvement of serotonin in depression arise from the observation that previously depressed, well-medicated, and symptom-free patients experience relapse of depressive symptoms within hours of serotonin depletion (Delgado et al., 1990). In healthy subjects, however, serotonin depletion does not in general cause a decrease in mood (Ruhé et al., 2007), but mood effects in subjects with a so-called vulnerable serotonergic system are observed (Booij et al., 2002). The vulnerability of the serotonin system of an individual is affected by factors such as previous depressive episodes, stressful life events, relatives with depression, polymorphism of the SERT gene, female gender, or neurotic personality (Booij et al., 2002;Jans et al., 2007). These observations from serotonin depletion studies have been pivotal to the current hypothesis regarding the pathophysiology of depression where a vulnerability of the serotonergic system is regarded as a disposing factor for the development of clinical depression (Jans et al., 2007). However, further studies are still needed to characterize serotonergic markers

that can differentiate serotonergic systems in vulnerable subjects from normal subjects. This could give insights to whether hypofunction of the serotonergic system is a triggering factor in the pathophysiology of depression.

PET measurements of the human 5-HT system

Positron emission tomography (PET) is an important tool for studies of the living brain in animals and humans. PET has been widely applied as a powerful technique to investigate neuroreceptor binding in vivo; however, it is mostly used in studies of cellular metabolism using labelled glucose analogues (most prominently ^{18}F-fluorodeoxyglucose, ^{18}F-FDG), but also for amyloid plaque binding, neurotransmitter release, blood-brain barrier (BBB) transport, and cerebral blood flow. For more than two decades, PET radioligands have been applied to investigate the serotonergic system in humans, and in vivo imaging studies have supplied the main fraction of knowledge gained since then on the function of this neurotransmitter system in the living brain. PET radioligands for imaging of 5-HT$_{1A}$, 5-HT$_{1B}$, 5-HT$_{2A}$, and 5-HT$_4$ receptors, and SERT are now used in clinical studies with multiple and diverse purposes.

In several studies, radioligand binding to serotonergic targets is used as a measure of receptor levels in human diseases and compared to binding in healthy controls. Studies from NRU have furthermore thoroughly characterized these markers in healthy controls in relation to demographical data, psychological traits, and genetic variation. In one study, 5-HT$_{2A}$ receptor binding measured with [^{18}F]altanserin was shown to decline with age (Adams et al., 2004). Furthermore, it was shown in a separate study that the cortical [^{18}F]altanserin binding was closer correlated in monozygotic than in dizygotic twins indicating that 5-HT$_{2A}$ receptor binding in humans is strongly genetically determined (Pinborg et al., 2008).

Besides these basic studies of neuroreceptor systems in patient or population groups, PET radioligands are also widely used directly as a tool in CNS drug discovery and development (Gee, 2003;Wong et al., 2009). In this respect, PET studies with the drug itself labelled with a positron emitter can measure the biodistribution, BBB penetration, brain concentration, and metabolism of the potential therapeutic. However, more often a well-characterized PET radioligand for the same target as the therapeutic target is used. In these types of studies, the displacement of PET radioligand is measured after a dosing regime of the investigated drug, and from this, the target occupancy of the given drug is measured, and small sample dose-finding studies can be conducted to determine which doses should be applied in further clinical studies. In the serotonin system, PET imaging is applied to measure target occupancy for clinical doses of SSRIs and antipsychotics at SERT and 5-HT$_{2A}$ receptors, respectively. Occupancy measurements of clinically relevant doses of all investigated SSRIs including citalopram, fluoxetine, sertraline, paroxetine, and venlafaxine at SERT were around 80% as determined using the PET radioligand [^{11}C]DASB (Meyer et al., 2004). These results show that for SSRI-antidepressants a close relationship between receptor occupancy

and clinical efficacy exists, and new potential SSRI would aim at doses achieving at least 80% SERT occupancy.

PET tracer development

The use of PET tracers for imaging is based on the underlying assumption that adding the positron emitting isotope does not change the biological properties of the molecule, and further that the PET tracer is administered in negligible amounts that do not perturbate biological function of the system examined. The availability of suitable PET tracers is a prerequisite for PET imaging, and as such the continuous development of novel PET tracers is essential for the evolution of PET imaging and for the field to be able to answer questions of increasing complexity.

PET tracer development is a sequential process, and the development of a successful PET tracer is somewhat similar to development of a successful therapeutic drug, as the PET tracer candidate may fail at any given step of the development process, thus PET tracer development is a complex and time-consuming process from which only a very small fraction of tested compounds actually goes through development and into clinical studies (Pike, 2009). Despite recent efforts to develop a screening platform for the prediction of PET radioligand performance based on in vitro data (Guo et al., 2009), PET radioligand development is currently still mostly based on empiricism and serendipity (Wong and Pomper, 2003). In order for a PET radioligand to succeed as a neuroimaging compound it must possess certain properties (see Table 1) and most of them can only be validated through in vivo studies.

Table 1. Ideal properties of a CNS PET radioligand and strategies for evaluation

Property	Experimental Method
• High affinity for target (usually K_D in nM range)	In vitro binding assay or autoradiography
• Selectivity for target	In vitro screening assays and in vivo blocking experiments
• Reliable radiolabelling at high specific radioactivity	Evaluation of chemical structure and test of labelling
• Penetration of the BBB	cLogD evaluation / In vivo scanning w/o efflux transporter blockade
• No BBB penetration of radiolabelled metabolites	HPLC analysis of plasma or tissue
• Suitable pharmacokinetics (observable brain uptake and washout)	In vivo PET scanning
• Safe for administration in low doses	Toxicological testing
• Low non-specific binding	In vivo PET scanning

First, the PET radioligand must bind the target with adequate affinity and selectivity. The affinity required is dependent on density of binding sites so that lower affinity is accepted for radioligands targeting receptors of higher density. Selectivity is the affinity towards the target receptor compared to the affinity towards non-target receptors, and generally, the more selectively a PET radioligand binds its target, the better a ligand it would be. However, since PET radioligand binding to any target can be regarded as the product of radioligand affinity for the receptor and the number of receptors, it is less of a problem for a radioligand to have affinity for a target if this target is of low density in the region to be examined. Both selectivity and affinity is usually determined by in vitro binding assays, and most PET radioligands display affinity in nanomolar range for their target. However, in vivo and in vitro affinities are often dissimilar due to differences in factors including receptor affinity state, microenvironment around the receptor, pH, and ion concentrations where binding occurs (Narendran et al., 2005). Additionally, in vivo affinities measurements are done in dynamic, non-steady state conditions whereas in vitro affinities are measured at equilibrium which also contribute to the differences between these affinity measures.

Also very important for a compound to be applicable as a PET radioligand, the compound must be able to be radiolabelled with a suited positron emitter, most often ^{11}C or [18]F. Since both these isotopes are relatively short-lived, radiolabelling and purification must occur quickly reliably, and preferably in a one-step reaction (Miller et al., 2008). ^{11}C-methyl groups are most frequently introduced by direct methylation of hydroxyl groups or amines using nucleophilic substitutions. ^{18}F-labels can be introduced in compounds with fluorine coupled to aliphatic side-chains by electrophilic fluorination or directly by aromatic ^{18}F-fluorination using nucleophilic substitution (Miller et al., 2008).

PET radioligands under development are often discarded due to high non-specific binding (NSB). NSB in PET scanning is the random and non-displaceable interaction between the PET radioligand and brain lipids and proteins that decrease target-to-background binding ratio. Since in vivo NSB of potential PET radioligand readily impose problems, much effort has been done to develop screening methods to predict NSB for PET radioligand development (Guo et al., 2009;Rosso et al., 2008). A practical and quick way of trying to predict NSB is looking at the lipophilicity of the radioligand. Increasing lipophilicity would tend to increase lipid interactions and thus increase NSB, however, evaluating lipophilicity alone is a poor predictor of in vivo NSB (Rosso et al., 2008), since this is influenced by numerous other factors including BBB penetration, diffusion and kinetic properties in the brain, and binding to non-target receptors. Therefore, the NSB of a PET radioligand can first really be assessed when applied for in vivo PET scanning.

Adequate penetration of the BBB is necessary for imaging of targets in the CNS (Pike, 2009). The BBB generally prevents hydrophilic or electrically changed molecules from passing, why PET radioligands should be somewhat lipophilic in order to cross the lipid bilayer in the BBB. However, very lipophilic compounds generally also are bound to plasma proteins to a greater extent which potentially could

impair brain penetrance, and they often also display greater NSB. Thus, an optimal lipophilicity for PET radiotracers is defined as a rule of thumb: $LogD_{7.4}$ – a widely used measure of lipophilicity – for PET radioligands should lie within 2.0-3.5 (Pike, 2009). Furthermore, penetration of the BBB is complicated by the presence of several efflux transporters effectively to removing unwanted substances from the brain, most prominent of these transporters is P-glycoprotein (P-gp). P-gp substrates show immensely structural diversity; small structural differences among compounds impact P-gp substrate behaviour dramatically and unpredictably, and P-gp also vary among animal species (Syvanen et al., 2009). Thus, whether a PET radioligand is a substrate for P-gp is usually tested through in vivo PET scanning.

Metabolism of the PET radioligand parent compound is also an issue during in vivo evaluation. If radiolabelled metabolites are formed and enter the brain this disturb the signal by increasing the background levels – this in the frequent case that the metabolites do not show affinity for the target receptor. If metabolites are formed outside the brain and enter the brain, the input function of these metabolites should also be taken into account which complicates quantification considerably. However, radiometabolites are usually less lipophilic than the parent radioligand and thus has reduced propensity to enter the brain (Pike, 2009). In the ideal case, a PET radioligand readily enter the brain without formation of radiolabelled metabolites, however, if the produced metabolites do not enter the brain then this profile of metabolism does not impact PET radioligand properties severely.

Finally, a requirement for an optimal PET radioligand is suitable in vivo kinetics, i.e. relatively fast kinetics are generally wanted to ensure that radioligand binding to the target receptor is reversible. The standard methods for radioligand binding quantification do not work if binding is irreversible over the time frame of PET scanning (Innis et al., 2007), therefore the ideal radioligand shows suitable pharmacokinetics in relation to the half-life of its radiolabel, i.e. both brain uptake and visible washout from the brain is observed within the time frame of the PET scanning.

Measuring endogenous neurotransmitter release with PET

PET has been widely applied to measure dopamine release using dopamine receptor 2 (D_2) antagonists radioligands such as [11C]raclopride. The release of dopamine is measured with e.g. [11C]raclopride through its displacement by endogenously released neurotransmitter. The released dopamine will compete with the labelled tracer for D_2 binding sites and in states of increased dopaminergic neurotransmission, [11C]raclopride binding to D_2 receptors is decreased and vice versa. This simplified model to describe the endogenous competition between dopamine and various D_2 radioligands is termed the classical occupancy model (Laruelle, 2000). The ability to measure dopamine levels with PET ligands sensitive to endogenous dopamine has revolutionized research within many diseases, including schizophrenia and drug addiction (Ginovart, 2005;Verhoeff, 1999). However, the full molecular mechanism underlying the measurement of dopamine levels with displaceable D_2 PET radioligands is not yet fully understood (Ginovart, 2005),

however the classical occupancy model probably is too simplified. One of its short-comings is that it does not take the agonist-mediated receptor internalization into account (Ginovart, 2005;Laruelle and Huang, 2001). But despite the lack of thorough knowledge on the molecular mechanisms, pharmacological challenges that increase extracellular dopamine levels, e.g. amphetamine or MDMA, are well-characterized to decrease D_2 PET radioligand binding in animal and human studies (Ginovart, 2005;Narendran et al., 2005;Narendran et al., 2010;Rosa-Neto et al., 2004). Similarly, it is also well-established that depletion of dopamine levels increases D_2 radioligand binding in human and animal studies (Cumming et al., 2002a;Seneca et al., 2008;Verhoeff et al., 2003). The application of D_2 radioligands and PET to measure dopamine release following challenges has been pivotal in understanding the role of dopamine in human behaviour and diseases. Thus, it was demonstrated that healthy volunteers playing a video game released dopamine in the striatum thus demonstrating the ability of in vivo imaging to detect physiological changes in dopamine levels (Koepp et al., 1998). And further in human disease states, it was demonstrated that schizophrenia patients show abnormally high levels and release of dopamine (Breier et al., 1997). These and similar in vivo imaging studies show a hyperreactivity of the dopaminergic system in response to challenges in schizophrenia, and this gain support from the classical dopaminergic hypothesis of schizophrenia, stating that the pathophysiology underlying this disease is caused by enhanced dopaminergic neurotransmission (Ginovart, 2005;Laruelle, 2000;Soares and Innis, 1999).

Although many D_2 receptor antagonist radioligands (e.g. [11C]raclopride and [123I]IBZM) are sensitive to endogenous dopamine release following pharmacological challenges, a growing body of evidence suggests that D_2 receptor agonists are superior to antagonists in measuring dopamine release. Theoretically, the ternary complex model of agonist-receptor interaction describes that agonist radioligands detect dopamine release better than antagonists, since these would only bind functional active receptors where the endogenous ligand/radioligand competition occurs. Studies in monkeys (Narendran et al., 2004;Seneca et al., 2006) and mice (Cumming et al., 2002b) have found that the degree of radioligand displacement was higher with agonist compound as compared to antagonist. This greater sensitivity towards endogenous competition with dopamine is attributed to the agonist only binding the high-affinity state of the D_2 receptors which specifically are susceptible to endogenous competition. The hypothesis that D_2 agonist radioligands only bind a subset of the total number of receptors is supported by a study in baboons showing fewer binding sites for the agonist tracer [11C]NPA as compared to the antagonist tracer [11C]raclopride (Narendran et al., 2005). These data support that agonists only bind high-affinity functional state of the receptors, and that agonist PET tracers are better radioligands for measuring endogenous competition.

Despite the conquest of valuable scientific landmarks using PET measurement of dopamine release with PET radioligands, the task of measuring endogenous neurotransmitter release has not been thoroughly accomplished for other neurotransmitter systems. Many factors complicate measurement of 5-HT release compared to DA release with PET (Paterson et al., 2010). These factors relate to the distribution and

localization of receptors, local endogenous ligand concentrations, and affinity state of the receptors. Speaking against the possibility for developing a 5-HT_{2A} radioligand usable to detect neurotransmitter release is that a greater fraction of 5-HT_{2A} receptors compared to the D_2 receptors are intracellulary localized (Cornea-Hebert et al., 2002) and as such not accessible for competition by endogenous neurotransmitter. Also, a smaller fraction of 5-HT_{2A} receptors is in the high-affinity state: ~20% for 5-HT_{2A} (Fitzgerald et al., 1999), 80% for D_2 (Narendran et al., 2005), and presumably the competition only occurs at high-affinity state of receptors. Finally, whereas D_2 receptors more frequently are localized in classical synapses, 5-HT_{2A} receptors are also localized extra-synaptically (De-Miguel and Trueta, 2005). 5-HT could potentially also compete with a radioligand for extra-synaptic sites, however, the predominant synaptic localization of D_2 receptors can cause increased concentration of dopamine in the proximity of the receptor thus to a greater extent facilitating local competition at these receptors.

Nevertheless, a serotonergic PET radioligand sensitive to endogenous changes in 5-HT could potentially serve as a non-invasive marker of 5-HT levels in humans. Such a marker would potentially grant invaluable insights to human diseases such as depression and AD which involve dysfunction of the 5-HT system. Much effort has put into testing the sensitivity of serotonergic PET radioligands to acutely altered 5-HT levels. Generally, these studies have found that serotonin receptor antagonist PET radioligands are not displaceable following pharmacological challenges that increase 5-HT. The binding of the 5-HT_{2A} receptor antagonist PET tracer [18F]Altanserin was not decreased following a citalopram/pindolol challenge to elevate endogenous 5-HT levels (Pinborg et al., 2004). Also, the 5-HT_4 receptor antagonist PET tracer [11C]SB207145 was found insensitive to citalopram-induced increases in 5-HT levels (Marner et al., 2010b). With the 5-HT_{1A} antagonist, [18F]MPPF, it was initially reported that increased levels of 5-HT decreased receptor binding using a beta-microprobe technique indicating that this ligand was sensitive to fluctuations in 5-HT in vivo (Rbah et al., 2003;Zimmer et al., 2002). However, a later study using a bolus/infusion approach in conscious monkeys found that [18F]MPPF binding was not reduced following a robust fenfluramine-mediated elevation of 5-HT during constant tracer levels in plasma (Udo de Haes et al., 2006). Finally, a very recent paper did, however, put forth interesting data showing that binding of the 5-HT_{1B} radioligand [11C]AZ10419369 is decreased following fenfluramine administration which could indicate that this PET tracer is sensitive to endogenously released 5-HT (Finnema et al., 2010). However, in this study the authors were not able to rule out a direct interaction between fenfluramine and the 5-HT_{1B} receptor, so more studies are needed to test the displaceability of [11C]AZ10419369 by 5-HT. Taken together, these data suggest that antagonist PET radioligands in the serotonergic system generally are not sensitive to endogenous competition by 5-HT (Paterson et al., 2010). So recently, 5-HT_{1A} agonist PET radioligands have been validated partly with the purpose to quantify 5-HT_{1A} receptor specifically in the high-affinity state, but also caused by the assumption that these agonist PET tracers could be more prone to displacement by endogenous 5-HT (Lemoine et al., 2010;Milak et al., 2008).

Aims

The overall aim of this thesis was to develop and validate methods for altering the serotonin system and to image the 5-HT$_{2A}$ receptor agonist binding sites in the pig brain. More specifically, the objectives of the studies were:

- To validate a porcine model of serotonin depletion using para-chlorophenylalanine (pCPA) to decrease cerebral 5-HT levels. Secondly, to investigate the effect of decreased levels of 5-HT on the most widely distributed 5-HT receptors.

- To develop [^{11}C]Cimbi-5 as a 5-HT$_{2A}$ receptor agonist PET tracer and validate its properties in the pig brain, including biodistribution and displaceability in vivo. Secondly, to improve PET tracer properties of [^{11}C]Cimbi-5 by changing of the labelling site and modification of the chemical structure of the PET tracer.

Methods

For the specific methods and materials used for each experimental set-up, please refer to the methodology section of the respective manuscript. The following sections will cover general aspects of the primary methods used in the present studies, as well as the reason for using them.

The pig as an experimental animal

For more than 40 years the pig (*sus scrofa*) has been used in human biomedical research due to the extensive similarity between human and porcine biology (Bustad and McClellan, 1966). For example, the pig is well-established in physiological research and surgical research and training (Tumbleson, 1986). Specifically in relation to neuroscience research, the pig brain, like the human brain, is gyrencephalic and thus resembles the human brain more than the lissencephalic brain of rodents. And due to the neuroanatomical and neurophysiological similarities between humans and pigs, the pig has gained increased popularity over the last decade as an experimental model animal in neuroscience research as recently reviewed (Lind et al., 2007). Furthermore, the large size of the pig brain favours modern imaging techniques such as magnetic resonance imaging (MRI) and PET using standard equipment designed for human use (Cumming et al., 2003;Watanabe et al., 2001). Also, the pig possesses several advantages over primates as a large non-rodent model for experimental research. Most obvious are the ethical and economical properties, but pigs are also more easily housed than primates and are readily available from farms in pork-producing countries. Over the last decades, the use of laboratory pigs as a non-rodent large animal model has also increased dramatically within toxicological testing (Lind et al., 2007).

Various breeds of pigs are normally chosen in experimental research based on the purpose of the study. The most common breed of pig used in research is the Landrace which is also the most common agricultural breed used in commercial pork production. However, due to different breeding standards among national agricultural organizations these breeds are not globally defined, and usually a more detailed distinction, e.g. Danish Landrace pig, is used in scientific literature (Lind et al., 2007). Furthermore, individual farms may not produce a pure breed, but rather a crossbreed of various breeds which favour larger litter sizes for commercial use. However, for research purposes a drawback is the use of a range of different and poorly defined breeds. Oppositely, the commercial use of the Danish Landrace holds economic and availability advantages in relation to research. Landrace pigs have been bred towards rapid growth and a high body weight of the mature animal which can be as heavy as 300 kg (Lind et al., 2007). Therefore, landrace pigs are most often only used at a young age, at a weight less than 40 kg, and most often only for relatively acute or short-term research studies. However, pig breeds exist, e.g. the Göttingen minipig, that are bred specifically for scientific purposes and at adult-hood obtain modest body weights around 35-45 kg (Köhn et al., 2008). These minipigs therefore provide a more practical choice of experimental pigs for longitudinal

studies over longer time, e.g. in the development of models of human diseases. The Göttingen minipig has been used successfully to generate an porcine animal model of Parkinson's disease (PD) (Mikkelsen et al., 1999). Also, in our lab we have established a method for in vivo gene transfer to the neonatal minipig brain using recombinant adeno-associated viral (rAAV) vectors with the objective to generate novel porcine animal models of CNS diseases such as AD (Kornum et al., 2010). Furthermore, the Göttingen minipigs are more widely used for behavioural testing as compared to the Landrace breeds (Kornum et al., 2007;Kornum and Knudsen, 2010;Nielsen et al., 2009). However, since the studies presented in this thesis all were are relatively short-term, the Danish Landrace was chosen as pig breed for the experiments.

The serotonin system in the pig has been used to model the developing human serotonergic neurotransmission finding a high degree of neurochemical and topographical resemblance during brain development in infants and piglets (Niblock et al., 2005). Furthermore, concentrations of 5-HT are comparable to humans with high concentrations in the raphe nucleus, thalamus, and basal ganglia (Swamy et al., 2004). The neuroanatomy of the porcine serotonin system has also been demonstrated to resemble the human serotonin system to a high degree, and the development of the medullary serotonin system shows equivalence in pigs and humans (Niblock et al., 2005). Also in several PET studies, pigs have been used to investigate in vivo binding of serotonergic targets finding similarities to human in the target distribution. SERT binding has been examined in pigs using various PET tracers showing that SERT distribution is similar in pigs and humans (Brust et al., 2003;Cumming et al., 2007;Smith et al., 1999;Smith et al., 2001). Also for 5-HT$_4$ receptor binding, the receptor distribution has been reported to be similar in pigs and humans (Kornum et al., 2009;Marner et al., 2010b).

In vitro quantification of 5-HT and metabolites

Measuring concentrations of small molecules is often done using high performance liquid chromatography (HPLC). HPLC relies on chromatographic separation of compounds in a solution such as a dialysate, a plasma sample, or a brain homogenate. The HPLC method of separation of molecules is based on high pressure forcing molecules through a column packed with beads which will retain molecules for different times depending on the physiochemical properties of the molecule and on the composition of the mobile phase used. Retention time in the column calibrated in comparison to external reference compounds allows for identification of specific molecules. Monoamines can be separated by reversed-phase HPLC (RP-HPLC) where changes in pH, ion concentrations, concentration of organic solvent, and ionic strength of the mobile phase all influence retention times of monoamines and their metabolites. In HPLC with electrochemical detection (ED), the eluted molecules pass over a glassy carbon electrode operating relative to an Ag/AgCl reference electrode. Here they are oxidized creating an electrical current that is measured by an amperometric detector, and this current is proportional to the number of molecules oxidized which is reflected as peak height on the resulting chromatogram. Monoamine peaks are identified in relation to

retention time of reference compounds and calibrated by the amounts of reference compounds applied. Concentrations of compounds in samples are then calculated by the area under curve (AUC) for the compound present in the samples relative to the AUC for the compound in the reference solution, tissue concentrations are determined by multiplying with the appropriate dilution factor. In Paper I, we quantified 5-HT, its main metabolite 5-HIAA, dopamine, and its main metabolites 3,4-dihydroxyphenylacetic acid and homovanillic acid in pig brain homogenates using a RP-HPLC with ED method as previously described (Weikop et al., 2007). Briefly, pieces of pig brain tissue were excised from discrete regions: frontal cortex, occipital cortex, striatum, hippocampus, caudal brain stem, rostral brain stem, and cerebellum. After homogenisation in perchloric acid saturated with disodium-EDTA, centrifugation, and filtering, the homogenates were loaded on the HPLC system.

A more precise estimation of extracellular 5-HT can be measured using in vivo microdialysis where canula probes are inserted directly into the brain of the animal colleting extracellular fluid that subsequently can be analysed with HPLC to determine monoamine concentrations. This method has successfully demonstrated increases in extracellular 5-HT concentrations after paroxetine administration in rats (Licht et al., 2010) and after fenfluramine administration in monkeys (Udo de Haes et al., 2006). However, since microdialysis is not thoroughly validated in the pig and is complicated by the thick porcine skull, lack of solid stereotaxic information on pig brain anatomy, and demand for proximate microdialysis and HPLC equipment, in Paper I, we used tissue concentration of 5-HT in brain homogenates as a marker for serotonergic neurotransmission. The validity of measurements of 5-HT tissue levels in homogenates compared to extracellular 5-HT measured by microdialysis during serotonin depletion has previously been confirmed (O'Connell et al., 1991) where homogenate measurements and microdialysis provide similar percentages of serotonin depletion following the same pharmacological intervention. Furthermore, extracellular monoamine concentrations measured by in vivo microdialysis may vary significantly both regionally and between animals making inter-animal comparisons difficult. 5-HT tissue has therefore often been applied to quantify the degree of serotonin depletion (Kornum et al., 2006;Lieben et al., 2004).

In vitro receptor autoradiography

The aim of this thesis was to study 5-HT receptors in the pig brain. In vitro receptor autoradiography is a widely used method to investigate receptor binding in vitro that employs radioactively labelled ligands which bind specifically but reversibly to particular receptors. Since the ligand/receptor binding ratio is 1, the signal can be quantified as number of receptors. For CNS applications, thin brain sections which preserve regional topography allow for quantification of binding in smaller structures than can be dissected for suspension based methods, e.g. receptor binding assay. Ligands can be labelled using a broad variety of isotopes including ^{14}C, ^{35}S, ^{32}P, ^{11}C, etc, however for receptor autoradiography, ^{125}I and ^{3}H (tritium) are most widely

used. Tritium labelling does not alter the biological structure of the ligand and allows labelling with relatively high specific activity (~2000 GBq/mmol). Furthermore, the long half-life of tritium (12.43 years) and low energy of β^--radiation (18.6 keV) enable long-term storage and use. Since receptors are detected in their native, properly folded state, the quality of autoradiograms is dependent on the availability of high-affinity ligands (incubation concentrations in nanomolar range) and high specific activity of the radiochemical synthesis.

As a general principle for in vitro binding, the total binding (TB) of the radioactive ligand comprises not only the specific binding (SB) of the ligand to the targeted receptor, but also the general non-specific binding (NSB) to tissue and other receptors, these interactions usually being of lower affinity. Thus, the SB can be calculated as TB subtracted NSB. The NSB is measured in the presence of a large excess (approx. 10000 fold) of an unlabelled ligand binding to the same receptor. The unlabelled ligand should preferably belong to another structural group than the labelled ligand allowing for subtraction of NSB from TB without the bias of displacing binding to other receptors by the labelled ligand. This general approach for calculating SB applies for both autoradiography and binding assay conducted in suspension.

In vitro receptor autoradiography can be performed as a saturation study where different concentrations of radioactive ligand are applied. In this type of study the equilibrium dissociation constant (K_d) (ligand concentration where 50% of the available receptors are occupied) can be determined. Conversely, when a saturating concentration of radioactively labelled ligand (~4-6 times K_d) is used, binding levels can be interpreted as a direct measure of the total concentration of receptor binding sites (B_{max}). This method is here applied in Paper I to investigate whether changes in receptor density occur.

Generally, the practical autoradiographic procedure comprises two steps, pre-incubation and incubation, that differ between the TB and the NSB sections followed by a washing step which is identical for TB and NSB. In the pre-incubation, sections are incubated relatively shortly in assay buffer omitting radioactively labelled ligand. The difference in pre-incubation buffers between TB and NSB is that an excess of un-labelled ligand with affinity for the investigated receptor has been added to the NSB buffer. Purposes of the pre-incubation step are to remove endogenous 5-HT from the tissue and allow the competitive ligand to access the tissue before addition of the labelled ligand. Following the pre-incubation, sections are incubated in assay buffers containing the radioactive ligand. The only difference between buffers for the TB and NSB is still the addition of excess un-labelled ligand.

Practically, the in vitro receptor autoradiography in Paper I was done on freshly frozen brains taken out quickly after decapitation and directly cooled on dry ice. Brains were stored at -80ºC until sectioning. The brains were sliced on a cryostat in 10 µm coronal sections, thaw-mounted on gelatine coated glass slides, and allowed to dry before storage at -80ºC. While sectioning, orientation in the coronal plane was maintained by referring to a stereotaxic atlas of the pig brain (Felix et al., 1999). Due to the maximal range of tritium radiation of 6 µm in water most activity will be absorbed in the tissue itself and thus not

result in a signal. This favours direct comparisons among quantifications done on different thicknesses of sections.

Autoradiograms and image analysis

The emitted radiation from isotope decay from sections processed for in vitro receptor autoradiography can be detected by photographic emulsion, photographic film, or phosphor imaging plates (IP) (Kuhar et al., 1986). In Paper I, we applied IPs for the detection of radioactive decay and measurements of receptor binding. The IP consists of a flexible plastic plate coated with phosphor crystals $(BaF(Br,I):Eu^{2+})$ combined with an organic binding. These crystals are capable of storing a fraction of the energy from the emitted radiation and when later stimulated by visible or infrared radiation, crystals emit photostimulated luminescence (PSL) at intensities proportional to the absorbed radiation energy (Amemiya and Miyahara, 1988). The PSL can be collected in a photomultiplier tube, amplified, and converted to a digital image by an image plate reader (IPR). The Fuji BAS 2500 was used as IPR in Paper I, and the IPs were scanned at a resolution of 100 µm which is sufficient to quantify binding in relatively small regions. Furthermore, tritium radiation-sensitive IPs (TR-IP) have been developed, and these are now widely used in receptor autoradiography at the expense of autoradiographic films (Pavey et al., 2002). Although, autoradiographic films hold a better resolution, the signal-to-noise ratio is better using IPs (Amemiya and Miyahara, 1988). Another important advantage of the TR-IPs is the marked reduction in exposure time (approx. 7-8 times) compared to tritium sensitive film (Pavey et al., 2002). In addition, the IPs are erasable, i.e. crystals in the IP can be reset by exposure to bright white light in an IP eraser allowing repetitive use of the same plate. This procedure can only be done, however, when tissue and ligand prior to exposure have been fixed in paraformalehyde vapour (Liberatore et al., 1999). When not fixed, the radioactive ligands will stick to the TR-IP plate itself leaving it unfit for reuse.

Since the PSL is proportional to the emitted radiation, and this is converted directly to a digital image, the in vitro receptor binding can be quantified by densitometric measurements of the resulting autoradiograms. This image analysis was in Paper I conducted using the free software ImageJ (Image Processing and analysis in Java, http://rsb.info.nih.gov/ij/). Image analysis was conducted by hand-drawing regions of interest (ROI) for each brain region, and the mean pixel density in the ROIs was measured. Image density in the ROI is expressed in arbitrary units as a gradation level with a value assigned to each pixel according to its density. In order to convert the mean pixel density measured to ligand binding, standard [3H]microscales were used which contain 8 activity levels (nCi/mg) of tritium (Amersham Biosciences). The [3H]microscale activity is embedded into a polymer structure and calibrated by the manufacturer to mimic the auto-absorbing features of brain grey matter providing a value of activity in units of nCi/mg estimated wet tissue equivalent (TE) (Geary et al., 1985). The visible bands of the higher (1-34 nCi/mg TE) and lower (0.07-6 nCi/mg TE) [3H]microscale were quantified using the same ROI. The measured densitometric

measurements were fitted to the decay-corrected [³H]microscale activity levels using a 3rd degree polynomial function. After this calibration is conducted, ImageJ utilizes the calibration function to compute results as binding (in nCi/mg TE) instead of the arbitrary unit pixel density. Thus, the [³H]microscale acts as an internal standard for each autoradiogram relating image densiometry to receptor binding. TB was hereafter measured within ROIs as nCi/mg TE, and the same ROIs were imposed on to the adjacent sections allowing for measurement of NSB. The difference between binding in adjacent sections comprised SB for all measured sections. Prior to the final analysis, the interobserver variation was assessed for each brain region by two observers that independently quantified SB, and for all procedures during quantitative autoradiography including sectioning, incubation, image analysis, and data processing, the identity of the sections was at all times blinded to the investigator. After measurements in ImageJ, TB, NSB, and SB were calculated in fmol/mg TE for each ROI using the decay-corrected specific activity of the ligand to convert from nCi to fmol. Moreover, the signal-to-noise ratio (SB/NSB) was also calculated. This parameter is often used as a measure of the quality of the protocol and is a parameter mainly influenced by the concentration and binding characteristics of the ligand, but can also be influenced by the addition of protective or blocking agent to the assay buffer or by changes in incubation or washing times.

Positron emission tomography (PET)

PET is a functional nuclear imaging modality based on the decay of positron emitting isotopes. When these radioisotopes decay, a positron (β^+) is emitted that upon an encounter with an electron (β^-) will undergo the physical phenomenon of annihilation. Annihilation literally translates to "to make into nothing"; however, the physical outcome of positron-electron annihilation is a pair of gamma photons with the energy of 511 keV. This pair of gamma photons is emitted at 180 degrees to each other making it possible to localize their source to a straight line between two detectors placed in a ring outside the radioisotope containing matter. Using the registered lines of response, image reconstruction estimates the radioactive concentration in a 3-dimensional area in a given temporal window. Radioisotopes widely used in PET include ^{11}C, ^{18}F, ^{15}O, ^{13}N, ^{82}Rb. These can be incorporated into compounds where a non-radioactive isotope of the same atom is normally present to yield labelled glucose analogues or receptor ligands. Such labelled receptor ligands are named radioligands or radiotracers, and Paper II/III of the present thesis concerns the development of 5-HT$_{2A}$ receptor agonist PET radiotracers.

In the current thesis, all PET scanning was conducted in young female Danish Landrace pigs using a high resolution research tomography (HRRT) scanner (Siemens AG, Germany) at the PET- and Cyclotron Unit, Copenhagen University Hospital, Rigshospitalet. The HRRT is a dedicated brain scanner offering the highest spatial resolution of any PET scanner. All PET scanning in Paper II and Paper III consisted of 90 minutes HRRT list mode data acquisition that was stated at the time of i.v. injection of the tracers, which were administered as a bolus injection in the catheter in the milk vein. Besides the venous

access, most pigs were also catheterized in the femoral artery. Here, arterial whole blood samples were taken eight times with increasing intervals during the PET scanning, and these blood samples were used to determine radioactive concentrations in plasma and whole blood, and radiolabelled metabolites were quantified with a HPLC system using a radiodetector. Furthermore, radioactivity in whole blood was continuously measured throughout the first 30 minutes of each scanning using an Allogg ABSS autosampler counting coincidences in a lead-shielded detector.

In Paper II and Paper III, all PET tracers were labelled with ^{11}C in one-step methylation reactions between the precursor and ^{11}C-methyl triflate. Generally, positron emitting isotopes have short half-life, however the half-life of ^{11}C is significantly shorter than that of ^{18}F (20.38 minutes vs. 109.77 minutes). Due to this difference, tracers labelled with ^{18}F are preferred for many purposes in relation to PET scanning yielding better count statistics in long scanning sessions and better possibility for distribution for PET scanning beyond immediate proximity of a cyclotron. Conversely, disadvantages using ^{18}F-labelled compared to ^{11}C-labelled PET tracers include the possibility of disturbing bone uptake of radioactive fluorine and also higher absorbed doses of radiation in human subjects. Moreover, the short half-life of ^{11}C enables blocking studies to be done within relatively short time, since carry-over of residual activity quickly decays. This allows a repeat scan in a condition of receptor blocking to be conducted as little as 2 hours after a baseline scan in the same animal. In this way, multiple PET scans in the same animal on the same day are allowed with ^{11}C-labelled PET tracers. In Paper II and Paper III, the in vivo selectivity of PET tracers was tested by challenges with a known 5-HT$_{2A}$ receptor antagonist ketanserin. After a baseline scan and 30 minutes prior to a second scan in the same animal, ketanserin was administered i.v., and the pig was re-scanned using the same PET protocol.

After scanning, the PET images were subsequently reconstructed into 38 dynamic frames of increasing length (6 × 10, 6 × 20, 4 × 30, 9 × 60, 3 × 120, 6 × 300, 4 × 600 s) using an iterative method as previously reported (Sureau et al., 2008). Images consisted of 207 planes of 256 × 256 voxels of 1.22 × 1.22 × 1.22 mm^3.

PET image analysis

PET images obtained during a dynamic PET investigation provide a quantitative estimation of the PET tracer concentration in a given volume of interest (VOI) over time. This relationship between regional radioactive concentrations of PET tracers is often visualized as a time-activity curve, and the activity outcome measure in time-activity curves is often expressed as radioactive concentration in VOI (in kBq/ml) normalized to the injected dose corrected for animal weight, in kBq/g yielding standardized uptake values (SUV) and the unit g/ml. Normalizing to the injected dose enable plotting of regional activity data from different animals and different injected doses on the same graph, this under the assumption that a given region takes up a constant fraction of injected PET tracer. Applying kinetic modelling, this regional data can be used to calculate the

distribution volume (V_T) of the PET tracer in a given VOI which, in this case of PET radioligands, is a measure of receptor concentration in the VOI.

Since both the time-activity curves and kinetic modelling require measurements of radioactivity in a given VOI, these must be carefully defined in anatomical space, preferably in a non-biased, automated way that is reproducible between animals. In Paper II and Paper III, a summed PET image of all counts in the 90 min scan was reconstructed for each pig and used for co-registration to a standardized MRI-based statistical atlas of the Danish Landrace pig brain (figure 2). This atlas was made in a similar way to what was previously reported for the Göttingen minipig (Watanabe et al., 2001), and the standard Danish Landrace pig brain atlas contains 20 predefined brain regions. Discrete points on the PET image is then co-registered to the atlas using the software Register as previously described (Kornum et al., 2009). Assigning regions using such an automated method avoids the possible bias from manually defining VOIs. After co-registration, radioactive concentrations in volumes of interest (VOI), including cerebellum, cortex (defined in the MRI-based atlas as entire cortical grey matter), hippocampus, lateral and medial thalamus, caudate nucleus, and putamen were extracted from the dynamic PET scanning. Radioactive concentrations (Bq/ml) in all VOIs were calculated as the average in left and right side.
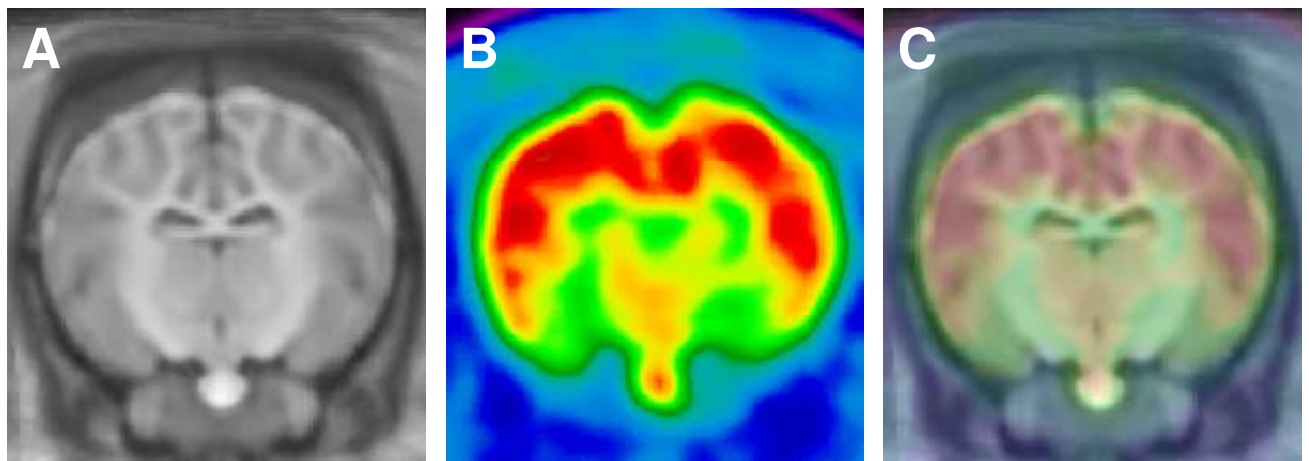
Figure 2. Illustration of co-registration of the HRRT PET images to the MRI-based atlas of the Danish Landrace pig brain. All sections are coronal summation images of 90 min of PET scanning viewed at the thalamic level. A: MRI-based atlas. B: [^{11}C]Cimbi-36 summed PET image at the same level as A. C: PET image overlaid on the atlas.

Several different models for kinetic modeling of PET data exist, but often regarded as the gold standard for receptor binding quantification is the compartmental analyses using parent-compound corrected arterial concentration as input function. So from PET scanning with successful measurements of plasma, whole blood, and radiometabolite measurements, the concentration of radioligand (C_{Tissue}) in a VOI relative to the plasma concentration (C_{Plasma}) can be calculated. This C_{Tissue}/C_{Plasma} ratio is defined as the V_T with the unit ml/cm^3 (Innis et al., 2007) and can be computed using one tissue or two tissue compartments model (1TC, 2TC). In Paper II and III, we calculated V_T for VOIs using 1TC or 2TC models in pigs with successful arterial input function measurements.

Also, neuroreceptor investigations using PET scanning are usually conducted using radioligands in tracer doses, i.e. doses of cold ligand do not occupy more than ~5% of receptors. Furthermore, PET radioligands must be administered in sufficiently low cold doses that do not perturbate or influence the biological system that is investigated. These assumptions both underlie the basic tracer principle.

For a PET radioligand to does indeed act as a tracer, does not occupy a significant fraction of the receptor, and the receptor system is not affected by the injection of cold compound, then the specific radioligand binding is at equilibrium approximated as binding potential (BP). First proposed by Mintun et al. (1984), BP is now the standard outcome measure of radioligand PET studies, but various forms of the BP exist dependent on what reference concentration of radioligand is chosen (Innis et al., 2007). BP_P is the equilibrium concentration of specifically bound radioligand to the concentration of radioligand in the plasma. Closely related to BP_P, the BP_F is specific radioligand binding to the free radioligand in plasma, i.e. radioligand not bound to plasma protein. Finally, non-displaceable binding potential (BP_{ND}) refers to the specifically bound radioligand at equilibrium relative to the radioligand concentration non-specifically bound in the tissue, BP_{ND} is typically measured with reference tissue models and is here the ratio of radioligand concentrations in the regions of high receptor density and a region devoid of target receptors. For all these versions of BP, the equilibrium conditions can be reached experimentally, however, most often the equilibrium is obtained after the application of a kinetic model to the experimental data. Based on in vitro binding nomenclature, BP is defined as the ratio between the concentration of binding sites (B_{max}) and the K_d of the radioligand, thus BP is proportional to both the affinity of the radioligand and to the receptor density (Mintun et al., 1984).

In Paper II, cortical BP_{ND} was calculated as $BP_{ND} = V_T/V_{ND} - 1$ (Innis et al., 2007) assuming that specific 5-HT$_{2A}$ receptor binding in cerebellum is negligible and that the V_{ND} is equal to the cerebellar V_T (Pinborg et al., 2003). For all pigs, BP_{ND} was also calculated with the simplified reference tissue model (SRTM, (Lammertsma and Hume, 1996)). The reference tissue models are generally accepted as valid for quantification of 5-HT$_{2A}$ receptor binding in PET studies (Meyer et al., 2010;Pinborg et al., 2003). However, for each PET tracers the application of reference tissue models should be validated in comparisons to compartment models. In paper III, we used SRTM BP_{ND} to approximate the target-to-background binding ratios of the tracers. All kinetic modelling was done with PMOD version 3.0 (PMOD Technologies Inc.). Goodness-of-fit was evaluated using the Akaike Information Criterion (AIC) which evaluates the fit of the kinetic model while taking the degrees of freedom into account.

Results and discussion

pCPA-treatment causes serotonin depletion in the pig brain

To validate a model of serotonin depletion in the pig brain, we treated female Danish Landrace pigs with the TPH inhibitor pCPA (i.m., 50 mg/kg or 100 mg/kg) once daily for four consecutive days and euthanized the animals on day five. No porcine model of serotonin depletion had previously been validated with regards to degree of depletion. Here, we found that serotonin immunoreactivity was decreased in most regions following pCPA treatment compared to saline (Paper I). Furthermore, to quantitatively validate the degree of serotonin depletion caused by the pCPA treatment, we excised tissue from seven distinct brain regions and analysed tissue levels of 5-HT and 5-HIAA with HPLC. On average, we found that the 5-HT tissue levels were decreased by 69±14% after 50 mg/kg pCPA and by 77±11% after 100 mg/kg pCPA across the brain regions (figure 2).
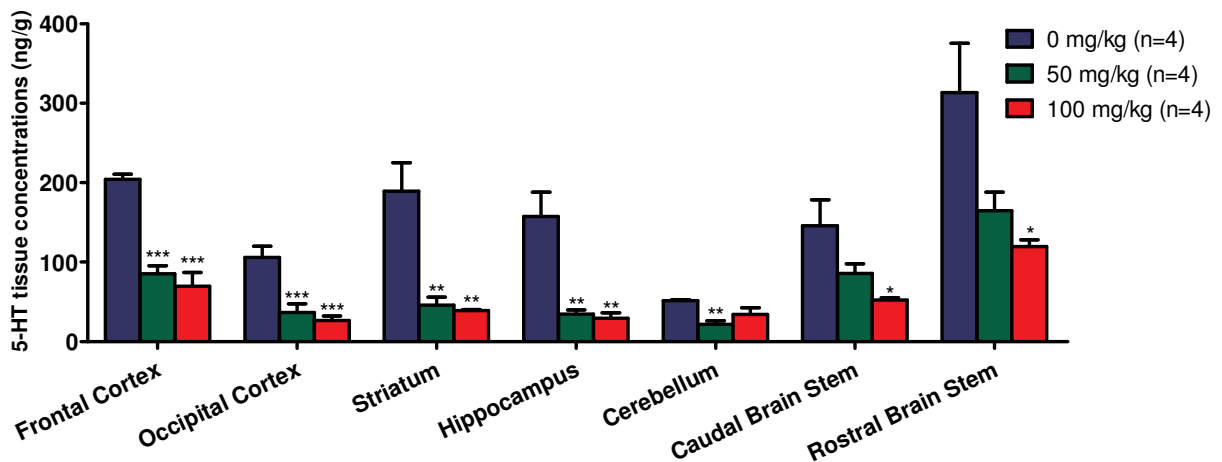
Figure 2. 5-HT tissue concentrations in pig brain regions following pCPA or saline. Error bars represent SEM. p-values are derived from a one-way analysis of variance (ANOVA) and tukey post-test compared to saline animals, *p<0.05, **p<0.01, ***p<0.001.

Similarly, the tissue concentrations of 5-HIAA were significantly decreased in all tested regions, and furthermore, 5-HIAA levels showed a greater extent of depletion by pCPA compared to 5-HT indicated by a significant main effect of pCPA treatment on 5-HT/5-HIAA ratios. That 5-HIAA levels display greater depletion by pCPA treatment as compared with 5-HT levels is consistent with previous studies in rats (Kornum et al., 2006), and this implies further that the pCPA treatment has additional effects on 5-HIAA levels other than the lowered concentration of 5-HT. Such a mechanism could be mediated through a down-regulation of MAO activity as dynamic compensatory change in the 5-HT system to restore 5-HT neurotransmission, however, a direct interaction between pCPA and MAO can also not be ruled out. Further

studies are needed to address the mechanism underlying the differential effects on 5-HIAA and 5-HT levels following pCPA treatment. Also, in paper I we find no effect of the pCPA treatment on tissue levels of dopamine or its metabolites indicating that the pCPA treatment caused selective depletion of serotonin in the pig brain. This is in line with pCPA, at least in the doses applied in Paper I, being a highly selective depletor of 5-HT (Koe and Weissman, 1966). Thus, the results from Paper I of the present thesis constitute a platform for future studies where effects of selective serotonin depletion can be examined in a large animal species. One specific application might be to use pCPA-treatment as a tool to investigate if serotonin depletion would increase binding of a serotonergic PET radioligand that is sensitive to endogenous competition by 5-HT in the pig brain, should such as PET tracer become available.

5-HT$_4$ receptor binding is increased in a porcine model of serotonin depletion

To investigate the effects of decreased 5-HT levels on the levels of 5-HT receptors in the pig brain following pCPA treatment, we performed in vitro receptor autoradiography using [^{3}H]WAY100635, [^{3}H]MDL100907, and [^{3}H]SB207145 to label 5-HT$_{1A}$, 5-HT$_{2A}$, and 5-HT$_4$ receptors, respectively. We also conducted SERT autoradiography using [^{3}H]escitalopram. 5-HT$_{2A}$ and 5-HT$_{1A}$ receptor binding as well as SERT binding in the pig brain were not affected by 5 days serotonin depletion. In contrast, 5-HT$_4$ receptor binding was significantly increased in the nucleus accumbens of pigs receiving pCPA compared to saline, and there was a general effect of pCPA treatment on 5-HT$_4$ receptor binding across all examined regions (figure 3). Furthermore, a significant correlation was found between 5-HT$_4$ receptor binding in the nucleus accumbens and 5-HT levels in the striatum.
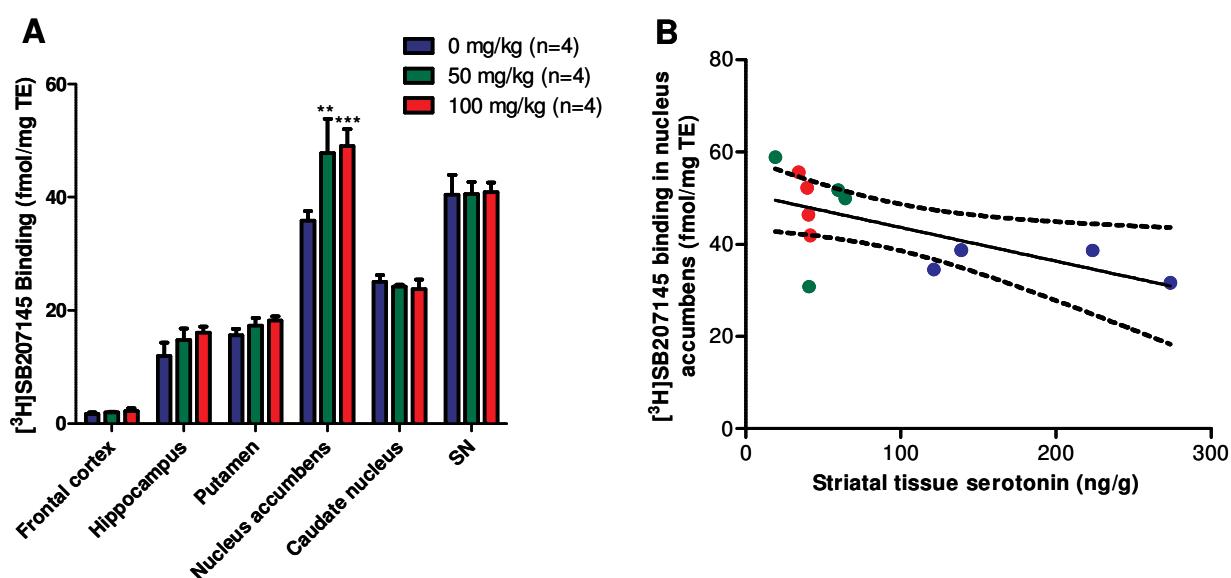
Figure 3. 5-HT$_4$ receptors binding measured with 1.2 nM [^{3}H]SB207145 in brain regions following pCPA treatment or saline. A: Differences among treatment groups are evaluated using a two-way ANOVA and Bonferroni post-tests for inter group comparisons in each brain region: **p<0.01 and ***p<0.001 compared to control. Error bars represent SEM. SN; substantia nigra. B: Correlation between specific 5-HT$_4$ receptor binding in the nucleus accumbens and 5-HT levels in the striatum of the contralateral hemisphere. Each point represents one animal: 0 mg/kg (blue), 50 mg/kg (green), and 100 mg/kg (red). Pearsons correlation coefficient is calculated at *p=0.014.

That 5-HT$_4$ receptors are effected by the levels of 5-HT, and that an inverse relationship exists between 5-HT levels and 5-HT$_4$ receptor levels, is in line with previous studies from NRU showing that chronic paroxetine treatment in rats decreased 5-HT$_4$ binding significantly, while serotonin depletion increased 5-HT$_4$ binding (Licht et al., 2009). Also, the inverse relationship between 5-HT levels and 5-HT$_4$ receptor levels has been shown in genetically modified mice that show over- and under-expression of SERT which impact extracellular 5-HT accordingly. SERT knock-out mice showed decreased 5-HT$_4$ receptor binding whilst SERT overexpressing mice showed increased 5-HT$_4$ receptor binding (Jennings et al., 2009).

In Paper I, we found no effect of five days pCPA treatment on 5-HT$_{2A}$ receptor binding in the pig brain. It was recently reported that acute tryptophan depletion in rats did not affect 5-HT$_{2A}$ receptor levels while three, but not one, weeks of chronic tryptophan depletion resulted in significantly increased 5-HT$_{2A}$ receptor binding (Cahir et al., 2007). Similarly, an increased 5-HT$_{2A}$ receptor binding was observed only 21 days after NDMA administration underlining the importance of the time-course of serotonin depletion for 5-HT$_{2A}$ receptor regulation (Reneman et al., 2002). These studies and Paper I suggest that short-term decreases in 5-HT levels do not regulate 5-HT$_{2A}$ receptors levels, however, in a more long-term state of decreased serotonergic neurotransmission, a compensatory up-regulation of 5-HT$_{2A}$ receptors may occur. These data taken together suggest that the 5-HT$_4$ receptor levels are more plastic than 5-HT$_{2A}$ and 5-HT$_{1A}$, and that the receptor is regulated in response to changes in the serotonergic transmission. Thus, this suggests that 5-HT$_4$ receptor binding may serve as an indirect measure of 5-HT levels, and further that these considerations should be taken into account when interpreting in vivo imaging studies investigating 5-HT$_4$ receptor binding in humans. In contrast, 5-HT$_{2A}$ receptor binding does not to the same extent seem to be affected by 5-HT levels suggesting that changes found in 5-HT$_{2A}$ receptor binding in human PET studies probably relate more to other changes in the brain function and anatomy than to fluctuations in extracellular 5-HT.

[^{11}C]Cimbi-5 is a novel 5-HT$_{2A}$ receptor agonist PET tracer

Currently, only selective 5-HT$_{2A}$ antagonistic PET radioligands are in use for mapping and quantifying 5-HT$_{2A}$ receptor binding in humans, e.g. [^{18}F]altanserin (Pinborg et al., 2003), [^{18}F]deuteroaltanserin (Soares et al., 2001), and [^{11}C]MDL100907 (Ito et al., 1998). However, 5-HT$_{2A}$ receptor agonist radioligands hold promise to selectively map 5-HT$_{2A}$ receptors in their G-protein coupled functional state. And therefore, agonist binding measured in vivo with PET may determine the number of high-affinity, membrane bound and active receptors as a more relevant measure for assessing dysfunction in the 5-HT$_{2A}$ receptor system in specific patient or population groups. To develop and validate a high-affinity 5-HT$_{2A}$ receptor agonist PET tracer, we identified a candidate compound in 2-(4-iodo-2,5-dimethoxyphenyl)-*N*-(2-methoxybenzyl)-ethanamine (25I-NBOMe, Cimbi-5) which was published as highly selective, highly potent and high-affinity 5-HT$_{2A}$ receptor agonist (Nichols et al., 2008). The N-benzyl substitution on the phenethylamine backbone,

as recognized from DOI, increase potency and affinity at the 5-HT$_{2A}$ receptor dramatically (Braden et al., 2006). To evaluate the potential of Cimbi-5 as a PET radioligand, we labelled this compound using an ^{11}C-methyltriflate methylation of the 2-hydroxybenzyl precursor which was BOC-protected at the secondary amine (figure 4).
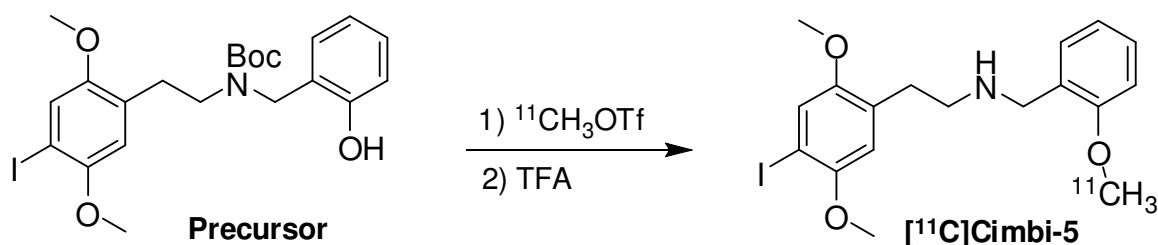
Figure 4. Radiochemical synthesis of 2-(4-iodo-2,5-dimethoxyphenyl)-N-(2-[^{11}C-OCH$_3$]methoxybenzyl)-ethanamine ([^{11}C]Cimbi-5). TFA, trifluoroacetic acid; Tf, triflate.

The properties of [^{11}C]Cimbi-5 as a PET tracer was then determined using HRRT scanning in Danish Landrace pigs. Following i.v. injection, [^{11}C]Cimbi-5 showed high cortical uptake in vivo in the pig brain, and low uptake in the cerebellum (figure 5). Thus, the [^{11}C]Cimbi-5 biodistributed in the pig brain was similar to the pattern expected from 5-HT$_{2A}$ receptor distribution as measured with 5-HT$_{2A}$ receptor antagonist PET tracers in humans (Adams et al., 2004;Ito et al., 1998) with high cortical uptake and low cerebellar uptake. Furthermore, the time-activity curves demonstrated a substantial separation between the cortical and cerebellar time-activity curves (figure 5) again indicating preferential cortical over cerebellar uptake. The time-activity curves peaked approximately 10 min post-injection and hereafter decreased implying that [^{11}C]Cimbi-5 binding is reversible over the 90 min scan time employed (Paper II).

To validate the specificity of the cortical [^{11}C]Cimbi-5 binding, we conducted in vivo blocking experiments after a bolus/infusion paradigm of ketanserin. The concentration of [^{11}C]Cimbi-5 in cortex was reduced almost to cerebellum levels following pre-treatment with ketanserin (figure 5). The cerebellar time-activity curve was practically unaltered by ketanserin administration (figure 5). This indicates that cortical [^{11}C]Cimbi-5 binding can be attributed to binding to 5-HT$_{2A}$ receptors in the pig brain. In humans, previous results indicate that specific [^{18}F]altanserin binding to 5-HT$_{2A}$ receptors is completely displaced by ketanserin as observed by cortical uptake declining completely to cerebellar levels following ketanserin administration (Pinborg et al., 2003).
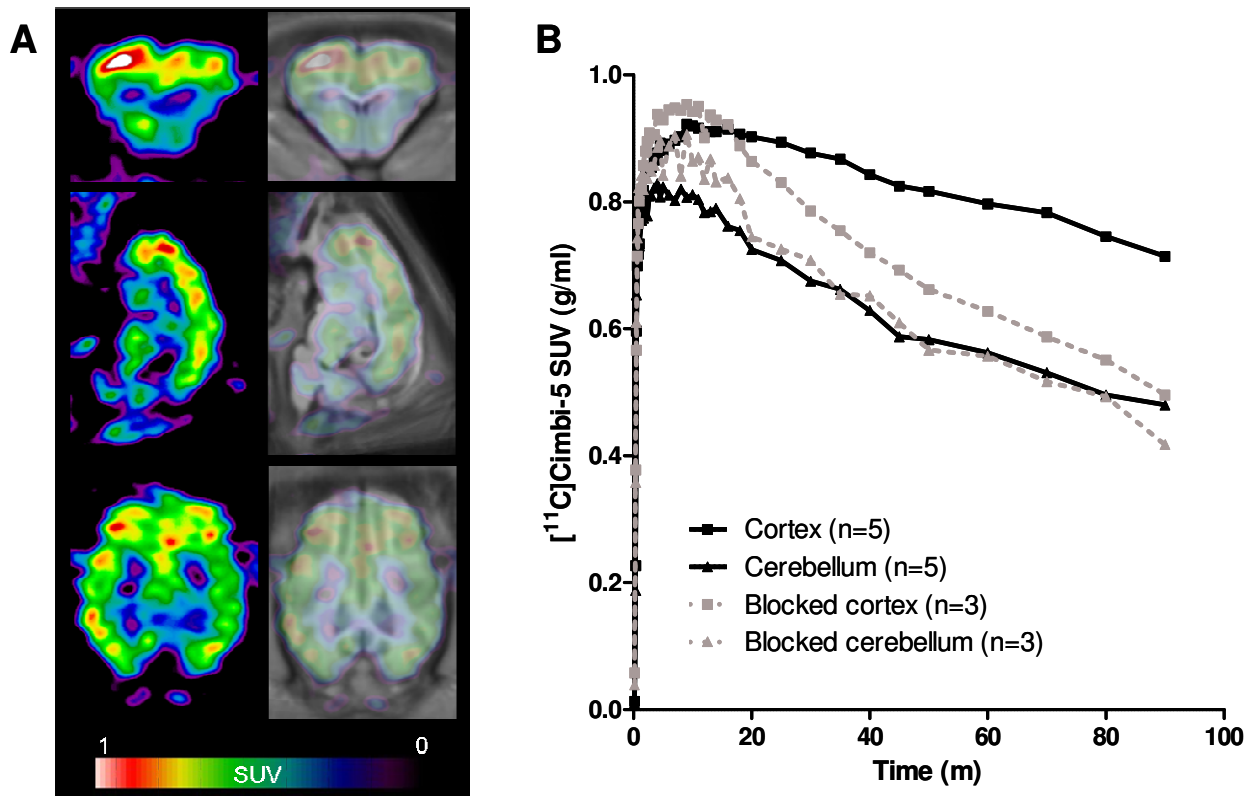
Figure 5. Colour coded representative coronal (top), sagittal (middle), and horizontal (bottom) standardized uptake value (SUV) PET images summed from 0-90 min scanning showing distribution of $[^{11}C]$Cimbi-5 in the pig brain. Left column show filtered PET, while right column show the same PET images aligned and overlaid on the standard pig brain after co-registration and transformation. B: Regional time-activity curves of $[^{11}C]$Cimbi-5 in the pig brain at baseline (black, solid line) or following i.v. ketanserin (3 mg/kg bolus, 1 mg/kg/h infusion) blockade (gray, dotted line). Number of pigs is indicated by the legends.

The target-to-background binding ratio of $[^{11}C]$Cimbi-5 was in Paper II evaluated as the cortical SRTM BP_{ND} with cerebellum as reference region. This is based on the specific 5-HT$_{2A}$ receptor binding in cerebellum being negligible, and most PET studies of 5-HT$_{2A}$ receptor binding apply this reference region for quantification (Meyer et al., 2010;Pinborg et al., 2003). The cortical SRTM BP_{ND} for $[^{11}C]$Cimbi-5 was 0.46 $\pm$ 0.11 (n=5) in Danish Landrace pig brain. This binding potential is lower than what is normally found with $[^{18}F]$altanserin in humans (Adams et al., 2004). However, in Paper II we compared the cortical SRTM BP_{ND} of $[^{11}C]$Cimbi-5 to that of $[^{18}F]$altanserin in the pig brain. Although, the $[^{18}F]$altanserin PET was done in a different type of PET scanner, in the different breed of pigs at a different age, the cortical SRTM BP_{ND} of $[^{18}F]$altanserin was strikingly similar (0.47 $\pm$ 0.10 (n=5)) to that of $[^{11}C]$Cimbi-5 (0.46 $\pm$ 0.11 (n=5)). Given that $[^{18}F]$altanserin is widely used in clinical settings as a 5-HT$_{2A}$ PET radioligand, and that $[^{18}F]$altanserin and $[^{11}C]$Cimbi-5 show similar target-to-background ratios in the pig brain, this underlines the potential of $[^{11}C]$Cimbi-5 for human PET scanning. Furthermore, in vitro test confirmed that Cimbi-5 was a high-affinity, highly potent agonist at 5-HT$_{2A}$ receptors (Paper II). Thus, $[^{11}C]$Cimbi-5 is the first promising PET

tracer described for labelling and quantification of high-affinity 5-HT_{2A} receptors in the human brain. Previous data with ^{123}I-labelled DOI for SPECT found that target-to-background binding ratios with this tracer was insufficient for further studies, and this tracer was also insensitive to ketanserin displacement (Zea-Ponce et al., 2002). Similarly, ^{11}C-labelled LSD used for PET scanning showed lower target-to-background binding ratios in monkeys (Wong et al., 1987) as compared to [^{11}C]Cimbi-5 in the pig brain. In conclusion, [^{11}C]Cimbi-5 is the first 5-HT_{2A} receptor agonist radioligand to show promising results in animals studies underscoring its potential as a PET tracer for in vivo quantification of high-affinity 5-HT_{2A} receptors. However, since effect sizes of the changes that potentially should be measured by a 5-HT_{2A} receptor agonist PET radioligand are not thought to be large, the target-to-background binding ratio with such a radioligand could prove crucial. For example, the effect of the SSRI-mediated 5-HT increase on PET radioligand binding is expected to be modest. Therefore, efforts should be made to identify the optimal PET tracer candidate before progressing with further studies, ultimately in humans.

[^{11}C]Cimbi-36 displays improved PET tracer properties over [^{11}C]Cimbi-5

To improve target-to-background binding ratios of the PET tracers, we tested a total of nine PET tracers, all analogues of [^{11}C]Cimbi-5. For 5-HT_{2A} receptor radioligands, the signal-to-noise ratio can be evaluated as the preferential binding of the radioligand in a 5-HT_{2A} receptor rich cortical region to the binding in cerebellum which essentially is devoid of 5-HT_{2A} receptors. Reliable quantification of this cortical 5-HT_{2A} receptor binding with antagonist PET radioligands was found using the reference tissue models (Meyer et al., 2010;Pinborg et al., 2003). Thus, the cortical SRTM BP_{ND} is regarded as a valid measure for the preferential binding in cortex relative to cerebellum, and in Paper II and III we used this as primary outcome for evaluating the target-to-background ratios of the tested 5-HT_{2A} receptor agonist PET radioligands.

In Paper III, we seeked to optimize the PET radioligand properties of [^{11}C]Cimbi-5, so we changed the labelling site and modified the chemical structure of the compound. Using an in vivo screening approach, we radiolabelled a total of nine new PET tracers, all showing close resemblance to [^{11}C]Cimbi-5, and evaluated their properties in the pig brain using the same PET protocol as for [^{11}C]Cimbi-5. Of these tested PET tracers, eight were different compounds as compared to [^{11}C]Cimbi-5, whereas [^{11}C]Cimbi-5-2 was structurally identical but ^{11}C-labelled at a different position (see figure 6 for structures). One HRRT PET scan was done for each tracer to identify compounds of particular promise and compounds that could be discarded in future studies. Of the novel PET tracers tested (figure 6), most showed somewhat similar properties as compared to [^{11}C]Cimbi-5 (figure 5) with regards to brain uptake and cortical SRTM BP_{ND}. However, the tracers [^{11}C]Cimbi-21 and [^{11}C]Cimbi-88 showed poor separation between cortex and cerebellum time-activity curves and lower cortical SRTM BP_{ND} compared to [^{11}C]Cimbi-5 (figure 5). These PET tracers were discarded for further studies due to low target-to-background binding ratios in the pig brain.
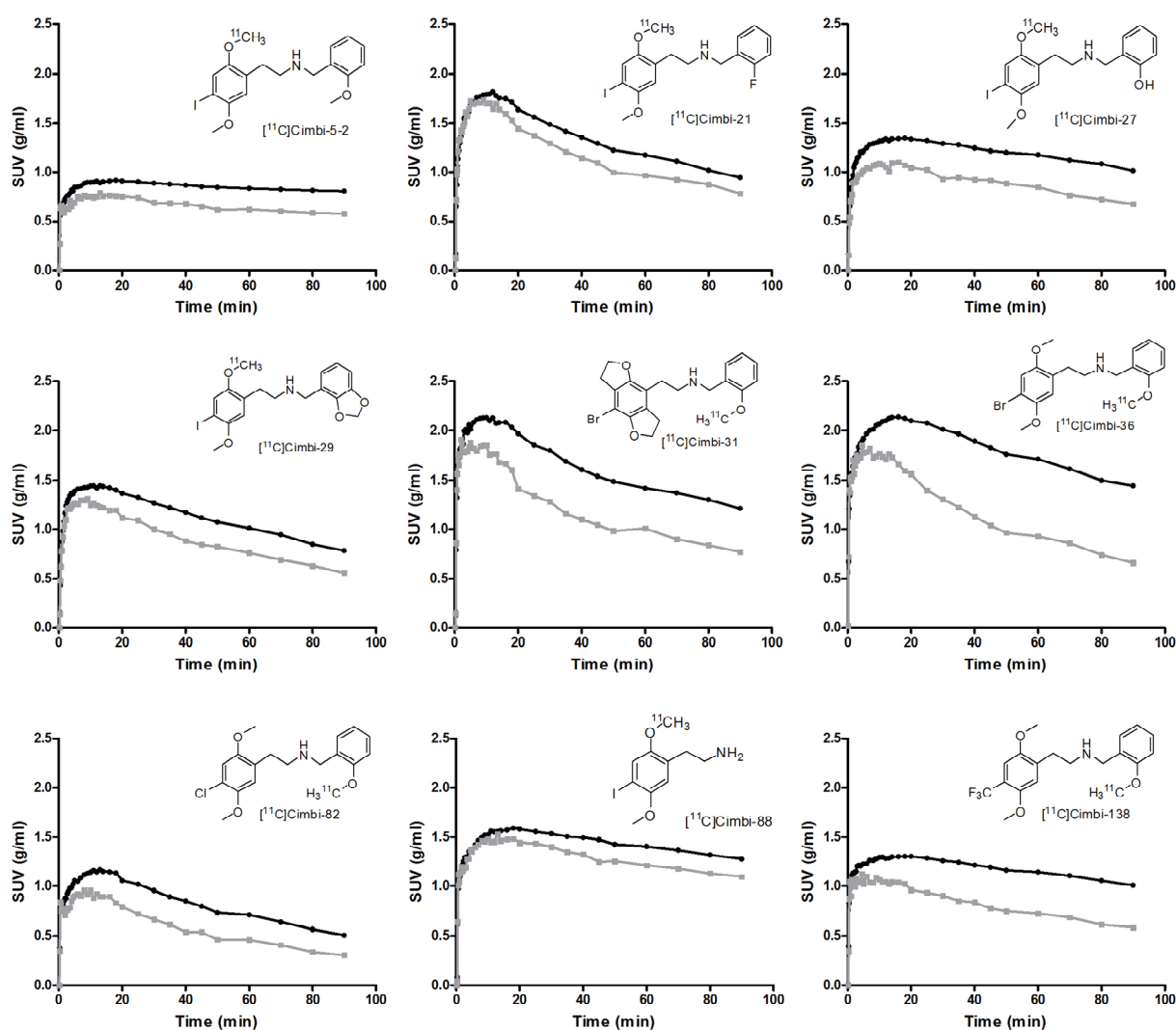
Figure 6. Regional time-activity curves of ^{11}C-labelled phenethylamines in the pig brain. Chemical structure and ^{11}C-label of the PET tracers are inserted by the corresponding time-activity curve. Circles connected by black line indicate radioactive concentration in cortex while squares connected by gray line indicate radioactive concentration in cerebellum. Standardized uptake values (SUV) in one pig brain are shown for each tracer.

[^{11}C]Cimbi-5-2 possessed the same chemical structure as [^{11}C]Cimbi-5 but was labelled in the phenethylamine-moiety (in the 2-position) rather than in the *N*-benzyl substituent. Previous studies with [^{11}C]WAY100635 have shown dramatically improved PET tracer properties by moving the ^{11}C-label from one part of the molecule to another due to the elimination of a lipophilic metabolite crossing the BBB (Pike, 2009). However, neither brain uptake nor cortical SRTM BP_{ND} was improved with [^{11}C]Cimbi-5-2 as compared to [^{11}C]Cimbi-5. Also, a lipophilic metabolite was observed in pig plasma both after [^{11}C]Cimbi-5-2 and [^{11}C]Cimbi-5 injections. These results suggest that metabolism of the radioligand was not grossly affected by changing the labelling site, and furthermore that this did not impact PET tracer properties. [^{11}C]Cimbi-27, [^{11}C]Cimbi-29, [^{11}C]Cimbi-31, and [^{11}C]Cimbi-82 all differed structurally from [^{11}C]Cimbi-

5, though, they were all *N*-benzyl substituted phenethylamines. These PET tracers showed roughly similar brain uptake and cortical SRTM BP_{ND} as the previously labelled candidate PET tracer. Given the close structural resemblance of these compounds to the previous candidate, it is perhaps not so surprising that the majority of the tested PET tracers showed similar properties in vivo in the pig brain.

Contrasting the other tracers, [^{11}C]Cimbi-36 and [^{11}C]Cimbi-138 showed better separation between cortex and cerebellum time-activity curves and higher cortical SRTM BP_{ND}, this also compared to the previous PET tracer candidate [^{11}C]Cimbi-5. Structurally, [^{11}C]Cimbi-5, [^{11}C]Cimbi-36, [^{11}C]Cimbi-82, and [^{11}C]Cimbi-138 only differ by the 4-substituent of the phenethylamine-moiety, this being iodine, bromine, chloride, and trifluoromethyl, respectively. In Paper III, we also conducted in vitro binding assays to determine to 5-HT_{2A} receptor affinity of the tested compounds and PI hydrolysis assays to determine in vitro potency of the tracer compound for 5-HT_{2A} receptor activation. With regards to their in vitro binding and activation properties, Cimbi-5, Cimbi-36, Cimbi-82, and Cimbi-138 showed similar properties, however [^{11}C]Cimbi-36 and [^{11}C]Cimbi-138 clearly possessed higher target-to-background ratios over [^{11}C]Cimbi-5 and [^{11}C]Cimbi-82 (Paper II and III). Cortical SRTM BP_{ND} was slightly higher, and brain uptake measured as SUV was also higher for [^{11}C]Cimbi-36 compared to [^{11}C]Cimbi-138. Thus, based on this in vivo screening [^{11}C]Cimbi-36 was the most promising candidate, and changing the 4-substituent from iodine to bromine did improve the PET tracer properties. A concurrent improvement obtained is implied by the regional time-activity curves for [^{11}C]Cimbi-36. These declined more clearly over the 90 min scanning time (figure 6) as compared to [^{11}C]Cimbi-5 (figure 5). Thus, [^{11}C]Cimbi-36 binding to the 5-HT_{2A} receptor is reversible and seemed more reversible as compared to the other tested tracers, e.g. [^{11}C]Cimbi-5-2, [^{11}C]Cimbi-27, and [^{11}C]Cimbi-138 (figure 6). Since reversible binding kinetics generally is a requisite for quantification (Innis et al., 2007), the faster kinetics of [^{11}C]Cimbi-36 in the pig brain may prove important in future studies since slower kinetics usually is found in humans.

To further characterize our primary 5-HT_{2A} receptor agonist PET radioligand, [^{11}C]Cimbi-36, we investigated its in vivo selectivity in a blocking study. We administered ketanserin i.v. to a pig after a [^{11}C]Cimbi-36 baseline scan and rescanned it after 30 min using the same PET protocol (figure 7). In the baseline and the blocked scan, the cortical SRTM BP_{ND} were 0.70 and 0.26, respectively, indicating that [^{11}C]Cimbi-36 binding in the pig cortex is displaceable by ketanserin and thus selective for 5-HT_{2A} receptors. These results further underline the potential of [^{11}C]Cimbi-36 for imaging 5-HT_{2A} receptor agonist binding sites in further studies.
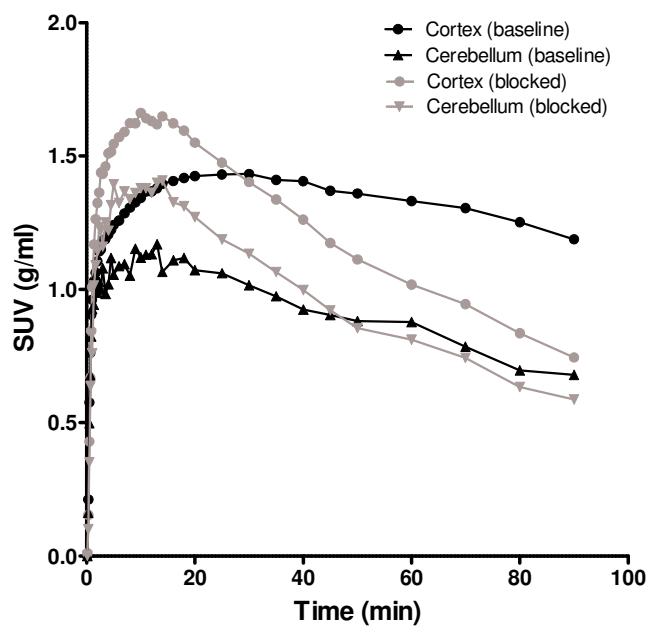
Figure 7. Cortical and cerebellar time-activity curves of [^{11}C]Cimbi-36 in pig brain at baseline (black line) and following pre-treatment i.v. with 10 mg/mg ketanserin (gray line). Squares and triangles indicate cortex and cerebellum, respectively. Standardized uptake values (SUV) normalized to injected dose per body weight is shown.

Conclusions and perspectives

The present PhD thesis concerns the validation of a porcine model of serotonin and the use of PET scanning in pigs to evaluate novel 5-HT$_{2A}$ receptor agonist radioligands. The pig is an increasingly applied experimental animal in neuroscience research; however, neurochemical studies and neuropharmacological manipulations in pig brain have only been sparsely reported. In Paper I, we show that 50 and 100 mg/kg pCPA effectively decrease tissue levels of 5-HT and 5-HIAA in the pig brain following four consecutive daily i.m. injections. This is the first pharmacological approach validated to cause serotonin depletion in the pig brain. Additionally, in paper I, we used this model of serotonin depletion to investigate the effects of decreased 5-HT levels on 5-HT receptor levels finding that 5-HT$_4$ receptors were more heavily affected by decreased 5-HT levels as compared to 5-HT$_{1A}$ and 5-HT$_{2A}$ receptors and SERT. The validation of a model of serotonin depletion in a large animal species like the pig can possibly aid future investigations of decreased serotonergic neurotransmission. In relation hereto, the pig is relevant for in vivo imaging studies due to its relatively large brain, and the pharmacological tool of pCPA treatment to decrease 5-HT levels may be useful to investigate effects of serotonin in the living brain. As an animal model of serotonergic dysfunction in humans, however, this porcine model of serotonin depletion only induces sub-chronic serotonin depletion; in comparison, the hypofunctional serotonin system in humans presumably develops over longer time. Therefore, it would be of interest to extend the time-course of serotonin depletion in the pig. Finally, studies of changes in 5-HT receptor densities following decreased serotonergic neurotransmission are also of significant translational value to many clinical imaging studies done at NRU and other places. Clinical PET studies often evaluate ligand binding as a measure of 5-HT receptor levels, and differences among groups of subjects are often reported as a trait of disease. However, present and other results indicate that 5-HT receptors, especially the 5-HT$_4$, are regulated in response to changes in levels of 5-HT which might have an impact on the 5-HT receptor binding measured in clinical imaging studies. Thus, the effects of differences in serotonergic tone between groups investigated should, at least in studies with 5-HT$_4$ radioligands, be taken into account when interpreting results. Moreover, 5-HT$_4$ receptor binding in humans could be speculated to be a marker of the state of the serotonergic system in the way that decreased tone could cause compensatory upregulation of 5-HT$_4$ receptor. Future studies will reveal whether 5-HT$_4$ receptor binding with PET could be a marker for human disease, and whether this marker is related to serotonergic function.

In paper II and III, we labelled and evaluated novel 5-HT$_{2A}$ receptor agonist PET tracers. These compounds are the first agonists to successfully label 5-HT$_{2A}$ receptors in vivo. In paper II, we show that [^{11}C]Cimbi-5 selectively labels 5-HT$_{2A}$ receptors with adequate signal-to-noise ratios in the pig, however in paper III, we report that [^{11}C]Cimbi-36 show even better properties with respect to both brain uptake and target-to-background binding ratios. We took the approach to optimize PET tracer properties to find the best candidate before moving forward with further studies of biological interest. The data in paper III illustrate the improved PET tracer properties of [^{11}C]Cimbi-36 over [^{11}C]Cimbi-5 and demonstrate the value of

optimizing novel PET tracers before moving forward with more extensive studies. To our knowledge, Paper III is the first of its kind to systematically and this extensively screen modified compounds by in vivo scanning to optimize PET tracer properties. Thus, [^{11}C]Cimbi-36 is currently our top candidate for a 5-HT$_{2A}$ receptor agonist PET tracer for human use. Future human use requires regulatory approval to use Cimbi-36 in microdosing range as an investigational new drug, and toxicological testing is necessary to ensure its safety. Thus, an additional argument for thoroughly identifying the most promising candidate PET tracer before progressing is provided, since these laborious and expensive efforts to obtain regulatory approval and in turn validating the PET tracer in humans should not be undertaken with a sub-optimal PET tracer.

[^{11}C]Cimbi-36 is hypothesized to selectively bind to a subpopulation of 5-HT$_{2A}$ receptors that are in the high-affinity state. It is relatively well-documented that different affinity states of 5-HT$_{2A}$ receptors exist in vitro, however, a 5-HT$_{2A}$ receptor agonist PET tracer is a necessary tool to demonstrate the existence of multiple affinity states in vivo. An elegant experimental approach to investigate this would be to compare [^{11}C]Cimbi-36 binding to that of an antagonist PET tracer such as [^{11}C]MDL100907 applying various specific radioactivities with both tracers to determine B$_{max}$ for each of the tracers. If the agonist PET tracer displays a lower number of binding sites compared to the antagonist PET tracer then multiple affinity states of 5-HT$_{2A}$ receptor exist in vivo, and the ratio of high- and low-affinity states is here determined by the ratio of B$_{max}$ of the tracers.

Another prominent perspective of the presented studies is to combine the methods developed in the present thesis. Thus, since pCPA treatment decreases tissue levels of 5-HT in the pig brain, and [^{11}C]Cimbi-36 is a promising PET tracer with the potential to measure changes in 5-HT in the living brain. However, the immediate question that at this point remains to be answered is whether [^{11}C]Cimbi-36 is sensitive to endogenously released 5-HT. To test this, a baseline scanning with [^{11}C]Cimbi-36 should be compared to a second challenge scan conducted on the same day. The appropriate challenge applied in this study would be a 5-HT releasing agent, e.g. fenfluramine, alternatively an SSRI could also be used to acutely elevate extracellular 5-HT levels. If [^{11}C]Cimbi-36 indeed is sensitive to endogenously released 5-HT, a natural next step would be to test [^{11}C]Cimbi-36 binding before and after serotonin depletion. The short half-life of ^{11}C in [^{11}C]Cimbi-36 enable these challenge studies to be conducted with short inter-scan intervals since carry-over residual activity can be disregarded. However, the methodologically ideal study to test sensitivity of a PET tracer would be with constant tracer levels in plasma as achievable with a bolus/infusion paradigm. Such a bolus/infusion paradigm for [^{11}C]Cimbi-36 would in this case also need to be validated.

If [^{11}C]Cimbi-36 should prove sensitive to fluctuations in endogenous 5-HT and the tracers safely could be used in humans, this would enable pivotal studies to improve the understanding of the serotonergic system in human disease. The hypothesis that hypofunction of the serotonergic system is implicated in the pathophysiology of depression could be investigated by comparing [^{11}C]Cimbi-36 binding in depressive patients to binding in healthy controls. Also, it would be of pharmaceutical interest to measure

the SSRI-mediated 5-HT release using a PET probe. The differential response to chronic SSRI treatment in depressive patients could possibly be related to the efficiency with which SSRI release 5-HT, and such a method to quantitatively address serotonin release of pharmacological challenges could potentially provide insights treatment resistance in depression.

References

Adams KH, Pinborg LH, Svarer C, Hasselbalch SG, Holm S, Haugbol S, Madsen K, Frokjaer V, Martiny L, Paulson OB, Knudsen GM (2004) A database of [(18)F]-altanserin binding to 5-HT(2A) receptors in normal volunteers: normative data and relationship to physiological and demographic variables. Neuroimage 21:1105-1113.

Alfieri AB, Cubeddu LX (1995) Treatment with para-chlorophenylalanine antagonises the emetic response and the serotonin-releasing actions of cisplatin in cancer patients. Br J Cancer 71:629-32.

Amemiya Y, Miyahara J (1988) Imaging plate illuminates many fields. Nature 336:89-90.

Barnes NM, Sharp T (1999) A review of central 5-HT receptors and their function. Neuropharmacology 38:1083-152.

Baumgarten HG, Björklund A (1976) Neurotoxic indoleamines and monoamine neurons. Annu Rev Pharmacol Toxicol 16:101-11.

Blin J, Baron JC, Dubois B, Crouzel C, Fiorelli M, ttar-Levy D, Pillon B, Fournier D, Vidailhet M, Agid Y (1993) Loss of brain 5-HT2 receptors in Alzheimer's disease. In vivo assessment with positron emission tomography and [18F]setoperone. Brain 116 (Pt 3):497-510.

Blokland A, Lieben C, Deutz NE (2002) Anxiogenic and depressive-like effects, but no cognitive deficits, after repeated moderate tryptophan depletion in the rat. J Psychopharmacol 16:39-49.

Bockaert J, Claeysen S, Becamel C, Dumuis A, Marin P (2006) Neuronal 5-HT metabotropic receptors: fine-tuning of their structure, signaling, and roles in synaptic modulation. Cell Tissue Res 326:553-72.

Booij L, Van der Does W, Benkelfat C, Bremner JD, Cowen PJ, Fava M, Gillin C, Leyton M, Moore P, Smith KA, Van der Kloot WA (2002) Predictors of mood response to acute tryptophan depletion. A reanalysis. Neuropsychopharmacology 27:852-61.

Braden MR, Parrish JC, Naylor JC, Nichols DE (2006) Molecular interaction of serotonin 5-HT2A receptor residues Phe339(6.51) and Phe340(6.52) with superpotent N-benzyl phenethylamine agonists. Mol Pharmacol 70:1956-1964.

Breier A, Su TP, Saunders R, Carson RE, Kolachana BS, de BA, Weinberger DR, Weisenfeld N, Malhotra AK, Eckelman WC, Pickar D (1997) Schizophrenia is associated with elevated amphetamine-induced synaptic dopamine concentrations: evidence from a novel positron emission tomography method. Proc Natl Acad Sci U S A 94:2569-2574.

Brust P, Zessin J, Kuwabara H, Pawelke B, Kretzschmar M, Hinz R, Bergman J, Eskola O, Solin O, Steinbach J, Johannsen B (2003) Positron emission tomography imaging of the serotonin transporter in the pig brain using [11C]()-McN5652 and S-([18F]fluoromethyl)-()-McN5652. Synapse 47:143-51.

Bustad LK, McClellan RO (1966) Swine in Biomedical Research. Science 152:1526-1530.

Cahir M, Ardis T, Reynolds GP, Cooper SJ (2007) Acute and chronic tryptophan depletion differentially regulate central 5-HT1A and 5-HT 2A receptor binding in the rat. Psychopharmacology (Berl) 190:497-506.

Chazal G, Ralston HJ (1987) Serotonin-containing structures in the nucleus raphe dorsalis of the cat: an ultrastructural analysis of dendrites, presynaptic dendrites, and axon terminals. J Comp Neurol 259:317-29.

Cornea-Hebert V, Watkins KC, Roth BL, Kroeze WK, Gaudreau P, Leclerc N, Descarries L (2002) Similar ultrastructural distribution of the 5-HT(2A) serotonin receptor and microtubule-associated protein MAP1A in cortical dendrites of adult rat. Neuroscience 113:23-35.

Cumming P, Gillings NM, Jensen SB, Bjarkam C, Gjedde A (2003) Kinetics of the uptake and distribution of the dopamine D(2,3) agonist (R)-N-[1-(11C]n-propylnorapomorphine in brain of healthy and MPTP-treated Gottingen miniature pigs. Nucl Med Biol 30:547-53.

Cumming P, Moller M, Benda K, Minuzzi L, Jakobsen S, Jensen SB, Pakkenberg B, Stark AK, Gramsbergen JB, Andreasen MF, Olsen AK (2007) A PET study of effects of chronic 3,4-methylenedioxymethamphetamine (MDMA, "ecstasy") on serotonin markers in Gottingen minipig brain. Synapse 61:478-87.

Cumming P, Wong DF, Dannals RF, Gillings N, Hilton J, Scheffel U, Gjedde A (2002a) The competition between endogenous dopamine and radioligands for specific binding to dopamine receptors. Ann N Y Acad Sci 965:440-450.

Cumming P, Wong DF, Gillings N, Hilton J, Scheffel U, Gjedde A (2002b) Specific binding of [(11)C]raclopride and N-[(3)H]propyl-norapomorphine to dopamine receptors in living mouse striatum: occupancy by endogenous dopamine and guanosine triphosphate-free G protein. J Cereb Blood Flow Metab 22:596-604.

De-Miguel FF, Trueta C (2005) Synaptic and extrasynaptic secretion of serotonin. Cell Mol Neurobiol 25:297-312.

Delgado PL, Charney DS, Price LH, Aghajanian GK, Landis H, Heninger GR (1990) Serotonin function and the mechanism of antidepressant action. Reversal of antidepressant-induced remission by rapid depletion of plasma tryptophan. Arch Gen Psychiatry 47:411-8.

Egan C, Grinde E, Dupre A, Roth BL, Hake M, Teitler M, Herrick-Davis K (2000) Agonist high and low affinity state ratios predict drug intrinsic activity and a revised ternary complex mechanism at serotonin 5-HT(2A) and 5-HT(2C) receptors. Synapse 35:144-150.

Felix B, Leger ME, Albe-Fessard D, Marcilloux JC, Rampin O, Laplace JP (1999) Stereotaxic atlas of the pig brain. Brain Res Bull 49:1-137.

Finnema SJ, Varrone A, Hwang TJ, Gulyas B, Pierson ME, Halldin C, Farde L (2010) Fenfluramine-induced serotonin release decreases [11C]AZ10419369 binding to 5-HT1B-receptors in the primate brain. Synapse 64:573-577.

Fitzgerald LW, Conklin DS, Krause CM, Marshall AP, Patterson JP, Tran DP, Iyer G, Kostich WA, Largent BL, Hartig PR (1999) High-affinity agonist binding correlates with efficacy (intrinsic activity) at the human serotonin 5-HT2A and 5-HT2C receptors: evidence favoring the ternary complex and two-state models of agonist action. J Neurochem 72:2127-2134.

Geary WA, Toga AW, Wooten GF (1985) Quantitative film autoradiography for tritium: methodological considerations. Brain Res 337:99-108.

Gee AD (2003) Neuropharmacology and drug development. Br Med Bull 65:169-177.

Ginovart N (2005) Imaging the dopamine system with in vivo [11C]raclopride displacement studies: understanding the true mechanism. Mol Imaging Biol 7:45-52.

Gonzalez-Maeso J, Sealfon SC (2009) Psychedelics and schizophrenia. Trends Neurosci 32:225-232.

Gonzalez-Maeso J, Weisstaub NV, Zhou M, Chan P, Ivic L, Ang R, Lira A, Bradley-Moore M, Ge Y, Zhou Q, Sealfon SC, Gingrich JA (2007) Hallucinogens recruit specific cortical 5-HT(2A) receptor-mediated signaling pathways to affect behavior. Neuron 53:439-52.

Gradwell PB, Everitt BJ, Herbert J (1975) 5-hydroxytryptamine in the central nervous system and sexual receptivity of female rhesus monkeys. Brain Res 88:281-93.

Griebel G (1995) 5-Hydroxytryptamine-interacting drugs in animal models of anxiety disorders: more than 30 years of research. Pharmacol Ther 65:319-95.

Gu Q (2002) Neuromodulatory transmitter systems in the cortex and their role in cortical plasticity. Neuroscience 111:815-35.

Guo Q, Brady M, Gunn RN (2009) A biomathematical modeling approach to central nervous system radioligand discovery and development. J Nucl Med 50:1715-1723.

Hasselbalch SG, Madsen K, Svarer C, Pinborg LH, Holm S, Paulson OB, Waldemar G, Knudsen GM (2008) Reduced 5-HT2A receptor binding in patients with mild cognitive impairment. Neurobiol Aging 29:1830-1838.

Hensler JG (2006) Serotonergic modulation of the limbic system. Neurosci Biobehav Rev 30:203-14.

Holm P, Ettrup A, Klein AB, Santini MA, El-Sayed M, Elvang AB, Stensbol TB, Mikkelsen JD, Knudsen GM, Aznar S (2010) Plaque Deposition Dependent Decrease in 5-HT2A Serotonin Receptor in AßPPswe/PS1dE9 Amyloid Overexpressing Mice. J Alzheimers Dis.

Innis RB, et al. (2007) Consensus nomenclature for in vivo imaging of reversibly binding radioligands. J Cereb Blood Flow Metab 27:1533-1539.

Ito H, Nyberg S, Halldin C, Lundkvist C, Farde L (1998) PET imaging of central 5-HT2A receptors with carbon-11-MDL 100,907. J Nucl Med 39:208-214.

Jans LA, Riedel WJ, Markus CR, Blokland A (2007) Serotonergic vulnerability and depression: assumptions, experimental evidence and implications. Mol Psychiatry 12:522-43.

Jennings KA, Licht CL, Bruce A, Lesch KP, Knudsen G.M., Sharp T (2009) Genetic variation in SERT expression changes brain 5-HT4 receptor levels. Society for Neuroscience343.15.

Koe BK, Weissman A (1966) p-Chlorophenylalanine: a specific depletor of brain serotonin. J Pharmacol Exp Ther 154:499-516.

Koepp MJ, Gunn RN, Lawrence AD, Cunningham VJ, Dagher A, Jones T, Brooks DJ, Bench CJ, Grasby PM (1998) Evidence for striatal dopamine release during a video game. Nature 393:266-268.

Köhn F, Sharifi AR, Taubert H, Malovrh S, Simianer H (2008) Breeding for low body weight in Goettingen minipigs. J Anim Breed Genet 125:20-8.

Kornum BR, Knudsen GM (2010) Cognitive testing of pigs (Sus scrofa) in translational biobehavioral research. Neurosci Biobehav Rev.

Kornum BR, Licht CL, Weikop P, Knudsen GM, Aznar S (2006) Central serotonin depletion affects rat brain areas differently: a qualitative and quantitative comparison between different treatment schemes. Neurosci Lett 392:129-134.

Kornum BR, Lind NM, Gillings N, Marner L, Andersen F, Knudsen GM (2009) Evaluation of the novel 5-HT4 receptor PET ligand [11C]SB207145 in the Gottingen minipig. J Cereb Blood Flow Metab 29:186-196.

Kornum BR, Stott SR, Mattsson B, Wisman L, Ettrup A, Hermening S, Knudsen GM, Kirik D (2010) Adeno-associated viral vector serotypes 1 and 5 targeted to the neonatal rat and pig striatum induce widespread transgene expression in the forebrain. Exp Neurol 222:70-85.

Kornum BR, Thygesen KS, Nielsen TR, Knudsen GM, Lind NM (2007) The effect of the inter-phase delay interval in the spontaneous object recognition test for pigs. Behav Brain Res 181:210-7.

Kuhar MJ, De Souza EB, Unnerstall JR (1986) Neurotransmitter receptor mapping by autoradiography and other methods. Annu Rev Neurosci 9:27-59.

Lammertsma AA, Hume SP (1996) Simplified reference tissue model for PET receptor studies. Neuroimage 4:153-158.

Lanctot KL, Herrmann N, Mazzotta P (2001) Role of serotonin in the behavioral and psychological symptoms of dementia. J Neuropsychiatry Clin Neurosci 13:5-21.

Laruelle M (2000) Imaging synaptic neurotransmission with in vivo binding competition techniques: a critical review. J Cereb Blood Flow Metab 20:423-451.

Laruelle M, Huang Y (2001) Vulnerability of positron emission tomography radiotracers to endogenous competition. New insights. Q J Nucl Med 45:124-138.

Lemoine L, Verdurand M, Vacher B, Blanc E, Le BD, Newman-Tancredi A, Zimmer L (2010) [18F]F15599, a novel 5-HT1A receptor agonist, as a radioligand for PET neuroimaging. Eur J Nucl Med Mol Imaging 37:594-605.

Leysen JE (2004) 5-HT2 receptors. Curr Drug Targets CNS Neurol Disord 3:11-26.

Liberatore GT, Wong JY, Krenus D, Jeffreys BJ, Porritt MJ, Howells DW (1999) Tissue fixation prevents contamination of tritium-sensitive storage phosphor imaging plates. Biotechniques 26:432-4.

Licht CL, Knudsen GM, Sharp T (2010) Effects of the 5-HT(4) receptor agonist RS67333 and paroxetine on hippocampal extracellular 5-HT levels. Neurosci Lett 476:58-61.

Licht CL, Marcussen AB, Wegener G, Overstreet DH, Aznar S, Knudsen GM (2009) The brain 5-HT4 receptor binding is down-regulated in the Flinders Sensitive Line depression model and in response to paroxetine administration. J Neurochem 109:1363-1374.

Lieben CK, Blokland A, Westerink B, Deutz NE (2004) Acute tryptophan and serotonin depletion using an optimized tryptophan-free protein-carbohydrate mixture in the adult rat. Neurochem Int 44:9-16.

Lieben CK, Steinbusch HW, Blokland A (2006) 5,7-DHT lesion of the dorsal raphe nuclei impairs object recognition but not affective behavior and corticosterone response to stressor in the rat. Behav Brain Res 168:197-207.

Lind NM, Moustgaard A, Jelsing J, Vajta G, Cumming P, Hansen AK (2007) The use of pigs in neuroscience: modeling brain disorders. Neurosci Biobehav Rev 31:728-51.

Liu Y, Yoo MJ, Savonenko A, Stirling W, Price DL, Borchelt DR, Mamounas L, Lyons WE, Blue ME, Lee MK (2008) Amyloid pathology is associated with progressive monoaminergic neurodegeneration in a transgenic mouse model of Alzheimer's disease. J Neurosci 28:13805-13814.

Lopez-Gimenez JF, Villazon M, Brea J, Loza MI, Palacios JM, Mengod G, Vilaro MT (2001) Multiple conformations of native and recombinant human 5-hydroxytryptamine(2a) receptors are labeled by agonists and discriminated by antagonists. Mol Pharmacol 60:690-699.

Magalhaes AC, Holmes KD, Dale LB, Comps-Agrar L, Lee D, Yadav PN, Drysdale L, Poulter MO, Roth BL, Pin JP, Anisman H, Ferguson SS (2010) CRF receptor 1 regulates anxiety behavior via sensitization of 5-HT2 receptor signaling. Nat Neurosci 13:622-629.

Mann JJ (1999) Role of the serotonergic system in the pathogenesis of major depression and suicidal behavior. Neuropsychopharmacology 21:99S-105S.

Marner L, Frokjaer VG, Kalbitzer J, Lehel S, Madsen K, Baare WF, Knudsen GM, Hasselbalch SG (2010a) Loss of serotonin 2A receptors exceeds loss of serotonergic projections in early Alzheimer's disease: a combined [(11)C]DASB and [(18)F]altanserin-PET study. Neurobiol Aging.

Marner L, Gillings N, Madsen K, Erritzoe D, Baare WF, Svarer C, Hasselbalch SG, Knudsen GM (2010b) Brain imaging of serotonin 4 receptors in humans with [11C]SB207145-PET. Neuroimage 50:855-861.

Meltzer CC, Price JC, Mathis CA, Greer PJ, Cantwell MN, Houck PR, Mulsant BH, Ben-Eliezer D, Lopresti B, DeKosky ST, Reynolds CF, III (1999) PET imaging of serotonin type 2A receptors in late-life neuropsychiatric disorders. Am J Psychiatry 156:1871-1878.

Meyer JH, Wilson AA, Sagrati S, Hussey D, Carella A, Potter WZ, Ginovart N, Spencer EP, Cheok A, Houle S (2004) Serotonin transporter occupancy of five selective serotonin reuptake inhibitors at different doses: an [11C]DASB positron emission tomography study. Am J Psychiatry 161:826-835.

Meyer PT, Bhagwagar Z, Cowen PJ, Cunningham VJ, Grasby PM, Hinz R (2010) Simplified quantification of 5-HT2A receptors in the human brain with [11C]MDL 100,907 PET and non-invasive kinetic analyses. Neuroimage 50:984-993.

Mikkelsen M, Moller A, Jensen LH, Pedersen A, Harajehi JB, Pakkenberg H (1999) MPTP-induced Parkinsonism in minipigs: A behavioral, biochemical, and histological study. Neurotoxicol Teratol 21:169-75.

Milak MS, Severance AJ, Ogden RT, Prabhakaran J, Kumar JS, Majo VJ, Mann JJ, Parsey RV (2008) Modeling considerations for 11C-CUMI-101, an agonist radiotracer for imaging serotonin 1A receptor in vivo with PET. J Nucl Med 49:587-596.

Miller PW, Long NJ, Vilar R, Gee AD (2008) Synthesis of 11C, 18F, 15O, and 13N radiolabels for positron emission tomography. Angew Chem Int Ed Engl 47:8998-9033.

Mintun MA, Raichle ME, Kilbourn MR, Wooten GF, Welch MJ (1984) A quantitative model for the in vivo assessment of drug binding sites with positron emission tomography. Ann Neurol 15:217-227.

Narendran R, Hwang DR, Slifstein M, Hwang Y, Huang Y, Ekelund J, Guillin O, Scher E, Martinez D, Laruelle M (2005) Measurement of the proportion of D2 receptors configured in state of high affinity for agonists in vivo: a positron emission tomography study using [11C]N-propyl-norapomorphine and [11C]raclopride in baboons. J Pharmacol Exp Ther 315:80-90.

Narendran R, Hwang DR, Slifstein M, Talbot PS, Erritzoe D, Huang Y, Cooper TB, Martinez D, Kegeles LS, bi-Dargham A, Laruelle M (2004) In vivo vulnerability to competition by endogenous dopamine: comparison of the D2 receptor agonist radiotracer (-)-N-[11C]propyl-norapomorphine ([11C]NPA) with the D2 receptor antagonist radiotracer [11C]-raclopride. Synapse 52:188-208.

Narendran R, Mason NS, Laymon CM, Lopresti BJ, Velasquez ND, May MA, Kendro S, Martinez D, Mathis CA, Frankle WG (2010) A comparative evaluation of the dopamine D(2/3) agonist radiotracer [11C](-)-N-propyl-norapomorphine and antagonist [11C]raclopride to measure amphetamine-induced dopamine release in the human striatum. J Pharmacol Exp Ther 333:533-539.

Nazarali AJ, Reynolds GP (1992) Monoamine neurotransmitters and their metabolites in brain regions in Alzheimer's disease: a postmortem study. Cell Mol Neurobiol 12:581-7.

Neumeister A (2003) Tryptophan depletion, serotonin, and depression: where do we stand? Psychopharmacol Bull 37:99-115.

Niblock MM, Luce CJ, Belliveau RA, Paterson DS, Kelly ML, Sleeper LA, Filiano JJ, Kinney HC (2005) Comparative anatomical assessment of the piglet as a model for the developing human medullary serotonergic system. Brain Res Brain Res Rev 50:169-83.

Nichols DE (2004) Hallucinogens. Pharmacol Ther 101:131-81.

Nichols DE, Frescas SP, Chemel BR, Rehder KS, Zhong D, Lewin AH (2008) High specific activity tritium-labeled N-(2-methoxybenzyl)-2,5-dimethoxy-4-iodophenethylamine (INBMeO): a high-affinity 5-HT2A receptor-selective agonist radioligand. Bioorg Med Chem 16:6116-6123.

Nielsen TR, Kornum BR, Moustgaard A, Gade A, Lind NM, Knudsen GM (2009) A novel spatial Delayed Non-Match to Sample (DNMS) task in the Gottingen minipig. Behav Brain Res 196:93-98.

O'Connell MT, Portas CM, Sarna GS, Curzon G (1991) Effect of p-chlorophenylalanine on release of 5-hydroxytryptamine from the rat frontal cortex in vivo. Br J Pharmacol 102:831-6.

O'Leary OF, Bechtholt AJ, Crowley JJ, Hill TE, Page ME, Lucki I (2007) Depletion of serotonin and catecholamines block the acute behavioral response to different classes of antidepressant drugs in the mouse tail suspension test. Psychopharmacology (Berl) 192:357-71.

Park DH, Stone DM, Baker H, Kim KS, Joh TH (1994) Early induction of rat brain tryptophan hydroxylase (TPH) mRNA following parachlorophenylalanine (PCPA) treatment. Brain Res Mol Brain Res 22:20-8.

Paterson L, Tyacke RL, Nutt DJ, Knudsen GM (2010) Measuring endogenous 5-HT release by emission tomography; promises and pitfalls. J Cereb Blood Flow Metab.

Pavey GM, Copolov DL, Dean B (2002) High-resolution phosphor imaging: validation for use with human brain tissue sections to determine the affinity and density of radioligand binding. J Neurosci Methods 116:157-63.

Paxinos G, Burt J, Atrens DM, Jackson DM (1977) 5-hydroxytryptamine depletion with para-chlorophenylalanine: effects on eating, drinking, irritability, muricide, and copulation. Pharmacol Biochem Behav 6:439-47.

Pei Q, Tordera R, Sprakes M, Sharp T (2004) Glutamate receptor activation is involved in 5-HT2 agonist-induced Arc gene expression in the rat cortex. Neuropharmacology 46:331-339.

Pike VW (2009) PET radiotracers: crossing the blood-brain barrier and surviving metabolism. Trends Pharmacol Sci 30:431-440.

Pinborg LH, Adams KH, Svarer C, Holm S, Hasselbalch SG, Haugbol S, Madsen J, Knudsen GM (2003) Quantification of 5-HT2A receptors in the human brain using [18F]altanserin-PET and the bolus/infusion approach. J Cereb Blood Flow Metab 23:985-996.

Pinborg LH, Adams KH, Yndgaard S, Hasselbalch SG, Holm S, Kristiansen H, Paulson OB, Knudsen GM (2004) [18F]altanserin binding to human 5HT2A receptors is unaltered after citalopram and pindolol challenge. J Cereb Blood Flow Metab 24:1037-1045.

Pinborg LH, Arfan H, Haugbol S, Kyvik KO, Hjelmborg JV, Svarer C, Frokjaer VG, Paulson OB, Holm S, Knudsen GM (2008) The 5-HT2A receptor binding pattern in the human brain is strongly genetically determined. Neuroimage 40:1175-1180.

Raleigh MJ, Brammer GL, Yuwiler A, Flannery JW, McGuire MT, Geller E (1980) Serotonergic influences on the social behavior of vervet monkeys (Cercopithecus aethiops sabaeus). Exp Neurol 68:322-34.

Raymond JR, Mukhin YV, Gelasco A, Turner J, Collinsworth G, Gettys TW, Grewal JS, Garnovskaya MN (2001) Multiplicity of mechanisms of serotonin receptor signal transduction. Pharmacol Ther 92:179-212.

Rbah L, Leviel V, Zimmer L (2003) Displacement of the PET ligand 18F-MPPF by the electrically evoked serotonin release in the rat hippocampus. Synapse 49:239-245.

Reneman L, Endert E, de Bruin K, Lavalaye J, Feenstra MG, de Wolff FA, Booij J (2002) The acute and chronic effects of MDMA ("ecstasy") on cortical 5-HT2A receptors in rat and human brain. Neuropsychopharmacology 26:387-96.

Rosa-Neto P, Gjedde A, Olsen AK, Jensen SB, Munk OL, Watanabe H, Cumming P (2004) MDMA-evoked changes in [11C]raclopride and [11C]NMSP binding in living pig brain. Synapse 53:222-233.

Rosso L, Gee AD, Gould IR (2008) Ab initio computational study of positron emission tomography ligands interacting with lipid molecule for the prediction of nonspecific binding. J Comput Chem 29:2397-2405.

Roth BL, Choudhary MS, Khan N, Uluer AZ (1997) High-affinity agonist binding is not sufficient for agonist efficacy at 5-hydroxytryptamine2A receptors: evidence in favor of a modified ternary complex model. J Pharmacol Exp Ther 280:576-583.

Ruhé HG, Mason NS, Schene AH (2007) Mood is indirectly related to serotonin, norepinephrine and dopamine levels in humans: a meta-analysis of monoamine depletion studies. Mol Psychiatry 12:331-59.

Santhosh L, Estok KM, Vogel RS, Tamagnan GD, Baldwin RM, Mitsis EM, Macavoy MG, Staley JK, van Dyck CH (2009) Regional distribution and behavioral correlates of 5-HT(2A) receptors in Alzheimer's disease with [(18)F]deuteroaltanserin and PET. Psychiatry Res 173:212-217.

Seneca N, Finnema SJ, Farde L, Gulyas B, Wikstrom HV, Halldin C, Innis RB (2006) Effect of amphetamine on dopamine D2 receptor binding in nonhuman primate brain: a comparison of the agonist radioligand [11C]MNPA and antagonist [11C]raclopride. Synapse 59:260-269.

Seneca N, Zoghbi SS, Skinbjerg M, Liow JS, Hong J, Sibley DR, Pike VW, Halldin C, Innis RB (2008) Occupancy of dopamine D2/3 receptors in rat brain by endogenous dopamine measured with the agonist positron emission tomography radioligand [11C]MNPA. Synapse 62:756-763.

Sibley DR, De LA, Creese I (1982) Anterior pituitary dopamine receptors. Demonstration of interconvertible high and low affinity states of the D-2 dopamine receptor. J Biol Chem 257:6351-6361.

Smith DF, Gee AD, Hansen SB, Moldt P, Nielsen EO, Scheel-Kruger J, Gjedde A (1999) Uptake and distribution of a new SSRI, NS2381, studied by PET in living porcine brain. Eur Neuropsychopharmacol 9:351-9.

Smith DF, Hansen SB, Ostergaard L, Gee AD, Danielsen E, Ishizu K, Bender D, Poulsen PH, Gjedde A (2001) [14C]Serotonin uptake and [O-methyl-11C]venlafaxine kinetics in porcine brain. Nucl Med Biol 28:633-638.

Soares JC, Innis RB (1999) Neurochemical brain imaging investigations of schizophrenia. Biol Psychiatry 46:600-615.

Soares JC, van Dyck CH, Tan P, Zoghbi SS, Garg P, Soufer R, Baldwin RM, Fujita M, Staley JK, Fu X, Amici L, Seibyl J, Innis RB (2001) Reproducibility of in vivo brain measures of 5-HT2A receptors with PET and [18F]deuteroaltanserin. Psychiatry Res 106:81-93.

Sureau FC, Reader AJ, Comtat C, Leroy C, Ribeiro MJ, Buvat I, Trebossen R (2008) Impact of image-space resolution modeling for studies with the high-resolution research tomograph. J Nucl Med 49:1000-1008.

Swamy HV, Smith TK, MacDonald EJ (2004) Effects of feeding blends of grains naturally contaminated with Fusarium mycotoxins on brain regional neurochemistry of starter pigs and broiler chickens. J Anim Sci 82:2131-9.

Syvanen S, Lindhe O, Palner M, Kornum BR, Rahman O, Langstrom B, Knudsen GM, Hammarlund-Udenaes M (2009) Species differences in blood-brain barrier transport of three positron emission tomography radioligands with emphasis on P-glycoprotein transport. Drug Metab Dispos 37:635-643.

Tumbleson M (1986) Swine in Biomedical Research. Plenum Press.

Udo de Haes JI, Harada N, Elsinga PH, Maguire RP, Tsukada H (2006) Effect of fenfluramine-induced increases in serotonin release on [18F]MPPF binding: a continuous infusion PET study in conscious monkeys. Synapse 59:18-26.

Van Oekelen D, Luyten WH, Leysen JE (2003) 5-HT2A and 5-HT2C receptors and their atypical regulation properties. Life Sci 72:2429-49.

Verhoeff NP (1999) Radiotracer imaging of dopaminergic transmission in neuropsychiatric disorders. Psychopharmacology (Berl) 147:217-249.

Verhoeff NP, Christensen BK, Hussey D, Lee M, Papatheodorou G, Kopala L, Rui Q, Zipursky RB, Kapur S (2003) Effects of catecholamine depletion on D2 receptor binding, mood, and attentiveness in humans: a replication study. Pharmacol Biochem Behav 74:425-432.

Versijpt J, Van Laere KJ, Dumont F, Decoo D, Vandecapelle M, Santens P, Goethals I, Audenaert K, Slegers G, Dierckx RA, Korf J (2003) Imaging of the 5-HT2A system: age-, gender-, and Alzheimer's disease-related findings. Neurobiol Aging 24:553-561.

Watanabe H, Andersen F, Simonsen CZ, Evans SM, Gjedde A, Cumming P (2001) MR-based statistical atlas of the Gottingen minipig brain. Neuroimage 14:1089-96.

Weikop P, Kehr J, Scheel-Kruger J (2007) Reciprocal effects of combined administration of serotonin, noradrenaline and dopamine reuptake inhibitors on serotonin and dopamine levels in the rat prefrontal cortex: the role of 5-HT1A receptors. J Psychopharmacol 21:795-804.

Wong DF, Lever JR, Hartig PR, Dannals RF, Villemagne V, Hoffman BJ, Wilson AA, Ravert HT, Links JM, Scheffel U, . (1987) Localization of serotonin 5-HT2 receptors in living human brain by positron emission tomography using N1-([11C]-methyl)-2-Br-LSD. Synapse 1:393-398.

Wong DF, Pomper MG (2003) Predicting the success of a radiopharmaceutical for in vivo imaging of central nervous system neuroreceptor systems. Mol Imaging Biol 5:350-362.

Wong DF, Tauscher J, Grunder G (2009) The role of imaging in proof of concept for CNS drug discovery and development. Neuropsychopharmacology 34:187-203.

Zea-Ponce Y, Kegeles LS, Guo N, Raskin L, Bakthavachalam V, Laruelle M (2002) Pharmacokinetics and brain distribution in non human primate of R(-)[123I]DOI, A 5HT(2A/2C) serotonin agonist. Nucl Med Biol 29:575-583.

Zimmer L, Mauger G, Le BD, Bonmarchand G, Luxen A, Pujol JF (2002) Effect of endogenous serotonin on the binding of the 5-hT1A PET ligand 18F-MPPF in the rat hippocampus: kinetic beta measurements combined with microdialysis. J Neurochem 80:278-286.

Paper I

Ettrup A, Kornum BR, Weikop P, Knudsen GM.

An Approach for Serotonin Depletion in Pigs: Effects on Serotonin Receptor Binding.

An Approach for Serotonin Depletion in Pigs: Effects on Serotonin Receptor Binding

ANDERS ETTRUP,[1]* BIRGITTE R. KORNUM,[1] PIA WEIKOP,[2] AND GITTE M. KNUDSEN[1]
[1]*Neurobiology Research Unit and Center for Integrated Molecular Brain Imaging (Cimbi),
Copenhagen University Hospital, Rigshospitalet, DK-2100 Copenhagen, Denmark*
[2]*NeuroSearch A/S, DK-2750 Ballerup, Denmark*

ABSTRACT   Depletion of central serotonin (5-HT) levels and dysfunction in serotonergic transmission are implicated in a variety of human CNS disorders. The mechanisms behind these serotonergic deficits have been widely studied using rodent models, but only to a limited extent in larger animal models. The pig is increasingly used as an experimental animal model especially in neuroscience research. Here, we present an approach for serotonin depletion in the pig brain. Central serotonin depletion in Danish Landrace pigs was achieved following 4 days treatment with *para*-chlorophenylalanine (*p*CPA). On day 5, tissue concentrations of 5-HT in seven distinct brain structures from one hemisphere: frontal and occipital cortex, striatum, hippocampus, cerebellum, rostral, and caudal brain stem, were determined. The other hemisphere was processed for receptor autoradiography. Treatments with 50 mg/kg and 100 mg/kg *p*CPA caused average decreases in 5-HT concentrations of 61% $\pm$ 14% and 66% $\pm$ 16%, respectively, and a substantial loss of 5-HT immunostaining was seen throughout the brain. The serotonin depletion significantly increased 5-HT$_4$ receptor binding in nucleus accumbens, but did not alter 5-HT$_{1A}$ and 5-HT$_{2A}$ receptor or serotonin transporter binding in any brain region. In conclusion, 4 days treatment with *p*CPA effectively reduces 5-HT levels in the pig brain. Further, whereas several 5-HT markers did not change after the *p*CPA treatment, 5-HT$_4$ receptors were consistently upregulated, indicating a greater susceptibility of this receptor to altered 5-HT levels. This porcine model of serotonin depletion will be useful in future studies of cerebral serotonergic dysfunction. **Synapse 00:000–000, 2010.**   © 2010 Wiley-Liss, Inc.

INTRODUCTION

The serotonin (5-HT) system is one of the most prominent and important neurotransmitter systems modulating a plethora of important behavioral effects, including anger, aggression, body temperature, mood, sleep, sexuality, and appetite. Impairments in the 5-HT system are also seen in various brain diseases including depression, schizophrenia, and Alzheimer's disease. Accordingly, investigations of the biochemical and behavioral effects of a decreased serotonergic neurotransmission can generate knowledge of the involvement of the 5-HT system in relation to these diseases. Serotonin depletion is, e.g., associated with acute relapse of depressive symptoms in previously depressed patients (Delgado et al., 1990) and other individuals particularly vulnerable to

affective disorders (Jans et al., 2007). Different experimental serotonin depletion regimes are used in rats, monkeys, and humans, including specific lesioning of serotonergic neurons, depletion of the 5-HT precursor, tryptophan, sustained 5-HT release, or inhibition of 5-HT synthesis. *para*-chlorophenylalanine (*p*CPA)

is a specific inhibitor of tryptophan hydroxylase, the rate-limiting enzyme in 5-HT biosynthesis, well-known to produce extensive and selective serotonin depletion in rats (Fusar-Poli et al., 2006; Kornum et al., 2006; O'Connell et al., 1991) and monkeys (Gradwell et al., 1975). The pig (*Sus scrofa*) has been widely used in human biomedical research due to its much closer similarity to human biology than the rodent (Vodicka et al., 2005), and over the last decade, pigs have also gained increasing popularity as an experimental animal in neuroscience, because of the considerable anatomical and genetic similarities between human and porcine neurobiology (Lind et al., 2007). Furthermore, the pig represents an alternative to rodent models, as avoiding the safety, ethical, and housing difficulties presented by research with non-human primates. Until now, a pig model for serotonin depletion has not been developed and validated.

The diverse effects of the 5-HT system is executed by the diversity and number of 5-HT receptor subtypes (Barnes and Sharp, 1999), and changes in post-synaptic 5-HT receptor levels are seen in a variety of human neuropsychiatric diseases. Among these, the 5-HT_{1A} receptor is the principal inhibitory 5-HT receptor, it rapidly regulates the activity of the serotonergic neurotransmission, and desensitization of pre-synaptic 5-HT_{1A} autoreceptors has been implicated in the delayed onset-of-action of selective serotonin reuptake inhibitor (SSRI) antidepressants. The 5-HT_{2A} receptor is the main excitatory 5-HT receptor subtype being directly involved in higher executive functions and perception and it is also the target of atypical antipsychotic drugs. Finally, 5-HT_4 receptors have been assigned a pivotal role in memory and learning (e.g., King et al., 2008).

The purpose of this study was to validate an approach for serotonin depletion in the pig brain, and to assess the effects of decreased 5-HT levels on the levels of 5-HT_{1A}, 5-HT_{2A}, and 5-HT_4 receptors, as well as the SERT.

MATERIALS AND METHODS
Animals and drug administration

Fourteen young (∼2 months old) female Danish Landrace pigs (mean weight ± SD: 17.6 kg ± 1.2 kg) were used in the study. After arrival, animals were housed in pairs under standard conditions and were allowed to acclimatize for 1 week before start of experiments. To minimize stress, the animals were provided with straw bedding and environment enrichment, in the form of plastic balls and metal chains.

For four consecutive days, the pigs were injected i.m. once daily in the neck with saline, 50 mg/kg, or 100 mg/kg *p*CPA methyl ester hydrochloride (Sigma, No. C3635). *p*CPA solutions adjusted to pH 7 by adding NaOH or saline were given as 10 ml injections.

Twenty-four hours after the final injection, animals were anesthetized and sacrificed via perfusion fixation or decapitation. All animal procedures were approved by the Danish Council for Animal Ethics (Journal No. 2006/561-1155).

5-HT immunostaining

One Danish Landrace pig received *p*CPA (100 mg/kg), whereas one control pig received saline. Animals were anesthetized by 0.1 ml/kg intramuscular injections of Zoletil veterinary mixture (Virbac Animal Health, France: 125 mg tiletamin and 125 mg zolazepam in 6.25 ml of 20 mg/ml xylazin, 1.25 ml of 100 mg/ml ketamine, 2 ml of 10 mg/ml metadon, and 2 ml of 10 mg/ml butorphanol). Animals were intravenously injected with 2000 mg sodium pentobarbital before undergoing surgical procedures. Heparinized saline was pumped directly into the aorta at a rate of 300 ml/min for 3 min followed by perfusion at the same flow rate with 4% paraformaldehyde (PFA) in phosphate buffer, pH 7.6. Stiffness of neck-musculature was used as an indicator of perfusion fixation of brain tissue, and this was further confirmed by the pale color of the perfused brain. The brains were carefully removed and postfixed for 2 h in PFA and hereafter immersed in cryoprotective solution [20% sucrose in phosphate buffered saline (PBS), pH = 7.6] and stored at 4°C for no longer than 2 days. Finally, cryoprotective freezing was conducted by immersion in isopentane (2-methylbutane, Sigma Aldrich) cooled to −70°C using liquid nitrogen. Cryoprotected frozen brains were stored at −80°C until processed. Coronal sections of perfusion fixated brain tissue were sliced in 50 µm sections at −25°C in a cryostat (Microm HM 500 OM) and collected in cryoprotective Olmose solution (30% ethylene glycol, 30% sucrose, 1% polyvinyl-pyrrolidone (PVP-40, Sigma) in PBS) and stored at −20°C. Free-floating sections were incubated in anti-5-HT antibodies (Sigma, No. S5545) diluted 1:5000 as previously described (Nielsen et al., 2006), and visualization of antigen binding was done in chromagen diaminobenzidine (DAB) solution (DAKO, Denmark). Sections were mounted on gelatin-coated glass slides, dried overnight, dehydrated, and cover slipped. DAB-stained sections were scanned in a flatbed desktop scanner (HP Scanjet 4850).

Tissue dissection and high-performance liquid chromatography analysis

Twelve Danish Landrace pigs were used in the quantitative study. Animals were sacrificed with injections of sodium pentobarbital under Zoletil anesthesia (as above), quickly decapitated, and their brains removed for immediate dissection. First, the caudal part of the brain stem was dissected by a cut just below cerebellar level. Then, the hemispheres

were split. For autoradiography, one hemisphere was frozen directly on an aluminum plate cooled by dry-ice and covered with crushed dry ice. The other hemisphere was dissected for measurement of regional concentrations of monoamines and metabolites: the rostral part of the brain stem was dissected at the level of the cerebellum. Thereafter, the hemisphere of cerebellum was excised, and hippocampus was dissected bluntly in its full length. Next, the frontal cortex was excised by an excision 2 cm from the rostral tip of the cerebrum. After exposing the striatum from the sagittal plane, this tissue was excised. Finally, occipital cortex was dissected by a cut 2 cm from the occipital lobe (the caudal tip of the cerebrum). Tissue was stored at $-80^\circ C$ and analyzed with high-performance liquid chromatography (HPLC) within 14 days. Tissue pieces were weighed and homogenized in perchloric acid (0.1 N, Bie and Bentsen No. 2527) saturated with disodium-EDTA (Bie and Bentsen No. K21193118) for 2×15 s using a polytron (IKA T10 basic). Thereafter, homogenates were centrifuged at $14,000g$ for 10 min at $4^\circ C$ (Eppendorf Centrifuge 5804R). Supernatant was filtered through a 0.20 μm cellulose acetate microfilter (Dismic—13 CP by Advantec). Finally, 20 μl of the filtrate was loaded to the HPLC-system.

Concentrations of 5-HT, 5-hydroxyindoleacetic acid (5-HIAA), dopamine (DA), 3,4-dihydroxyphenylacetic acid (DOPAC), and homovanillic acid (HVA) in tissue homogenates were determined by reversed phase HPLC with electrochemical detection as previously described (Weikop et al., 2007). The limits of detection (at signal-to-noise ratio of 3) for all compounds were in the range of 30–160 fmol/sample, i.e., 1.5–3 nM. Tissue concentrations of 5-HT, 5-HIAA, DA, DOPAC and HVA were calculated using a reference solution containing 0.5 or 1 pmol/sample of all investigated compounds. The following reference compounds were used: DA (Sigma H8502), HVA (Sigma H1252), DOPAC (Sigma 850217), 5-HIAA (Sigma H8876), and 5-HT (Sigma H4511). Monoamine and metabolites concentrations in homogenate samples were calculated by the area under curve (AUC) for the peak of the compound relative to the AUC for the reference compound and reported relative to the weight of the tissue (ng/g tissue). Reference solutions were quantified before each set of homogenates was measured.

Quantitative in vitro receptor autoradiography

Coronal 10 μm sections for quantitative receptor autoradiography were sliced on a cryostat (Microm HM 500 OM) and thaw-mounted on gelatin-coated glass slides. Sections were stored at $-80^\circ C$ until processing. As sectioning, orientation in the coronal plane was maintained by referring to a stereotaxic atlas of the pig brain (Felix et al., 1999). Following incubation

at room temperature (RT) and washing procedures, sections were fixed overnight in PFA vapor in a desiccator jar at $4^\circ C$, dried for 3 h at in an air-tight plastic box using beads of silica gel as desiccant at RT, and exposed to a pre-erased BAS TR2040 tritium sensitive imaging plates (TR-IP) (Fuji Film, Japan) at $4^\circ C$ in a radiation-shielded IP cassette. Slides were coexposed with four [^{3}H]microscales (Amersham Biosciences, USA). TR-IPs were scanned in a BAS-2500 bioimaging analyser (Fuji Film).

The autoradiographic protocol to determine 5-HT$_{1A}$ receptor binding in the pig brain was based on previous studies in rats (Cahir et al., 2007). In a saturation study, the K_d of [methoxy-^{3}H]WAY100635 (GE Healthcare, United Kingdom, No. TRK1034) on pig brain sections was determined at 0.29 ± 0.02 nM (data not shown), and concurrently, assay buffer composition and incubation time was adjusted to optimize the specific-to-nonspecific binding ratio. Briefly, 5-HT$_{1A}$ receptor binding in pig brain sections was determined as follows: Sections were preincubated for 15 min in assay buffer (50 mM Tris-HCl, buffer 0.01% ascorbic acid, pH 7.4). [^{3}H]WAY100635 was added to the incubation buffer, to reach a final concentration 1.5 nM, and the slides were then incubated for 2 h. Nonspecific binding (NSB) was determined in the presence of 10 μM 5-HT (Sigma No. H9523). Following incubation procedures, slides were washed in ice-cold 50 mM Tris-HCl buffer (pH 7.4) for 2×10 min and in distilled water for 20 s to remove buffer salts before being dried for 30 min under a gentle air stream. Sections were exposed to the TR-IPs for 14 days.

5-HT$_{2A}$ receptor binding was quantified with the tritiated high-affinity 5-HT$_{2A}$ receptor antagonist [^{3}H]MDL100907 (kindly provided by Prof. Christer Halldin, Karolinska Institute, Stockholm, Sweden): K_d of [^{3}H]MDL100907 has previously been determined at 0.3 nM (Kristiansen et al., 2005). NSB was determined in the presence of 10 μM of unlabeled ketanserin (Sigma, No. S006). Pig brain sections were preincubated for 15 min (50 mM Tris-HCl buffer, 0.01% ascorbic acid, 10 μM pargyline, pH 7.4). After preincubation, slides were incubated for 1 h in the same buffer with addition of 1.0 nM [^{3}H]MDL100907. Following incubation, sections were washed in 50 mM Tris-HCl buffer for 2×20 s and in distilled water for 20 s. Sections were exposed to the TR-IPs for 7 days.

5-HT$_4$ receptor binding was quantified with the tritiated 5-HT$_4$ receptor selective antagonist [^{3}H]SB207145 as previously described (Licht et al., 2009). The affinity of [^{3}H]SB207145 for the porcine 5-HT$_4$ receptor is 0.39 nM in brain homogenate (Kornum et al., 2009). Briefly, sections were preincubated for 15 min (50 mM Tris-HCl buffer, 0.01% ascorbic acid, 10 μM pargyline, pH 7.4) followed by 1 h incubation in the same buffer added 1.2 nM [^{3}H]SB207145 (kindly provided by Christine Parker, GSK). Washing was done first with

Tris-HCl buffer (2×20 s), then with distilled water (1×20 s). Sections were exposed to the TR-IPs for 14 days. NSB was measured in the presence of 10 μM high-affinity 5-HT$_4$ receptor antagonist, RS39604 (Tocris, No. 0991).

SERT binding was determined using the tritiated SSRI [^{3}H]escitalopram as previously described (Thomsen and Helboe, 2003). NSB was measured in the presence of 10 μM of the structurally different SSRI paroxetine (GSK, UK). Briefly, sections were preincubated for 20 min at RT (50 mM Tris-HCl buffer, 120 mM NaCl, 5 mM KCl, pH 7.4) followed by 1 h incubation at RT in the same buffer added 2 nM [^{3}H]escitalopram (kindly provided by Lundbeck A/S, Denmark). Washing was conducted in Tris-HCl buffer (3×2 min) subsequent in distilled water (1×10 s). Sections were exposed to the TR-IPs for 8 days.

Image and data analysis

Densitometric image analysis of autoradiograms were conducted using the free software ImageJ (Image Processing and analysis in Java, http://rsb.info.nih.gov/ij/), version 1.38x. Regions of interest (ROI) were hand-drawn around anatomical landmarks, e.g., borders of a section, for each brain region and the mean pixel density in the ROIs was measured as outcome. A 3rd degree exponential calibration function of decay-corrected [^{3}H]microscales activity steps was used to convert the mean pixel density in the ROI to radioactivity. The calibration fit yielded r^2-values greater than 0.99 with no systematic deviations for all autoradiograms. The subsequent outcome, nCi/mg estimated wet tissue equivalent (TE), was for each ROI converted to fmol/mg TE using the decay-corrected specific activity of the ligand, and the specific binding (SB) was calculated as the total binding minus the NSB, as determined on adjacent sections.

The treatment group was blinded to the investigator during the quantitative assessments of autoradiography and sectioning, incubation, image analysis, and data processing.

Statistical analyses

Statistical tests were performed using Prism version 5.0 (GraphPad software, USA). When significant interactions between dose and regions were found in a two-way analysis of variance (ANOVA), tests for significant treatment effects were conducted using one-way ANOVA and tukey-test for multiple comparisons between dose groups for each distinct region. In analyses of 5-HT/5-HIAA ratios and receptor binding data, a two-way ANOVA analysis was applied when no significant interaction between region and treatment was found, using Bonferroni post-test correction for multiple comparisons. Correlations were carried

out by evaluating the Pearsons correlation coefficient assuming Gaussian distribution of the variables receptor binding and tissue concentrations. P-values below 0.05 were considered statistically significant. Results are expressed in mean ± standard error of the mean (SEM) unless otherwise stated.

RESULTS
5-HT immunoreactivity and tissue concentrations of monoamines and metabolites

pCPA treatment was associated with a significant loss of 5-HT immunoreactivity in frontal cortex, hippocampus, thalamus, parietal cortex, occipital cortex, and caudal brain stem (Fig. 1). When compared with cortical regions, 5-HT immunoreactivity in the substantia nigra (SN) was only slightly affected by pCPA (Fig. 1B). In the absence of primary antibodies, no staining was found in any sections.

In pCPA treated pigs, tissue concentrations of 5-HT and 5-HIAA were significantly decreased in all seven brain regions examined (Table I). In the examined brain regions, tissue concentrations of 5-HT were on average decreased by 61% ± 14% after treatment with 50 mg/kg pCPA and by 66% ± 16% after treatment with 100 mg/kg pCPA. When compared with saline-treated pigs, tissue concentrations of 5-HIAA were on average decreased by 69% ± 14% after 50 mg/kg pCPA and by 77% ± 11% after 100 mg/kg pCPA. The most extensive depletion was found in hippocampus and striatum, whereas the least effective depletion was observed in the brain stem areas and in the cerebellum. There was no statistically significant difference between treatment regimes with 50 mg/kg vs. 100 mg/kg. In all examined brain regions, except for the rostral brain stem, 5-HIAA tissue levels showed a greater extent of depletion by pCPA compared with 5-HT, and there was a significant main effect of pCPA treatment on 5-HT/5-HIAA ratios ($F_{2,63} = 6.43$, $P < 0.01$) indicating that regional tissue concentrations of 5-HT and 5-HIAA were affected differently by pCPA.

The pigs tolerated the pCPA treatment well and gained in average 1.3 kg (SD: 0.4 kg, $n = 14$) over the 5 days with no significant difference in gained weight among the treatment groups ($F_{2,11} = 1.42$, $P = 0.28$). No overt behavioral differences were observed between saline and pCPA treated pigs. Furthermore, no significant effects of pCPA in any dose on DA, DOPAC, or HVA were found in any region, however, rather large variations in the measurements within the treatment groups were concurrently found (Table II).

5-HT$_{1A}$ receptor autoradiography

Figure 2 shows [^{3}H]WAY100635 autoradiograms from different brain areas. The highest binding was seen in the hippocampus and in the frontal cortex. In the brain stem, [^{3}H]WAY100635 binding was generally
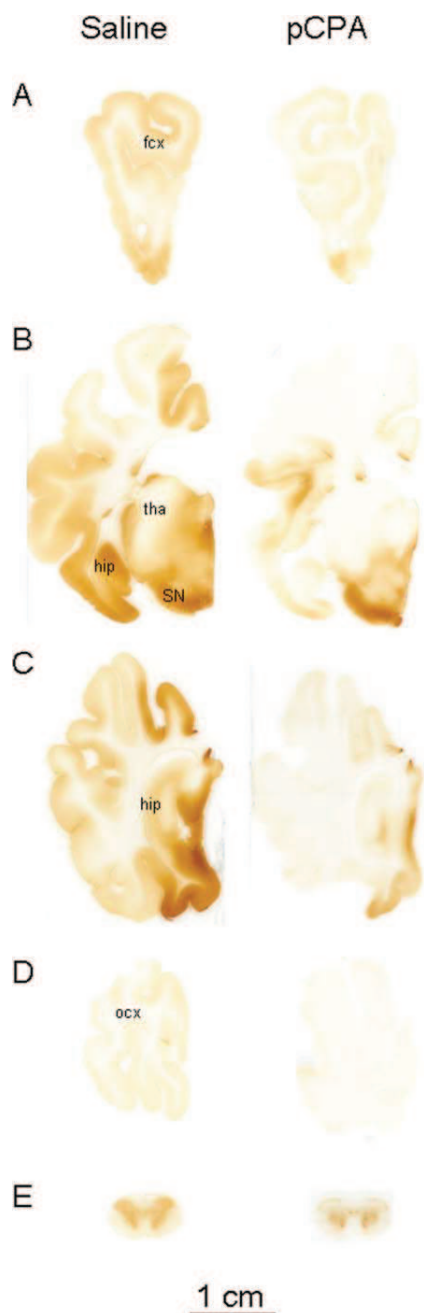
Fig. 1. 5-HT immunostaining of saline and *p*CPA treated animals. Representative images of coronal sections from one hemisphere of a saline treated animal (left panel) and a *p*CPA injected animal (right panel) are shown. Regions from rostral (top) to caudal (bottom) are (**A**) frontal cortex (fcx); (**B**) hippocampus (hip), substantia nigra (SN), and thalamus (tha); (**C**) hippocampus (hip); (**D**) occipital cortex (ocx); and (**E**) spinal cord.

low, but high binding was seen in the dorsal raphe nucleus (DRN). As [³H]WAY100635 binding was very low in the striatum, olfactory bulb, and the thalamus, 5-HT$_{1A}$ binding was only quantified in frontal cortex,

hippocampus, and DRN (Table III). In those regions, no significant interaction between region and treatment was found ($F_{4,27} = 1.31$, $P > 0.28$) and no main effect of treatment on [³H]WAY100635 binding was found ($F_{2,27} = 1.31$, $P > 0.30$, Table II).

5-HT$_{2A}$ receptor autoradiography

In the [³H]MDL100907 autoradiograms (Fig. 2), high binding was seen in the cerebral cortex and olfactory bulb. Moderate [³H]MDL100907 binding was found in the hippocampus and low binding in thalamus and in the brain stem. Overall, *p*CPA treatment did not alter [³H]MDL100907 binding ($F_{2,45} = 1.28$, $P > 0.28$, Table III) and no interaction between region (frontal cortex, hippocampus, caudate nucleus, putamen, and brain stem) and treatment was found ($F_{8,45} = 0.82$, $P > 0.58$).

5-HT$_4$ receptor autoradiography

In the [³H]SB207145 autoradiograms (Fig. 2), the highest binding was seen in the nucleus accumbens and SN. High-binding levels were also observed in the hippocampus, caudate nucleus, and putamen, whereas [³H]SB207145 binding was low in the cerebral cortex. [³H]SB207145 binding was quantified in caudate nucleus, putamen, nucleus accumbens, frontal cortex, hippocampus, and SN (Table III). There was no interaction between region and treatment ($F_{10,54} = 1.17$, $P > 0.10$), but a significant effect of *p*CPA treatment on [³H]SB207145 binding was found ($F_{2,54} = 3.70$, $P = 0.031$), and Bonferroni post-test revealed significant differences in the nucleus accumbens between both 50 and 100 mg/kg *p*CPA relative to control. In the nucleus accumbens, [³H]SB207145 binding correlated inversely and statistically significantly to 5-HT levels in the striatum (Fig. 3) ($r_{0.05(2),10} = -0.67$, $P = 0.018$).

SERT autoradiography

In the [³H]escitalopram autoradiograms (Fig. 2) high binding was seen in the DRN, moderate binding in striatum and low binding in the remaining regions, including hippocampus and cortical areas. [³H]escitalopram binding was quantified in frontal cortex, hippocampus, caudate nucleus, and putamen (Table III). [³H]escitalopram binding was unaffected by *p*CPA treatment ($F_{2,42} = 1.17$, $P > 0.32$) and there was no interaction between region and treatment ($F_{8,42} = 0.29$, $P > 0.96$).

DISCUSSION

The present results show that *p*CPA-mediated inhibition of tryptophan hydroxylase effectively reduced 5-HT levels in the pig brain to ~40% of baseline levels. The reduction in 5-HT was validated both qualita-

TABLE I. Effect of pCPA on 5-HT and 5-HIAA content in pig brain regions (ng/g tissue)

	0 mg/kg (n=4) Mean ± SEM	50 mg/kg (n=4) Mean ± SEM	100 mg/kg (n=4) Mean ± SEM	% depletion	
				50 mg/kg	100 mg/kg
5-HT:					
Frontal cortex	204.2 ± 6.5	85.2 ± 10.3*	69.9 ± 17.1*	58	66
Occipital cortex	106.1 ± 14.0	36.7 ± 10.6*	26.6 ± 5.9*	65	75
Striatum	189.3 ± 35.9	45.8 ± 10.3**	38.9 ± 1.7**	76	79
Hippocampus	157.4 ± 30.6	34.7 ± 5.4**	29.6 ± 7.0**	78	81
Cerebellum	51.4 ± 1.6	21.6 ± 4.3**	34.4 ± 8.1	58	33
Caudal brain stem	146.0 ± 32.3	86.1 ± 11.4	52.4 ± 2.9***	41	64
Rostral brain stem	313.5 ± 61.8	164.6 ± 23.6	119.6 ± 8.4***	48	62
5-HIAA:					
Frontal cortex	329.6 ± 42.6	123.1 ± 25.1**	62.1 ± 9.6**	63	81
Occipital cortex	183.4 ± 27.2	45.1 ± 17.9**	38.0 ± 13.7**	75	79
Striatum	515.8 ± 60.3	114.3 ± 6.4*	71.4 ± 4.9*	78	86
Hippocampus	429.7 ± 79.1	58.8 ± 5.3*	41.4 ± 10.6*	86	90
Cerebellum	92.6 ± 14.2	26.3 ± 5.8**	24.9 ± 10.0**	72	73
Caudal brain stem	230.7 ± 47.4	88.0 ± 5.5***	58.5 ± 11.2***	62	75
Rostral brain stem	355.1 ± 41.1	197.8 ± 19.2**	153.9 ± 15.2**	44	57

Differences between treatment groups are evaluated vs. saline groups using one-way ANOVA for each brain region and Tukey post-test for multiple comparisons: *p<0.001, **p<0.01, ***p<0.05.

tively by immunostaining and quantitatively by HPLC analysis. pCPA treatment leads to a profound decrease of 5-HT immunoreactivity, in a similar regional pattern as seen in rats (Kornum et al., 2006), with a larger loss of staining in cortical areas than in, e.g., the SN. The regional differences in the pCPA-induced loss of 5-HT immunostaining have previously been ascribed to morphological differences in serotonergic fibers, i.e., thin serotonergic projections in cortical areas deplete more easily than the thicker projections in the SN and in the cell soma in the DRN and the medial raphe nucleus (Kornum et al., 2006).

Our data from the pig brain are in line with similar studies in rats where pCPA is found to effectively and selectively decrease 5-HT and 5-HIAA tissue concentrations (Koe and Weissman, 1966; Kornum et al., 2006; O'Connell et al., 1991). The higher percentages of serotonin depletion (>90%) achieved in rats are likely to be explained by the higher doses of pCPA (~250–400 mg/kg) and perhaps also by the route of administration (intraperitoneal vs. intramuscular) (Kornum et al., 2006; O'Leary et al., 2007; Paxinos et al., 1977), and furthermore, 100 mg/kg pCPA given to rats only resulted in 30% cortical serotonin depletion (Datla and Curzon, 1996). We did not identify any added effect on 5-HT or 5-HIAA tissue concentrations when using 100 mg/kg instead of 50 mg/kg pCPA in any brain region indicating that the two doses caused a similar degree of serotonin depletion. This lack of a clear dose-response relationship may either be due to a threshold effect or to a limited bioavailability from intramuscular administration. We cannot exclude that a larger degree of serotonin depletion could be achieved in the pig brain by using either a different route of administration or a different treatment scheme. Although reducing 5-HT levels more effectively, higher pCPA doses also induce a minor depletion of DA (O'Leary et al., 2007), and it could also be argued that a greater than 90% serotonin depletion is less relevant in terms of modeling a dysfunctional serotonergic system.

In consistency with previous rat studies, we found pCPA treatment to be associated with a relatively larger depletion of 5-HIAA than 5-HT (Datla and Curzon, 1996; Kornum et al., 2006; O'Connell et al., 1991), suggesting that in addition to the effects arising from the lower 5-HT levels, pCPA effects 5-HIAA levels separately. Such a mechanism could be mediated through a downregulation of MAO activity either through direct inhibition by pCPA or by dynamic compensatory changes in the 5-HT system to restore 5-HT neurotransmission, but further studies are needed to address this question.

This is the first study to examine the autoradiographic 5-HT$_{1A}$ and 5-HT$_{2A}$ receptor distribution in the pig brain. For both the 5-HT$_{1A}$ receptor (Hall et al., 1997) and the 5-HT$_{2A}$ receptor (Hall et al., 2000), the regional binding in the pig brain is overall concordant with that in the human brain. In humans, however, cortical cell layers I-II have higher 5-HT$_{1A}$ receptor binding than the deeper cortical layers V-VI (Burnet et al., 1997; Hall et al., 1997). In contrast, rats have higher 5-HT$_{1A}$ receptor binding in the deeper layers compared with the superficial (Compan et al., 1998). In the pig brain, 5-HT$_{1A}$ receptor binding is higher in the deeper layers compared with the superficial (Fig. 2), so with respect to laminar distribution of 5-HT$_{1A}$ receptors, it seems that the pig brain resembles the rat brain more than the human brain. Conversely, the laminar distribution of porcine 5-HT$_{2A}$ receptors in cortical areas (Fig. 2) resembles that of humans and nonhuman primates with the highest density of 5-HT$_{2A}$ receptors superficially located (Hall et al., 2000; Lopez-Gimenez et al., 1998, 2001) in contrast to the rat brain, where the highest density is found in the

TABLE II. Effect of pCPA on DA, DOPAC, and HVA content in pig brain regions (ng/g tissue)

	DA			DOPAC			HVA		
	0 mg/kg (n=4) Mean ± SEM	50 mg/kg (n=4) Mean ± SEM	100 mg/kg (n=4) Mean ± SEM	0 mg/kg (n=4) Mean ± SEM	50 mg/kg (n=4) Mean ± SEM	100 mg/kg (n=4) Mean ± SEM	0 mg/kg (n=4) Mean ± SEM	50 mg/kg (n=4) Mean ± SEM	100 mg/kg (n=4) Mean ± SEM
Frontal cortex	6.9 ± 2.2	4.1 ± 2.0	3.1 ± 0.8	38.2 ± 15.3	20.6 ± 3.0	14.4 ± 5.1	36.4 ± 13.1	19.3 ± 4.7	25.9 ± 6.8
Occipital cortex	2.1 ± 0.8	3.4 ± 1.5	1.7 ± 0.6	39.1 ± 19.4	19.7 ± 1.0	8.3 ± 1.8	12.5 ± 2.0	12.7 ± 3.6	12.1 ± 2.0
Striatum	1341 ± 466	1449 ± 666	858 ± 289	1472 ± 452	1865 ± 682	1008 ± 412	1989 ± 260	1912 ± 733	1939 ± 1433
Hippocampus	8.8 ± 5.1	4.4 ± 1.0	5.5 ± 2.0	23.3 ± 8.0	18.2 ± 2.9	12.9 ± 3.0	27.4 ± 6.4	34.8 ± 4.2	26.7 ± 2.1
Cerebellum	1.6 ± 0.7	6.0 ± 3.2	3.7 ± 1.6	28.5 ± 10.6	25.5 ± 1.2	14.5 ± 4.1	10.9 ± 2.2	24.2 ± 2.9	18.7 ± 5.1
Caudal brain stem	6.3 ± 2.8	4.8 ± 2.6	3.6 ± 1.2	25.4 ± 7.3	18.7 ± 5.3	8.9 ± 3.2	21.8 ± 4.1	21.2 ± 3.6	24.6 ± 3.2
Rostral brain stem	19.3 ± 8.5	19.8 ± 3.1	15.2 ± 1.9	30.7 ± 6.1	40.7 ± 9.3	21.0 ± 7.3	38.3 ± 5.3	45.7 ± 4.5	41.0 ± 4.8

deeper cortical layer V (Fischette et al., 1987; Lopez-Gimenez et al., 1997).

We found in the Danish Landrace pig brain the same regional distribution and relative intensity of [^{3}H]SB207145 binding as in the Göttingen minipig (Kornum et al., 2009) and in humans (Pike et al., 2003; Varnäs et al., 2003). Similarly, the SERT distribution in this study resembles that previously found using autoradiography in the pig brain (Cumming et al., 2001).

No significant effect of the pCPA treatment on 5-HT$_{1A}$ receptor binding was seen. After 5 days of pCPA administration (300 mg/kg), the 5-HT$_{1A}$ receptor binding as measured with [^{3}H]-8-OH DPAT was increased in the rat frontal cortex (Compan et al., 1998), but this was not seen with a selective serotonergic lesion by intracerebroventricular injection of 5,7-dihydroxytryptamine (5,7-DHT) (Gobbi et al., 1994), and similarly, 5-HT$_{1A}$ receptor binding was unaffected after MDMA administration in pigs (Cumming et al., 2007). Further, cortical 5-HT$_{1A}$ receptor binding was unaltered following subchronic and chronic tryptophan depletion in rats (Cahir et al., 2007). Taken together, the postsynaptic 5-HT$_{1A}$ receptor density does not seem to be sensitive to subchronically decreased serotonergic neurotransmission.

pCPA treatment did in our study not alter [^{3}H]MDL100907 binding in the pig brain. A complete serotonergic lesion by intraraphe 5,7-DHT injections lead to significant decreases in 5-HT$_{2A/2C}$ [^{125}I]-DOI binding in rat cerebral cortex after 21 days (Compan et al., 1998). By contrast, no changes in cortical 5-HT$_{2A}$ receptor binding was seen following administration of 5,7-DHT (Fischette et al., 1987) indicating that only a near to complete depletion of 5-HT downregulate 5-HT$_{2A}$ receptors (Licht et al., 2009). Moderate, chronic serotonin depletion also increases 5-HT$_{2A}$ receptor binding in rats where 21 days of MDMA administration resulted in an inverse association between cerebral 5-HT concentrations and 5-HT$_{2A}$ receptor binding (Reneman et al., 2002). Finally, 21, but not 5, days of tryptophan depletion caused a significant increase in 5-HT$_{2A}$ receptor binding (Cahir et al., 2007). Taken together, these studies suggest that 5-HT$_{2A}$ receptors upregulate only in response to more chronically decreased serotonergic neurotransmission.

pCPA treatment did in our study not alter SERT binding. Compounds that cause serotonin depletion concurrent with degeneration of serotonergic afferents, e.g., MDMA and 5,7-DHT, consistently decrease SERT binding in regions receiving serotonergic input in rats (Chalon et al., 2004; McGregor et al., 2003) and in pigs (Cumming et al., 2007). However, in line with our observation, subchronic serotonin depletion using pCPA has not been reported to cause changes in SERT binding (Rattray et al., 1996).
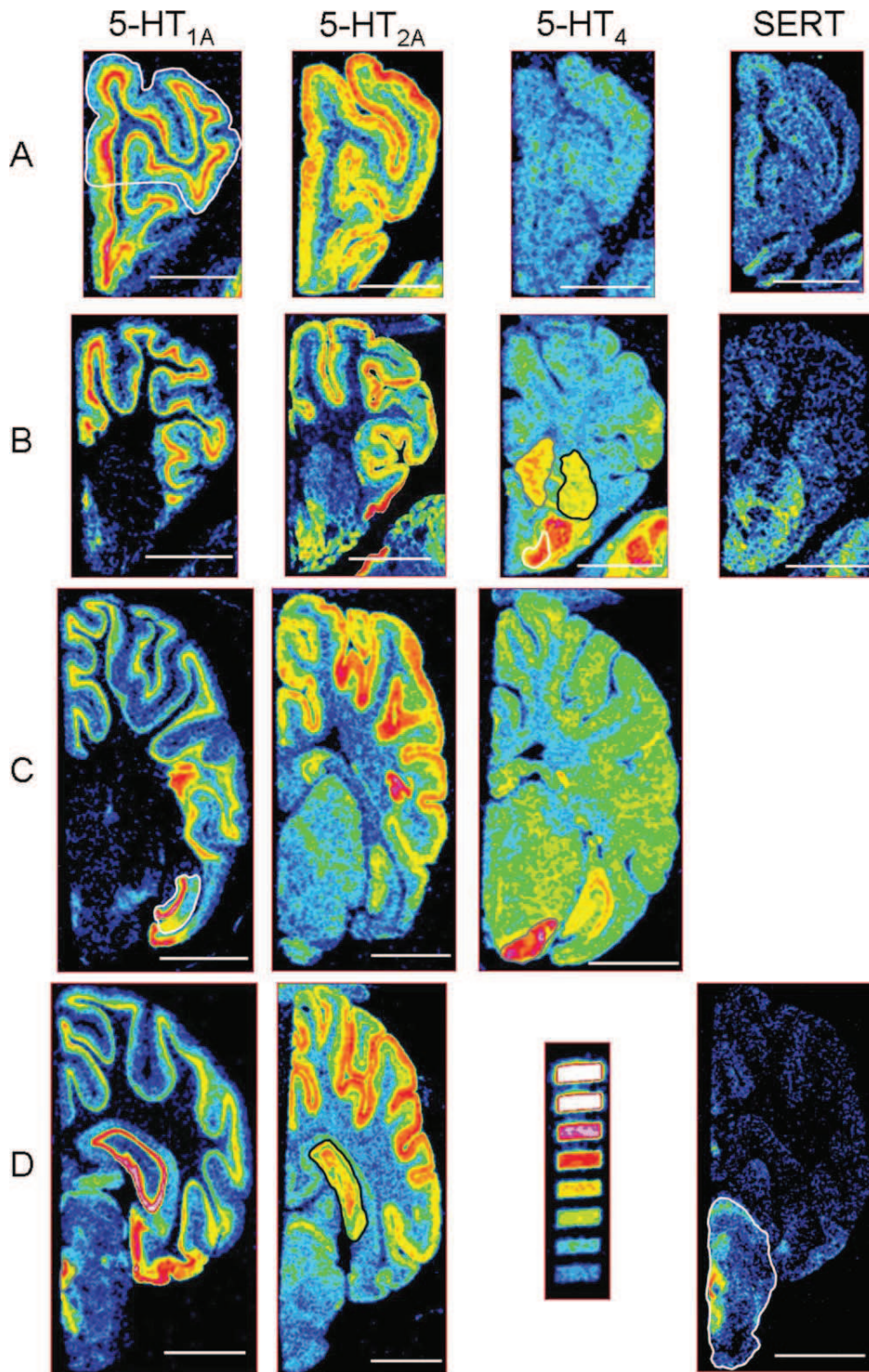
Fig. 2. Representative coronal sections of 5-HT$_{1A}$, 5-HT$_{2A}$, 5-HT$_4$, and SERT autoradiography in pig brain. Sections were incubated in the presence of 1.5 nM [^{3}H]WAY100635 for 5-HT$_{1A}$, 1.0 nM [^{3}H]MDL100907 for 5-HT$_{2A}$, 2.0 nM [^{3}H]SB207145 for 5-HT$_4$, and 1.5 nM [^{3}H]escitalopram for SERT. Sections are shown rostral to caudal and ROIs are delineated as indicated. **A**: Frontal cortex (white); (**B**) caudate nucleus (gray), putamen (black, and nucleus accumbens (white); (**C**) hippocampus (gray) and SN (gray); and (**D**) brain stem (white), raphé nucleus (gray), hippocampus (black). Radioactivity of the steps of the [^{3}H]microscale used as internal standard are: 385, 242, 156, 95, 61, 40, 25, 17 fmol/mg TE (top to bottom). In all sections, white bars correspond to 1 cm.

TABLE III. *Effect of pCPA on serotonin receptor and SERT binding in pig brain regions (fmol/mg TE)*

Region:	0 mg/kg (n=4) Mean ± SEM	50 mg/kg (n=4) Mean ± SEM	100 mg/kg (n=4) Mean ± SEM
5-HT$_{1A}$ (N.S.)			
Frontal cortex	16.50 ± 1.59	17.13 ± 0.83	14.68 ± 1.39
Hippocampus	46.31 ± 2.54	44.64 ± 3.61	46.52 ± 3.60
Dorsal raphe nucleus	25.28 ± 7.21	14.99 ± 1.67	27.42 ± 4.09
5-HT$_{2A}$ (N.S.)			
Frontal cortex	16.33 ± 1.04	18.36 ± 1.60	19.35 ± 1.08
Hippocampus	1.58 ± 0.20	1.67 ± 0.28	2.14 ± 0.50
Brain stem	1.25 ± 0.10	0.93 ± 0.09	1.01 ± 0.06
Caudate nucleus	6.88 ± 0.62	8.06 ± 1.17	7.33 ± 1.18
Putamen	3.55 ± 0.75	4.38 ± 1.04	4.42 ± 0.60
5-HT$_4$ (P = 0.03[a])			
Frontal cortex	1.71 ± 0.28	2.01 ± 0.13	2.23 ± 0.53
Hippocampus	11.96 ± 2.35	14.76 ± 2.08	16.04 ± 1.11
Putamen	15.62 ± 1.16	17.30 ± 1.37	18.21 ± 0.74
Nucleus accumbens	35.86 ± 1.72	47.83 ± 6.00*	49.03 ± 3.04**
Caudate nucleus	25.08 ± 1.17	24.23 ± 0.33	23.77 ± 1.70
Substantia nigra	40.46 ± 3.52	40.61 ± 2.06	40.86 ± 1.74
SERT (N.S.)			
Frontal cortex	3.59 ± 0.52	4.68 ± 0.28	3.60 ± 0.05
Caudate nucleus	4.71 ± 0.21	5.05 ± 0.99	4.53 ± 1.29
Putamen	8.02 ± 0.48	9.54 ± 0.27	7.87 ± 0.92
Hippocampus	0.47 ± 0.22	0.61 ± 0.43	0.83 ± 0.46

*$p<0.01$ and **$p<0.001$ Bonferroni corrected post-tests for differences in mean vs. control.[a]Indicate significant main-effect of treatment on mean.

In contrast to the absent effects of the pCPA treatment on other 5-HT markers, the abundance of 5-HT$_4$ receptor binding sites labeled with [^{3}H]SB207145 was significantly increased the in the nucleus accumbens of the pig brain, and therefore, it seems that the 5-HT$_4$ receptor is more sensitive to 4 days serotonin depletion in comparison to 5-HT$_{1A}$ and 5-HT$_{2A}$ receptors. In rats treated with 5,7-DHT (Compan et al., 1996) or pCPA/fenfluramine (Licht et al., 2009), serotonin depletion is also associated with increases in cerebral 5-HT$_4$ receptor binding. In this study, sections were incubated with [^{3}H]SB207145 concentrations 4–6 times higher than K_d, such that the increase in 5-HT$_4$ receptor binding most likely is due to an increase in receptor number rather than an increase in affinity. The increased 5-HT$_4$ receptor levels is speculated to be a compensatory response to decreased serotonergic neurotransmission; this is in line with recently published data in rats where 2 and 3 weeks (but not 1 day) of SSRI treatment downregulated 5-HT$_4$ receptors across multiple brain regions (Licht et al., 2009). Only in the nucleus accumbens, however, we found a statistically significant negative correlation between 5-HT levels and 5-HT$_4$ receptor binding suggesting decreased 5-HT levels in this region downreregulates 5-HT$_4$ receptor binding. Optimally, this correlation should have been made between 5-HT measurements in nucleus accumbens and not the entire striatum of which nucleus accumbens is only part of. However, as the nucleus accumbens cannot be macroscopically reliably identified and dissected, the entire striatum was used as an index for the 5-HT levels in the nucleus accumbens. The restriction of statistical significance to this one brain region may be due to the lim-
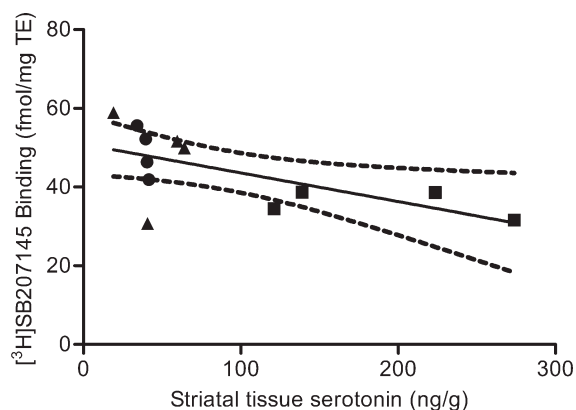
Fig. 3. Correlation between 5-HT$_4$ receptor binding in the nucleus accumbens and 5-HT levels in the striatum of the contralateral hemisphere. Each point represents one animal treated with 0 mg/kg (■), 50 mg/kg (▲), and 100 mg/kg (●) pCPA. Pearsons correlation coefficient is calculated at *$P = 0.014$.

ited sample size. Taken together, our findings suggest that the 5-HT$_4$ receptor is particularly susceptible to subchronic changes in 5-HT levels.

In conclusion, this study is the first to validate an approach for serotonin depletion in the pig brain and also to describe the regional distribution of 5-HT$_{1A}$ and 5-HT$_{2A}$ receptors in the pig brain. We show that 5-HT$_4$ receptor binding is significantly increased in this model, whereas 5-HT$_{1A}$, 5-HT$_{2A}$, and SERT binding is unaffected by the treatment. This provides an excellent setting for future studies of serotonergic neurotransmission regulations in the pig brain using both in vitro and in vivo methods.

REFERENCES

Barnes NM, Sharp T. 1999. A review of central 5-HT receptors and their function. Neuropharmacology 38:1083–1152.

Burnet PW, Eastwood SL, Harrison PJ. 1997. [3H]WAY-100635 for 5-HT1A receptor autoradiography in human brain: A comparison with [3H]8-OH-DPAT and demonstration of increased binding in the frontal cortex in schizophrenia. Neurochem Int 30:565–574.

Cahir M, Ardis T, Reynolds GP, Cooper SJ. 2007. Acute and chronic tryptophan depletion differentially regulate central 5-HT1A and 5-HT 2A receptor binding in the rat. Psychopharmacology (Berl) 190:497–506.

Chalon S, Bronquard C, Vercouillie J, Kodas E, Garreau L, Bodard S, Emond P, Besnard JC, Guilloteau D. 2004. ADAM is an effective tool for in vivo study of serotonergic function: Validation in rat models. Synapse 52:136–142.

Compan V, Daszuta A, Salin P, Sebben M, Bockaert J, Dumuis A. 1996. Lesion study of the distribution of serotonin 5-HT4 receptors in rat basal ganglia and hippocampus. Eur J Neurosci 8:2591–2598.

Compan V, Segu L, Buhot MC, Daszuta A. 1998. Differential effects of serotonin (5-HT) lesions and synthesis blockade on neuropeptide-Y immunoreactivity and 5-HT1A, 5-HT1B/1D and 5-HT2A/2C receptor binding sites in the rat cerebral cortex. Brain Res 795:264–276.

Cumming P, Kretzschmar M, Brust P, Smith DF. 2001. Quantitative radioluminography of serotonin uptake sites in the porcine brain. Synapse 39:351–355.

Cumming P, Moller M, Benda K, Minuzzi L, Jakobsen S, Jensen SB, Pakkenberg B, Stark AK, Gramsbergen JB, Andreasen MF, Olsen AK. 2007. A PET study of effects of chronic 3,4-methylene-dioxymethamphetamine (MDMA, "ecstasy") on serotonin markers in Gottingen minipig brain. Synapse 61:478–487.

Datla KP, Curzon G. 1996. Effect of p-chlorophenylalanine at moderate dosage on 5-HT and 5-HIAA concentrations in brain regions of control and p-chloroamphetamine treated rats. Neuropharmacology 35:315–320.

Delgado PL, Charney DS, Price LH, Aghajanian GK, Landis H, Heninger GR. 1990. Serotonin function and the mechanism of antidepressant action. Reversal of antidepressant-induced remission by rapid depletion of plasma tryptophan. Arch Gen Psychiatry 47:411–418.

Felix B, Leger ME, Albe-Fessard D, Marcilloux JC, Rampin O, Laplace JP. 1999. Stereotaxic atlas of the pig brain. Brain Res Bull 49:1–137.

Fischette CT, Nock B, Renner K. 1987. Effects of 5,7-dihydroxy-tryptamine on serotonin1 and serotonin2 receptors throughout the rat central nervous system using quantitative autoradiography. Brain Res 421:263–279.

Fusar-Poli P, Allen P, McGuire P, Placentino A, Cortesi M, Perez J. 2006. Neuroimaging and electrophysiological studies of the effects of acute tryptophan depletion: A systematic review of the literature. Psychopharmacology (Berl) 188:131–143.

Gobbi M, Regondi MC, Pompeiano M, Palacios JM, Mennini T. 1994. Differential effects of 5,7-dihydroxytryptamine-induced serotoninergic degeneration of 5-HT1A receptors and 5-HT uptake sites in the rat brain. J Chem Neuroanat 7:65–73.

Gradwell PB, Everitt BJ, Herbert J. 1975. 5-Hydroxytryptamine in the central nervous system and sexual receptivity of female rhesus monkeys. Brain Res 88:281–293.

Hall H, Lundkvist C, Halldin C, Farde L, Pike VW, McCarron JA, Fletcher A, Cliffe IA, Barf T, Wikstrom H, Sedvall G. 1997. Autoradiographic localization of 5-HT1A receptors in the post-mortem human brain using [3H]WAY-100635 and [11C]way-100635. Brain Res 745:96–108.

Hall H, Farde L, Halldin C, Lundkvist C, Sedvall G. 2000. Autoradiographic localization of 5-HT(2A) receptors in the human brain using [(3)H]M100907 and [(11)C]M100907. Synapse 38:421–431.

Jans LA, Riedel WJ, Markus CR, Blokland A. 2007. Serotonergic vulnerability and depression: Assumptions, experimental evidence and implications. Mol Psychiatry 12:522–543.

King MV, Marsden CA, Fone KC. 2008. A role for the 5-HT(1A), 5-HT4 and 5-HT6 receptors in learning and memory. Trends Pharmacol Sci 29:482–492.

Koe BK, Weissman A. 1966. p-Chlorophenylalanine: A specific depletor of brain serotonin. J Pharmacol Exp Ther 154:499–516.

Kornum BR, Licht CL, Weikop P, Knudsen GM, Aznar S. 2006. Central serotonin depletion affects rat brain areas differently: A qualitative and quantitative comparison between different treatment schemes. Neurosci Lett 392:129–134.

Kornum BR, Lind NM, Gillings N, Marner L, Andersen F, Knudsen GM. 2009. Evaluation of the novel 5-HT4 receptor PET ligand [11C]SB207145 in the Gottingen minipig. J Cereb Blood Flow Metab 29:186–196.

Kristiansen H, Elfving B, Plenge P, Pinborg LH, Gillings N, Knudsen GM. 2005. Binding characteristics of the 5-HT2A receptor antagonists altanserin and MDL 100907. Synapse 58:249–257.

Licht CL, Marcussen AB, Wegener G, Overstreet DH, Aznar S, Knudsen GM. 2009. The brain 5-HT4 receptor binding is down-regulated in the flinders sensitive line depression model and in response to paroxetine administration. J Neurochem 109:1363–1374.

Lind NM, Moustgaard A, Jelsing J, Vajta G, Cumming P, Hansen AK. 2007. The use of pigs in neuroscience: Modeling brain disorders. Neurosci Biobehav Rev 31:728–751.

Lopez-Gimenez JF, Mengod G, Palacios JM, Vilaro MT. 1997. Selective visualization of rat brain 5-HT2A receptors by autoradiography with [3H]MDL 100,907. Naunyn Schmiedebergs Arch Pharmacol 356:446–454.

Lopez-Gimenez JF, Vilaro MT, Palacios JM, Mengod G. 1998. [3H]MDL 100,907 labels 5-HT2A serotonin receptors selectively in primate brain. Neuropharmacology 37:1147–1158.

Lopez-Gimenez JF, Vilaro MT, Palacios JM, Mengod G. 2001. Mapping of 5-HT2A receptors and their mRNA in monkey brain: [3H]MDL100,907 autoradiography and in situ hybridization studies. J Comp Neurol 429:571–589.

McGregor IS, Clemens KJ, Van der PG, Li KM, Hunt GE, Chen F, Lawrence AJ. 2003. Increased anxiety 3 months after brief exposure to MDMA ("Ecstasy") in rats: Association with altered 5-HT transporter and receptor density. Neuropsychopharmacology 28:1472–1484.

Nielsen K, Brask D, Knudsen GM, Aznar S. 2006. Immunodetection of the serotonin transporter protein is a more valid marker for serotonergic fibers than serotonin. Synapse 59:270–276.

O'Connell MT, Portas CM, Sarna GS, Curzon G. 1991. Effect of p-chlorophenylalanine on release of 5-hydroxytryptamine from the rat frontal cortex in vivo. Br J Pharmacol 102:831–836.

O'Leary OF, Bechtholt AJ, Crowley JJ, Hill TE, Page ME, Lucki I. 2007. Depletion of serotonin and catecholamines block the acute behavioral response to different classes of antidepressant drugs in the mouse tail suspension test. Psychopharmacology (Berl) 192: 357–371.

Paxinos G, Burt J, Atrens DM, Jackson DM. 1977. 5-Hydroxytryptamine depletion with para-chlorophenylalanine: Effects on eating, drinking, irritability, muricide, and copulation. Pharmacol Biochem Behav 6:439–447.

Pike VW, Halldin C, Nobuhara K, Hiltunen J, Mulligan RS, Swahn CG, Karlsson P, Olsson H, Hume SP, Hirani E, Whalley J, Pilowsky LS, Larsson S, Schnell PO, Ell PJ, Farde L. 2003. Radioiodinated SB 207710 as a radioligand in vivo: Imaging of brain 5-HT4 receptors with SPET. Eur J Nucl Med Mol Imaging 30:1520–1528.

Rattray M, Baldessari S, Gobbi M, Mennini T, Samanin R, Bendotti C. 1996. p-Chlorophenylalanine changes serotonin transporter mRNA levels and expression of the gene product. J Neurochem 67:463–472.

Reneman L, Endert E, de Bruin K, Lavalaye J, Feenstra MG, de Wolff FA, Booij J. 2002. The acute and chronic effects of MDMA ("ecstasy") on cortical 5-HT2A receptors in rat and human brain. Neuropsychopharmacology 26:387–396.

Thomsen C, Helboe L. 2003. Regional pattern of binding and c-Fos induction by (R)- and (S)-citalopram in rat brain. Neuroreport 14:2411–2414.

Varnäs K, Halldin C, Pike VW, Hall H. 2003. Distribution of 5-HT4 receptors in the postmortem human brain—an autoradiographic study using [125I]SB 207710. Eur Neuropsychopharmacol 13:228–234.

Vodicka P, Smetana K Jr, Dvorankova B, Emerick T, Xu YZ, Ourednik J, Ourednik V, Motlik J. 2005. The miniature pig as an animal model in biomedical research. Ann N Y Acad Sci 1049:161–171.

Weikop P, Kehr J, Scheel-Kruger J. 2007. Reciprocal effects of combined administration of serotonin, noradrenaline and dopamine reuptake inhibitors on serotonin and dopamine levels in the rat prefrontal cortex: The role of 5-HT1A receptors. J Psychopharmacol 21:795–804.

Paper II

Ettrup A, Palner M, Gillings N, Santini MA, Hansen M, Kornum BR,
Rasmussen LK, Någren K, Madsen J, Begtrup M, Knudsen GM.

Radiosynthesis and evaluation of ^{11}C-CIMBI-5 as a high affinity
5-HT$_{2A}$ receptor agonist radioligand for PET.

Radiosynthesis and Evaluation of ^{11}C-CIMBI-5 as a 5-HT$_{2A}$ Receptor Agonist Radioligand for PET

Anders Ettrup[1], Mikael Palner[1], Nic Gillings[2], Martin A. Santini[1], Martin Hansen[3], Birgitte R. Kornum[1], Lars K. Rasmussen[3], Kjell Någren[2], Jacob Madsen[2], Mikael Begtrup[3], and Gitte M. Knudsen[1]

[1]Neurobiology Research Unit and Center for Integrated Molecular Brain Imaging (CIMBI), Copenhagen University Hospital, Rigshospitalet, Copenhagen, Denmark; [2]PET and Cyclotron Unit, Copenhagen University Hospital, Rigshospitalet, Copenhagen, Denmark;; and [3]Department of Medicinal Chemistry, Faculty of Pharmaceutical Sciences, University of Copenhagen, Copenhagen, Denmark

PET brain imaging of the serotonin 2A (5-hydroxytryptamine 2A, or 5-HT$_{2A}$) receptor has been widely used in clinical studies, and currently, several well-validated radiolabeled antagonist tracers are used for in vivo imaging of the cerebral 5-HT$_{2A}$ receptor. Access to 5-HT$_{2A}$ receptor agonist PET tracers would, however, enable imaging of the active, high-affinity state of receptors, which may provide a more meaningful assessment of membrane-bound receptors. In this study, we radiolabel the high-affinity 5-HT$_{2A}$ receptor agonist 2-(4-iodo-2,5-dimethoxyphenyl)-N-(2-[^{11}C-OCH$_3$]methoxybenzyl)ethanamine (^{11}C-CIMBI-5) and investigate its potential as a PET tracer. **Methods:** The in vitro binding and activation at 5-HT$_{2A}$ receptors by CIMBI-5 was measured with binding and phosphoinositide hydrolysis assays. Ex vivo brain distribution of ^{11}C-CIMBI-5 was investigated in rats, and PET with ^{11}C-CIMBI-5 was conducted in pigs. **Results:** In vitro assays showed that CIMBI-5 was a high-affinity agonist at the 5-HT$_{2A}$ receptor. After intravenous injections of ^{11}C-CIMBI-5, ex vivo rat studies showed a specific binding ratio of 0.77 ± 0.07 in the frontal cortex, which was reduced to cerebellar levels after ketanserin treatment, thus indicating that ^{11}C-CIMBI-5 binds selectively to the 5-HT$_{2A}$ receptor in the rat brain. The PET studies showed that the binding pattern of ^{11}C-CIMBI-5 in the pig brain was in accordance with the expected 5-HT$_{2A}$ receptor distribution. ^{11}C-CIMBI-5 gave rise to a cortical binding potential of 0.46 ± 0.12, and the target-to-background ratio was similar to that of the widely used 5-HT$_{2A}$ receptor antagonist PET tracer ^{18}F-altanserin. Ketanserin treatment reduced the cortical binding potentials to cerebellar levels, indicating that in vivo ^{11}C-CIMBI-5 binds selectively to the 5-HT$_{2A}$ receptor in the pig brain. **Conclusion:** ^{11}C-CIMBI-5 showed a cortex-to-cerebellum binding ratio equal to the widely used 5-HT$_{2A}$ antagonist PET tracer ^{18}F-altanserin, indicating that ^{11}C-CIMBI-5 has a sufficient target-to-background ratio for future clinical use and is displaceable by ketanserin in both rats and pigs. Thus, ^{11}C-CIMBI-5 is a promising tool for investigation of 5-HT$_{2A}$ agonist binding in the living human brain.

Serotonin 2A (5-hydroxytryptamine 2A, or 5-HT$_{2A}$) receptors are implicated in the pathophysiology of human diseases such as depression, Alzheimer's disease, and schizophrenia. Also, 5-HT$_{2A}$ receptor stimulation exerts the hallucinogenic effects of recreational drugs such as lysergic acid diethylamide and 1-(2,5-dimethoxy-4-iodophenyl)-2-aminopropane (1), and atypical antipsychotics have antagonistic or inverse agonistic effects on the 5-HT$_{2A}$ receptor (2).

Currently, there are 3 selective 5-HT$_{2A}$ antagonistic PET ligands—^{18}F-altanserin (3), ^{18}F-deuteroaltanserin (4), and ^{11}C-MDL100907 (5)—in use for mapping and quantifying 5-HT$_{2A}$ receptor binding in the human brain. However, whereas 5-HT$_{2A}$ antagonists bind to the total pool of receptors, 5-HT$_{2A}$ agonists bind only to the high-affinity state of the receptor (6,7). Thus, a 5-HT$_{2A}$ receptor agonist ligand holds promise for the selective mapping of 5-HT$_{2A}$ receptors in their functional state; therefore, alterations in agonist binding measured in vivo with PET may be more relevant for assessing dysfunction in the 5-HT$_{2A}$ receptor system in specific patient or population groups. Furthermore, because many of the 5-HT$_{2A}$ receptors are intracellularly localized (8,9), combining measurements with antagonist and agonist PET tracers would enable determination of the ratio of the high-affinity, membrane-bound, and active receptors to the low-affinity, intracellular, and inactive receptors (10). Thus, quantification of functionally active 5-HT$_{2A}$ receptors in vivo using an agonist PET tracer is hypothesized to be superior to antagonist measurements of total number of 5-HT$_{2A}$ receptors for studying alterations in receptor function in human diseases such as depression.

D$_2$ receptor agonist radiotracers are now known to be superior to antagonist radiotracers in measuring dopamine release in vivo in monkeys (11) and mice (10). In humans,

most studies have found that 5-HT_{2A} receptor antagonist PET tracers are not displaceable by elevated levels of endogenous serotonin (5-HT) (*12*). This suggests that agonist PET tracers may be better suited for measuring endogenous competition than antagonist tracers, so that 5-HT_{2A} receptor agonists would be more prone to displacement by competition with endogenously released 5-HT. Monitoring the release of endogenous 5-HT is highly relevant in relation to human diseases such as depression and Alzheimer's disease, which involve dysfunction of the 5-HT system.

2-(4-iodo-2,5-dimethoxyphenyl)-*N*-(2-methoxybenzyl) ethanamine (25I-NBOMe, or CIMBI [Center for Integrated Molecular Brain Imaging]-5) has recently been described as a potent and selective 5-HT_{2A} receptor agonist, and phosphoinositide hydrolysis assays revealed that it has a 12-fold lower half-maximal effective concentration (EC_{50}) than 5-HT itself (*13*). Although this compound has been tritiated (*14*), its in vivo biological distribution and possible PET tracer potential have not been investigated.

Here, we present the synthesis of ^{11}C-labeled CIMBI-5 and biological evaluation of this novel PET tracer. The compound was characterized in vitro, and ^{11}C-CIMBI-5 was investigated after intravenous injection both ex vivo in rats and in vivo in pigs with PET.

MATERIALS AND METHODS

In Vitro Binding and Activation

Inhibition constant (K_i) determinations against various neuroreceptors (Table 1) were provided by the Psychoactive Drug Screening Program (PDSP; experimental details are provided at http://pdsp.med.unc.edu/). In our laboratory, competition binding experiments were performed on a NIH-3T3 cell line (GF62) stably transfected with the rat 5-HT_{2A} receptor as previously described

[Table 1]

TABLE 1
PDSP Screening Result: Inhibition Constants (K_i) for CIMBI-5 Versus Serotonin and Other Receptors

Receptor	K_i (nM)
5-HT_{2A}	2.2 ± 0.1
5-HT_{2B}	2.3 ± 0.2
5-HT_{2C}	7.0 ± 1.0
5-HT_6	58 ± 17
5-HT_{1A}	85 ± 16
D_3	117 ± 14
α_{2C}	348 ± 17
D_4	647 ± 37
Serotonin transporter	$1,009 \pm 84$
α_{2A}	$1,106 \pm 206$
M_5	$1,381 \pm 231$
D_2	$1,600 \pm 333$
5-HT_7	$1,670 \pm 125$
5-HT_{5A}	$2,200 \pm 385$
D_1	$3,718 \pm 365$
5-HT_{1B}	$3,742 \pm 553$
Norepinephrine transporter	$4,574 \pm 270$
Dopamine transporter	$5,031 \pm 343$
D_5	$7,872 \pm 933$

(*15*) using 0.2 nM ^{3}H-MDL100907 (kindly provided by Prof. Christer Halldin) and 8 different concentrations of CIMBI-5 (1 μM to 1 pM) in a total of 1 mL of buffer (500 mM Tris base, 1,500 mM NaCl, and 200 mM ethylenediaminetetraacetic acid). Nonspecific binding was determined with 1 μM ketanserin. Incubation was performed for 1 h at 37°C.

The 5-HT_{2A} receptor activation by CIMBI-5 was measured on GF62 cells using a phosphoinositide hydrolysis assay as previously described (*16*). Briefly, cells were incubated with myo-(*1,2*)-^{3}H-inositol (Amersham) in labeling medium. Subsequently, the cells were washed and incubated at 37°C with CIMBI-5 (1 μM to 0.1 pM). The formed inositol phosphates were extracted and counted with a liquid scintillation counter.

Radiochemical Synthesis of ^{11}C-CIMBI-5

^{11}C-methyl trifluoromethanesulfonate (triflate) produced using a fully automated system was transferred in a stream of helium to a 1.1-mL vial containing 0.3–0.4 mg of the labeling precursor (**3**; Fig. 1) and 2 μL of 2 M NaOH in 300 μL of acetonitrile, and the [**Fig. 1**] resulting mixture was heated at 40°C for 30 s. Subsequently, 250 μL of trifluoroacetic acid:CH$_3$CN (1:1) were added and the mixture heated at 80°C for 5 min (Fig. 2). After neutralization [**Fig. 2**] with 750 μL of 2 M NaOH, the reaction mixture was purified by high-performance liquid chromatography (HPLC) on a Luna C18 column (Phenomenex Inc.) (250 × 10 mm; 40:60 acetonitrile:25 mM citrate buffer, pH 4.7; and flow rate, 5 mL/min). The chemical synthesis of the labeling precursor is described in detail in the supplemental data (supplemental materials are available online only at http://jnm.snmjournals.org).

The fraction corresponding to the labeled product ($\sim$12.5 min) was collected in 50 mL of 0.1% ascorbic acid, and the resulting solution was passed through a solid-phase C18 Sep-Pak extraction column (Waters Corp.), which had been preconditioned with 10 mL of ethanol, followed by 20 mL of 0.1% ascorbic acid. The column was flushed with 3 mL of sterile water. Then, the trapped radioactivity was eluted with 3 mL of ethanol, followed by 3 mL of 0.1% ascorbic acid into a 20-mL vial containing 9 mL of phosphate buffer (100 mM, pH 7), giving a 15 mL solution of ^{11}C-CIMBI-5 with a pH of approximately 7. In a total synthesis time of 40–50 min, 1.5–2.5 GBq of ^{11}C-CIMBI-5 was produced, with radiochemical purity greater than 97% and specific radioactivity in the range 64–355 GBq/μmol. The lipophilicity of CIMBI-5 (cLogD$_{7.4}$ [log of calculated distribution coefficient, octanol/buffer pH 7.4]) was calculated using 2 different programs, which were in good agreement (CSLogD [ChemSilico], cLogD$_{7.4}$ = 3.33; Pallas 3.5 [CompuDrug Inc.], cLogD$_{7.4}$ = 3.21).

Ex Vivo Uptake in Rats

Twenty-two Sprague–Dawley rats (mean weight, 295 ± 53 g; Charles River) were included in the study. All animal experiments were performed in accordance with the European Communities Council Resolves of November 24, 1986 (86-609/ECC), and approved by the Danish State Research Inspectorate (journal no. 2007/561-1320). Rats were maintained on a 12-h light–dark cycle, with free access to food and water.

The ex vivo uptake and brain distribution were evaluated as previously described (*17*). Briefly, rats were injected in the tail vein with ^{11}C-CIMBI-5 (3.9 ± 3.5 MBq/kg; specific radioactivity, 30.9 GBq/μmol). The rats were decapitated at 5 ($n = 2$), 15 ($n = 2$), 30 ($n = 4$), 45 ($n = 2$), and 60 min ($n = 4$); the brains were quickly removed, placed on ice, and dissected into frontal cortex
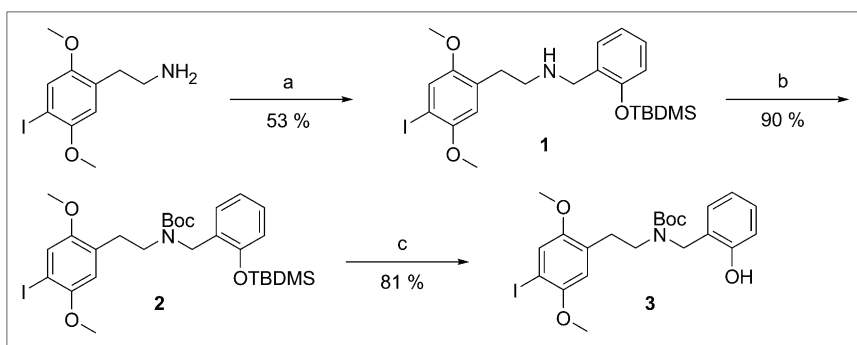
FIGURE 1. Synthesis of labeling precursor for ^{11}C-CIMBI-5 (*3*): (a) 2-(*tert*-butyldimethyl-silyloxy)benzaldehyde, NaBH$_4$, MeOH; (b) Boc$_2$O, THF; and (c) TBAF, NH$_4$Cl, THF. OTBDMS = t-butyldimethylsiloxy; THF = tetrahydrofuran.

(first 3 mm of the brain) and cerebellum. Blood from the trunk was collected immediately, and plasma was isolated by centrifugation (1,500 rpm, 10 min). All brain tissue samples were collected in tared counting vials and counted for 20 s in a γ-counter (Cobra 5003; Packard Instruments).

For ex vivo blocking studies, rats were divided in vehicle (saline) and ketanserin-treated groups ($n = 5–6$). Rats were intravenously injected with vehicle or 1 mg/kg of ketanserin (Sigma) 45 min before tracer administration. ^{11}C-CIMBI-5 was injected in the tail vein, and after 30 min, the rats were decapitated. Brain regions and plasma were extracted and counted.

PET in Pigs

Six female Danish Landrace Pigs were used in this study (mean weight, 17.8 ± 1.4 kg). After arrival, animals were housed under standard conditions and were allowed to acclimatize for 1 wk before scanning. On the scanning day, pigs were tranquilized by intramuscular injection of 0.5 mg/kg of midazolam. Anesthesia was induced by 0.1 mL/kg intramuscular injections of Zoletil veterinary mixture (Virbac Animal Health; 125 mg of tiletamine and 125 mg of zolazepam in 8 mL of 5 mg/mL midazolam). After induction, anesthesia was maintained by a 10 mg/kg/h intravenous infusion of propofol (B. Braun Melsugen AG). During anesthesia, animals were endotracheally intubated and ventilated (volume, 250 mL; frequency, 15 per min). Venous access was granted through 2 Venflons (Becton Dickinson) in the peripheral milk veins, and an arterial line for blood sampling measurement was obtained by a catheter in the femoral artery after a minor incision. Vital signs including blood pressure, temperature, and heart rate were monitored throughout the duration of the PET scan. Immediately after scanning, animals were sacrificed by intravenous injection of pentobarbital–lidocaine. All animal procedures were approved by the Danish Council for Animal Ethics (journal no. 2006/561-1155).

PET Protocol

In 5 pigs, ^{11}C-CIMBI-5 was given as intravenous bolus injections, and the pigs were subsequently PET-scanned for 90 min in list mode with a high-resolution research tomography scanner
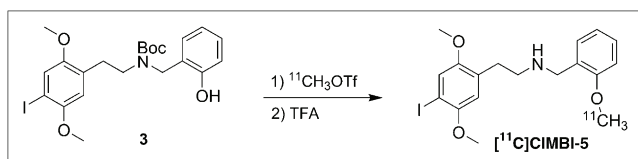
FIGURE 2. Radiochemical synthesis of ^{11}C-CIMBI-5. OTf = triflate; TFA = trifluoroacetic acid.

(Siemens AG). Scanning began at the time of injection. After the baseline scan, 3 pigs were maintained in anesthesia and scanned a second time using the same PET protocol. The 5-HT$_{2A}$ receptor antagonist ketanserin tartrate (Sigma) was administered at 30 min before the second scan (3 mg/kg bolus, followed by 1 mg/kg/h infusion for the duration of the scan). For all ^{11}C-CIMBI-5 PET scans, the injected radioactivity was on average 238 MBq (range, 96–418 MBq; $n = 9$), the specific radioactivity at the time of injection was 75 GBq/μmol (range, 28–133 GBq/μmol; $n = 9$), the average injected mass was 1.85 μg (range, 0.37–5.49 μg; $n = 9$), and there were no significant differences in these parameters between the baseline and blocked scans. In 2 pigs, arterial whole-blood samples were taken throughout the entire scan. During the first 15 min after injection, radioactivity in whole blood was continuously measured using an ABSS autosampler (Allogg Technology) counting coincidences in a lead-shielded detector. Concurrently, blood samples were manually drawn at 2.5, 5, 10, 20, 30, 50, 70, and 90 min, and the radioactivity in whole blood and plasma was measured using a well counter (Cobra 5003; Packard Instruments) that was cross-calibrated to the high-resolution research tomography scanner and autosampler. Also, radiolabeled parent compound and metabolites were measured in plasma as in the "HPLC Analysis of Pig Plasma and Pig Brain Tissue" section.

The free fraction of ^{11}C-CIMBI-5 in plasma, f_p, was estimated using an equilibrium dialysis chamber method as previously described (*18*). Briefly, the dialysis was conducted in chambers (Harvard Biosciences) separated by a cellulose membrane with a protein cutoff of 10,000 Da. Small amounts of ^{11}C-CIMBI-5 (~10 MBq) were added to a 5-mL plasma sample from the pig. Plasma (500 μL) was then dialyzed at 37°C against an equal volume of buffer (135 mM NaCl, 3.0 mM KCl, 1.2 mM CaCl$_2$, 1.0 mM MgCl$_2$, and 2.0 mM KH$_2$PO$_4$, pH 7.4). Counts per minute in 400 μL of plasma and buffer were determined in a well counter after various dialysis times, and f_p of ^{11}C-CIMBI-5 was calculated as counts per minute in buffer divided by counts per minute in plasma. The samples were taken from the dialysis chambers after equilibrium had been obtained between the 2 chambers.

HPLC Analysis of Pig Plasma and Pig Brain Tissue

Whole-blood samples (10 mL) drawn during PET were centrifuged (3,500 rpm, 4 min), and the plasma was passed through a 0.45-μm filter before HPLC analysis with online radioactivity detection, as previously described (*19*).

Also, the presence of radioactive metabolites of ^{11}C-CIMBI-5 in the pig brain was investigated. Twenty-five minutes after intravenous injection of approximately 500 MBq of ^{11}C-CIMBI-5, the pig was killed by intravenous injection of pentobarbital and

decapitated, and the brain was removed. At the same time, a blood sample was drawn manually. Within 30 min of decapitation, brain tissue was homogenized in 0.1N perchloric acid (Bie and Bentsen) saturated with sodium–ethylenediaminetetraacetic acid (Sigma) for 2×30 s using a Polytron homogenizer (Kinematica, Inc.). After centrifugation, the supernatant was neutralized using phosphate buffer, filtered (0.45 μm), and analyzed by HPLC. A plasma sample taken at the time of decapitation was analyzed concurrently.

Quantification of PET Data

Ninety-minute high-resolution research tomography, list-mode PET data were reconstructed into 38 dynamic frames of increasing length (6×10, 6×20, 4×30, 9×60, 3×120, 6×300, and 4×600 s). Images consisted of 207 planes of 256×256 voxels of $1.22 \times 1.22 \times 1.22$ mm. A summed image of all counts in the 90-min scan was reconstructed for each pig and used for coregistration to a standardized MRI-based statistical atlas of the Danish Landrace pig brain, similar to that previously reported for the Göttingen minipig (20), using the program Register as previously described (18). The temporal radioactivity in volumes of interest (VOIS), including the cerebellum, cortex (defined in the MRI-based atlas as entire cortical gray matter), hippocampus, lateral and medial thalamus, caudate nucleus, and putamen, was calculated. Radioactivity in all VOIs was calculated as the average of radioactive concentration (Bq/mL) in the left and right sides. Outcome measure in the time–activity curves was calculated as radioactive concentration in VOI (in kBq/mL) normalized to the injected dose corrected for animal weight (in kBq/g), yielding standardized uptake values (g/mL).

In 1 pig in which full arterial input function, including metabolite correction, was measured, we calculated ^{11}C-CIMBI-5 distribution volumes (V_T) for VOIs based on either 1-tissue- or 2-tissue-compartment models (1TC or 2TC, respectively) using plasma corrected for parent compound as the arterial input function (Supplemental Table 1). Cortical nondisplaceable binding potential (BP_{ND}) was calculated as $BP_{ND} = V_T/V_{ND} - 1$ (21), assuming that specific 5-HT$_{2A}$ receptor binding in the cerebellum was negligible and that the nondisplaceable volume of distribution (V_{ND}) was equal to the cerebellar V_T (3). For all 5 pigs, BP_{ND} was also calculated with the simplified reference tissue model (SRTM) (22), both at baseline and in the ketanserin-blocked condition, with the cerebellum as the reference region (Supplemental Table 1). Kinetic modeling was done with PMOD software (version 3.0; PMOD Technologies Inc.). Goodness of fit was evaluated using the Akaike information criterion.

Statistical Analysis

All statistical tests were performed using Prism (version 5.0; GraphPad Software). P values below 0.05 were considered statistically significant. Results are expressed in mean $\pm$ SD unless otherwise stated.

RESULTS

Chemistry

The labeling precursor was synthesized in 3 steps (Fig. 1): reductive amination with t-butyldimethylsilyl–protected salicylaldehyde, followed by *tert*-butoxycarbonyl (Boc) protection of the secondary amine and removal of the t-butyldimethylsilyl group, which gave the labeling precursor (**3**). Synthesis of the reference compound has been described previously (13).

In Vitro Binding Affinity

CIMBI-5 had the highest affinity for the 5-HT$_{2A}$ receptor, in agreement with previous studies (14). Between the subtypes of the 5-HT$_2$ receptors, CIMBI-5 did not show a higher affinity toward 5-HT$_{2A}$ receptors than it did toward 5-HT$_{2B}$ receptors; however, approximately a 3-fold higher affinity of CIMBI-5 for 5-HT$_{2A}$ receptors than for 5-HT$_{2C}$ receptors was found. Against targets other than 5-HT$_2$ receptors, CIMBI-5 showed at least a 30-fold lower affinity for any other of the investigated receptors than for 5-HT$_{2A}$ receptors (Table 1). In vitro binding assays conducted in our laboratory determined K_i of CIMBI-5 against 2 nM ^{3}H-MDL100907 at 1.5 ± 0.7 nM, thus confirming nanomolar affinity of CIMBI-5 for 5-HT$_{2A}$ receptors.

In Vitro Functional Characterization

The functional properties of CIMBI-5 toward the 5-HT$_{2A}$ receptor were assessed by measuring its effect on phosphoinositide hydrolysis in GF62 cells overexpressing the 5-HT$_{2A}$ receptor. CIMBI-5 was found to be an agonist with an EC$_{50}$ of 1.02 ± 0.17 nM (Supplemental Fig. 1), in agreement with previous reports (13). Pretreatment with 1 μM ketanserin completely inhibited CIMBI-5–induced phosphoinositide hydrolysis (data not shown). Furthermore, CIMBI-5 showed $84.6\% \pm 1.9\%$ of the 5-HT$_{2A}$ activation achieved by 10 μM 5-HT, demonstrating that CIMBI-5 functioned nearly as a full agonist.

Ex Vivo Distribution in Rats

After injection of ^{11}C-CIMBI-5 in awake rats, the time–activity curves measured as standardized uptake values showed highest uptake in the frontal cortex, whereas uptake in the cerebellum (equivalent to nondisplaceable uptake) was lower and paralleled the plasma time–activity curve. The brain uptake peaked in all regions at 15 min after injection and thereafter slowly declined (data not shown).

The specific binding ratio (SBR) in the frontal cortex region of interest, calculated as SBR = (region of interest − cerebellum)/cerebellum, peaked 30 min after injection, reaching a level of 0.77 ± 0.07, after which the SBR slowly declined (Fig. 3A). Thus, 30 min after injection was chosen [Fig. 3] as a reference time point and used in the blocking experiment with ketanserin. Ketanserin pretreatment reduced the SBR in the frontal cortex to levels not significantly different from zero (0.076 ± 0.12) (Fig. 3B).

In Vivo Distribution and Ketanserin Blockade in Pig Brain

[11]C-CIMBI-5 showed high cortical uptake in vivo in the pig brain with PET, medium uptake in striatal and thalamic regions, and low uptake in the cerebellum (Fig. 4). Furthermore, the time–activity curves demonstrated a substantial separation between the cortical and cerebellar time–activity curves (Fig. 5A). The time–activity curves peaked at approximately 10 min after injection and thereafter decreased, implying that ^{11}C-CIMBI-5 binding is reversible over the 90-min scan time used in this study. [Fig. 4] [Fig. 5]
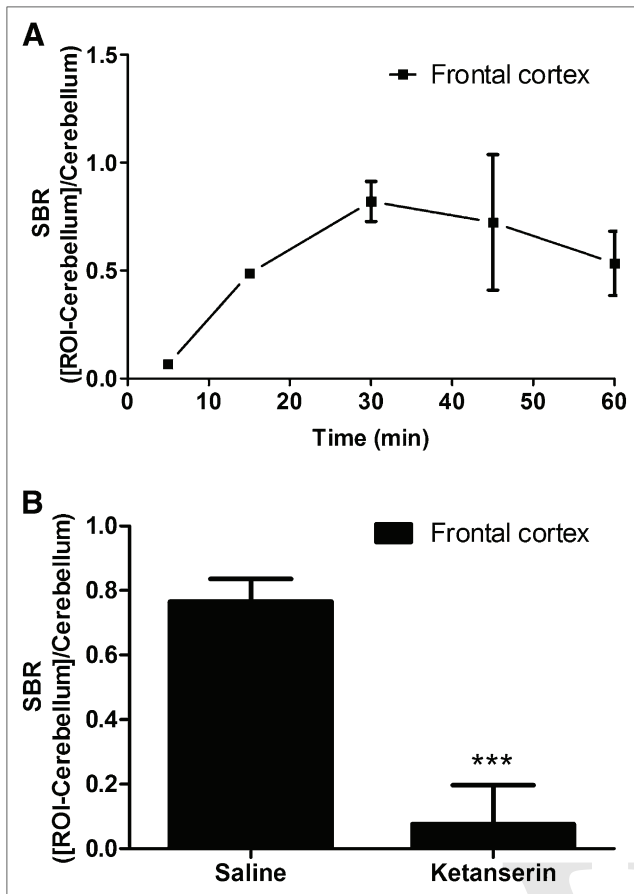
FIGURE 3. Time-dependent ex vivo distribution of ^{11}C-CIMBI-5 and displacement by ketanserin. (A) SBRs in frontal cortex in rats are shown relative to time after injection. (B) After ketanserin pretreatment (1 mg/kg intravenously), SBR in frontal cortex at 30 min after ^{11}C-CIMBI-5 injection is significantly decreased. ***$P < 0.0001$ in Student t test of ketanserin vs. saline. ROI = region of interest.

After ketanserin treatment, the concentration of ^{11}C-CIMBI-5 in the cortex was reduced almost completely to cerebellar levels (Fig. 5A). The cerebellar time–activity curve was unaltered by ketanserin administration (Fig. 5A).

Kinetic Modeling

With the SRTM, baseline cortical BP_{ND} of ^{11}C-CIMBI-5 was 0.46 ± 0.11 ($n = 5$). After the ketanserin bolus and infusion, the cortical BP_{ND} was significantly decreased by 75% (mean blocked BP_{ND}, 0.11 ± 0.06; $n = 3$). For the fitted SRTM, no significant difference in goodness of fit was found between baseline and blocked condition (Supplemental Table 1). In 1 pig in which full metabolite-corrected arterial input was measured, V_T was calculated from 1TC and 2TC models. Ratios between V_T in the cortex and cerebellum were 1.57 and 1.61, corresponding to a BP_{ND} of 0.57 and 0.61 with the 1TC and 2TC model, respectively. After ketanserin blockade, cortical ^{11}C-CIMBI-5 BP_{ND} was reduced to 0.13 and 0.11 in the 1TC and 2TC, respectively (Supplemental Table 1).

RGB
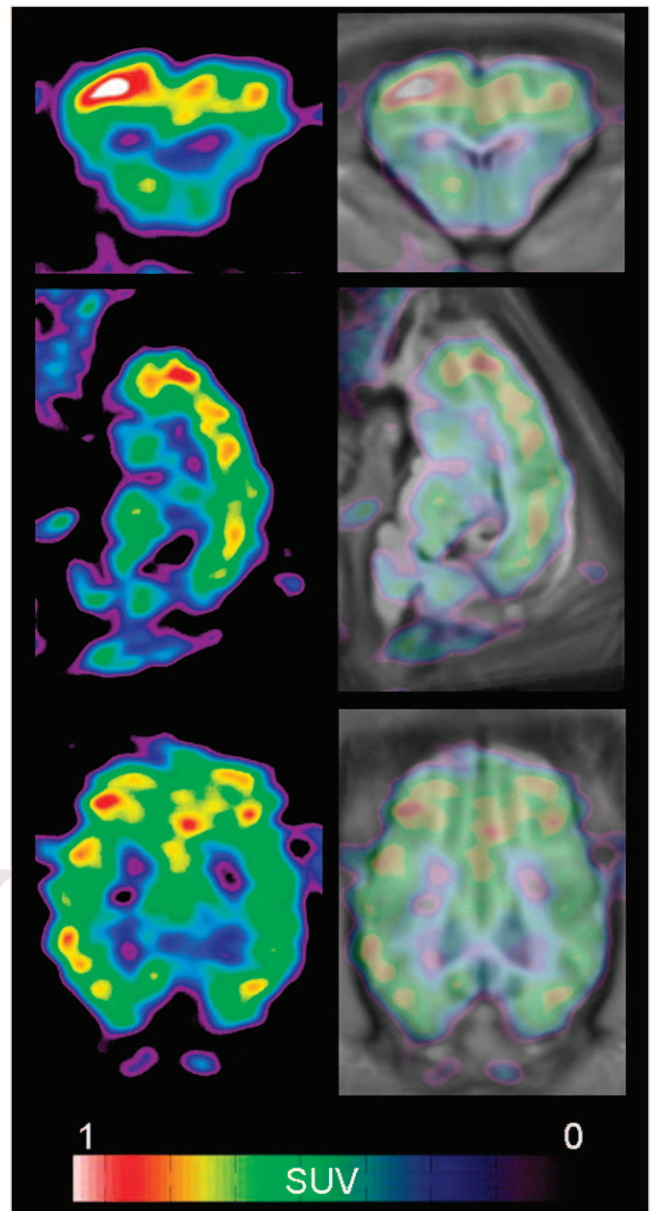
FIGURE 4. Representative coronal (top), sagittal (middle), and horizontal (bottom) PET images summed from 0 to 90 min of scanning showing distribution of ^{11}C-CIMBI-5 in pig brain. Left column shows PET images after $3 \times 3 \times 3$ mm gaussian filtering. Right column shows same PET images aligned and overlaid on a standardized MRI-based atlas of the pig brain after coregistration. SUV = standardized uptake value.

Radiolabeled Metabolites

In the radio-HPLC analysis, a lipophilic radioactive metabolite accounting for up to 20% of the total plasma radioactivity was found, and it maintained stable plasma levels after 20 min and throughout the scan (Fig. 6). The HPLC retention time of [**Fig. 6**] ^{11}C-CIMBI-5 and its metabolite in the HPLC column suggest that the metabolite is slightly less lipophilic than ^{11}C-CIMBI-5 itself (Fig. 7). However, this metabolite was found only in [**Fig. 7**] negligible amounts in homogenized pig brain tissue, compared with plasma from the same animal (Fig. 7).

FIGURE 6. HPLC analysis of radioactive metabolites in pig plasma after intravenous injection of ^{11}C-CIMBI-5. ■ = parent compound ^{11}C-CIMBI-5; ▼ = lipophilic metabolite; ● = polar metabolites.

FIGURE 5. Time–activity curves of 5-HT$_{2A}$ agonist and antagonist PET tracers in pig brain. (A) ^{11}C-CIMBI-5 time–activity curves in Danish Landrace pig brain at baseline (black solid line) or after intravenous ketanserin (3 mg/kg bolus, 1 mg/kg/h infusion) blockade (gray dotted line). (B) ^{18}F-altanserin time–activity curves in minipigs. Mean standardized uptake values normalized to injected dose per body weight are shown. SUV = standardized uptake value.

The free fraction of ^{11}C-CIMBI-5 in pig plasma at 37°C was 1.4% ± 0.3% using a dialysis chamber method, in which equilibrium between chambers was reached after 60 min.

DISCUSSION

In the current study, we report the in vitro, ex vivo, and in vivo validation of ^{11}C-CIMBI-5, a novel 5-HT$_{2A}$ receptor agonist PET tracer. To our knowledge, this is the first ago-nist 5-HT$_{2A}$ receptor PET tracer that has been developed. In vitro assays performed at our laboratory, along with assays performed through the PDSP screening program, confirmed the nanomolar affinity of CIMBI-5 for the 5-HT$_{2A}$ receptor as previously reported (13,14). In the current study, the K$_i$ for CIMBI-5 against ^{3}H-MDL100907 was 1.5 ± 0.7 nM, in agreement with the PDSP value of 2.2 nM for K$_i$ of CIMBI-5 against ^{3}H-ketanserin. The somewhat lower value (K$_i$ = 0.15 nM against ^{3}H-ketanserin) previously reported (13) may have been because that assay was performed at 25° C, whereas the values reported here were obtained at 37°C. We also confirmed that CIMBI-5 has agonistic properties at the 5-HT$_{2A}$ receptor, with an EC$_{50}$ value of 1.02 ± 0.17 nM, in agreement with previous reports (13). In addition, we showed that CIMBI-5 is nearly a full agonist, with 85% of the 5-HT$_{2A}$ activation, compared with 5-HT itself. The data on binding and receptor activation, taken together with the PDSP screening for CIMBI-5 (Table 1), show that CIMBI-5 is a high-affinity agonist for 5-HT$_{2A}$ receptors. CIMBI-5 had an affinity similar to that of the 5-HT$_{2A}$ and the 5-HT$_{2B}$ receptors and a 3-fold lower affinity to 5-HT$_{2C}$ receptor. The eventual presence and distribution of 5-HT$_{2B}$ receptors in the brain is still questionable, and specific 5-HT$_{2B}$ receptor binding in the brain has to our knowledge not yet been demonstrated. For 5-HT$_{2C}$ receptors, density of this subtype of receptors in cortical areas, compared with density of 5-HT$_{2A}$ receptors, is negligible (23,24). Therefore, the cortical ^{11}C-CIMBI-5 binding signal stems from its 5-HT$_{2A}$ receptor binding.

^{11}C-CIMBI-5 uptake and distribution in the rat brain after ex vivo dissection were similar to those in previous rat studies with ^{18}F-altanserin (25), showing high uptake in the frontal cortex and no displaceable binding in the cerebellum. Also, the specific uptake in the frontal cortex of the rat brain was blocked by ketanserin pretreatment, indicating that ^{11}C-CIMBI-5 binding is selective for the 5-HT$_{2A}$ receptor. Similarly, ^{11}C-CIMBI-5 distributed in the pig

jnm074021-pm ■ 10/8/10
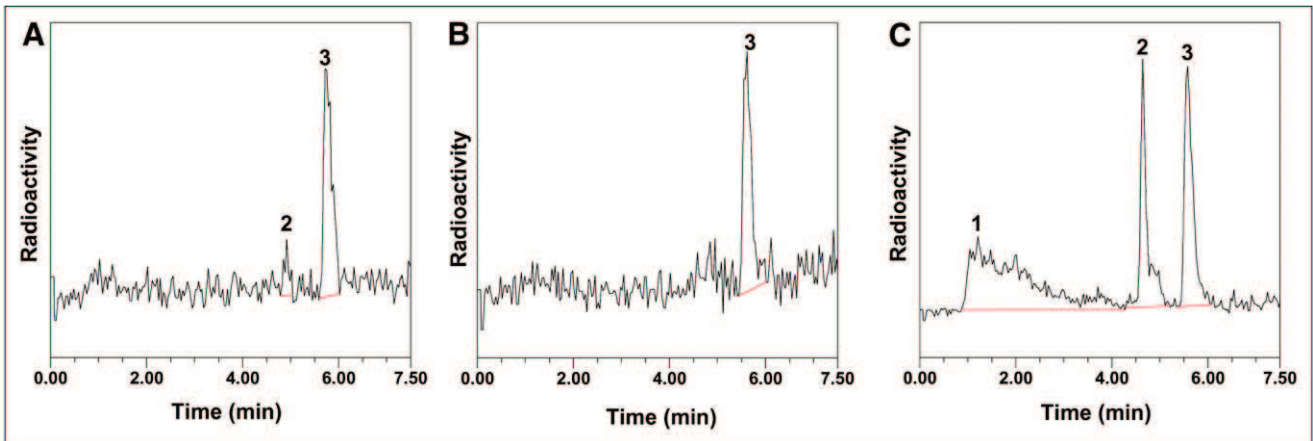
FIGURE 7. HPLC analysis of brain extracts and plasma at 25 min after injection of ^{11}C-CIMBI-5: frontal cortex (A), cerebellum (B), and plasma (C). Peaks: 1 = polar metabolites, 2 = lipophilic metabolites, and 3 = parent compound.

brain in a pattern resembling the 5-HT$_{2A}$ receptor distribution as measured with 5-HT$_{2A}$ receptor antagonist PET tracers in pigs (*25*) and in humans (*5,26*), with high cortical uptake and low cerebellar uptake. Further, the 5-HT$_{2A}$ selectivity of in vivo cortical ^{11}C-CIMBI-5 binding in the pig was confirmed in the blocking study in which cortical ^{11}C-CIMBI-5 binding was decreased by a ketanserin bolus and infusion, whereas the cerebellar uptake was unaffected.

BP$_{ND}$ for ^{11}C-CIMBI-5 with the cerebellum as a reference region was calculated using compartmental models, reference tissue approaches, and noninvasive Logan methods (Supplemental Table 1). For 5-HT$_{2A}$ receptor antagonist PET tracers, such as ^{18}F-altanserin, the cerebellum is generally regarded as a valid reference region (*3*). Also, because negligible amounts of 5-HT$_{2A}$ receptors are present in the cerebellum, compared with cortical areas, the preferential binding of a 5-HT$_{2A}$ receptor PET ligand, as measured, for example, by the SRTM BP$_{ND}$, is indicative of the target-to-background ratio of 5-HT$_{2A}$ PET ligands. At baseline, ^{11}C-CIMBI-5 showed an average SRTM BP$_{ND}$ of 0.46. Given that an agonist PET tracer, compared with the antagonist, would bind only a high-affinity subpopulation of 5-HT$_{2A}$ receptors, the maximum number of binding sites for such an agonist tracer would be lower than the antagonist, and—given that the radioligand affinities are comparable—it is anticipated that a lower BP$_{ND}$ for an agonist tracer would be found. When compared with human data from 5-HT$_{2A}$ receptor antagonist PET tracers (*5,26*), the cortical binding potential of ^{11}C-CIMBI-5 was indeed lower, but further studies are required to explore whether the somewhat low binding potential measured in pigs will translate to humans.

To compare the time–activity curves for ^{11}C-CIMBI-5 to a known 5-HT$_{2A}$ antagonist PET tracer in the same animal species, we compared it to ^{18}F-altanserin pig data obtained from our laboratory (*25*). ^{11}C-CIMBI-5 and ^{18}F-altanserin in pigs showed similar cortex-to-cerebellum uptake and equal SRTM BP$_{ND}$, 0.46 ± 0.11 and 0.47 ± 0.10, respectively. Thus, in the pig brain ^{11}C-CIMBI-5 and ^{18}F-altanserin

have similar target-to-background binding ratios, and ^{11}C-CIMBI-5 therefore holds promise for clinical use.

After injection of ^{11}C-CIMBI-5, a radiolabeled metabolite only slightly less lipophilic than ^{11}C-CIMBI-5 appeared in the pig plasma. On the basis of previous studies describing the metabolism of the 5-HT$_{2A}$ receptor agonist compound 1-(2,5-dimethoxy-4-iodophenyl)-2-aminopropane (*27*) in rats, we speculated that this metabolite is the result of *O*-demethylation at a methoxy group in the iododimethoxyphenyl moiety of the tracer. Lipophilic radiolabeled metabolites impose a problem if they cross the blood–brain barrier because their presence will contribute to nonspecific binding. This has been observed for other antagonistic PET tracers in the serotonin system (*3*). Our brain homogenate experiments suggested that the lipophilic metabolite does not enter the pig brain, at least not to any large extent, and consequently the radiolabeled metabolite does not contribute to the nonspecific binding of ^{11}C-CIMBI-5.

Taken together, the results indicate that ^{11}C-CIMBI-5 is a promising tracer for visualization and quantification of high-affinity 5-HT$_{2A}$ receptor agonist binding sites using PET. More specifically, studies of ^{11}C-CIMBI-5 could reveal differences in the number of binding sites measured with an agonist versus antagonist tracer, thus giving insights to whether high- and low-affinity states of 5-HT$_{2A}$ receptors coexist in vivo as is described for the dopamine system (*28*). Optimally, a larger cortical BP$_{ND}$ and higher brain uptake of the PET tracer is preferred. Also, the time–activity curves of ^{11}C-CIMBI-5 suggested relatively slow kinetics, which potentially would be a more pronounced phenomenon in primates and humans complicating quantification. Therefore, it may be worthwhile to pursue development of ^{11}C-CIMBI-5 analogs with modified chemical structures to improve these PET tracer properties.

CONCLUSION

The novel high-affinity 5-HT$_{2A}$ receptor agonist PET tracer ^{11}C-CIMBI-5 distributes in the brain in a pattern compatible with the known 5-HT$_{2A}$ receptor distribution,

and its binding can be blocked by ketanserin treatment. ^{11}C-CIMBI-5 is a promising PET tracer for in vivo imaging and quantification of high-affinity-state 5-HT$_{2A}$ receptors in the human brain.

ACKNOWLEDGMENTS

REFERENCES

1. Gonzalez-Maeso J, Weisstaub NV, Zhou M, et al. Hallucinogens recruit specific cortical 5-HT$_{2A}$ receptor-mediated signaling pathways to affect behavior. *Neuron.* 2007;53:439–452.
2. Kim SW, Shin IS, Kim JM, et al. The 5-HT2 receptor profiles of antipsychotics in the pathogenesis of obsessive-compulsive symptoms in schizophrenia. *Clin Neuropharmacol.* 2009;32:224–226.
3. Pinborg LH, Adams KH, Svarer C, et al. Quantification of 5-HT2A receptors in the human brain using [18F]altanserin-PET and the bolus/infusion approach. *J Cereb Blood Flow Metab.* 2003;23:985–996.
4. Soares JC, van Dyck CH, Tan P, et al. Reproducibility of in vivo brain measures of 5-HT2A receptors with PET and [18F]deuteroaltanserin. *Psychiatry Res.* 2001;106:81–93.
5. Ito H, Nyberg S, Halldin C, Lundkvist C, Farde L. PET imaging of central 5-HT2A receptors with carbon-11-MDL 100,907. *J Nucl Med.* 1998;39:208–214.
6. Fitzgerald LW, Conklin DS, Krause CM, et al. High-affinity agonist binding correlates with efficacy (intrinsic activity) at the human serotonin 5-HT2A and 5-HT2C receptors: evidence favoring the ternary complex and two-state models of agonist action. *J Neurochem.* 1999;72:2127–2134.
7. Song J, Hanniford D, Doucette C, et al. Development of homogeneous high-affinity agonist binding assays for 5-HT2 receptor subtypes. *Assay Drug Dev Technol.* 2005;3:649–659.
8. Cornea-Hebert V, Watkins KC, Roth BL, et al. Similar ultrastructural distribution of the 5-HT$_{2A}$ serotonin receptor and microtubule-associated protein MAP1A in cortical dendrites of adult rat. *Neuroscience.* 2002;113:23–35.
9. Peddie CJ, Davies HA, Colyer FM, Stewart MG, Rodriguez JJ. Colocalisation of serotonin2A receptors with the glutamate receptor subunits NR1 and GluR2 in the dentate gyrus: an ultrastructural study of a modulatory role. *Exp Neurol.* 2008;211:561–573.
10. Cumming P, Wong DF, Gillings N, Hilton J, Scheffel U, Gjedde A. Specific binding of [11C]raclopride and N-[3H]propyl-norapomorphine to dopamine receptors in living mouse striatum: occupancy by endogenous dopamine and guanosine triphosphate-free G protein. *J Cereb Blood Flow Metab.* 2002;22:596–604.
11. Narendran R, Hwang DR, Slifstein M, et al. In vivo vulnerability to competition by endogenous dopamine: comparison of the D2 receptor agonist radiotracer (−)-N-[11C]propyl-norapomorphine ([11C]NPA) with the D2 receptor antagonist radiotracer [11C]-raclopride. *Synapse.* 2004;52:188–208.
12. Pinborg LH, Adams KH, Yndgaard S, et al. [18F]altanserin binding to human 5HT2A receptors is unaltered after citalopram and pindolol challenge. *J Cereb Blood Flow Metab.* 2004;24:1037–1045.
13. Braden MR, Parrish JC, Naylor JC, Nichols DE. Molecular interaction of serotonin 5-HT2A receptor residues Phe339(6.51) and Phe340(6.52) with superpotent N-benzyl phenethylamine agonists. *Mol Pharmacol.* 2006;70:1956–1964.
14. Nichols DE, Frescas SP, Chemel BR, Rehder KS, Zhong D, Lewin AH. High specific activity tritium-labeled N-(2-methoxybenzyl)-2,5-dimethoxy-4-iodophenethylamine (INBMeO): a high-affinity 5-HT2A receptor-selective agonist radioligand. *Bioorg Med Chem.* 2008;16:6116–6123.
15. Herth MM, Kramer V, Piel M, et al. Synthesis and in vitro affinities of various MDL 100907 derivatives as potential 18F-radioligands for 5-HT2A receptor imaging with PET. *Bioorg Med Chem.* 2009;17:2989–3002.
16. Kramer V, Herth MM, Santini MA, Palner M, Knudsen GM, Rosch F. Structural combination of established 5-HT receptor ligands: new aspects of the binding mode. *Chem Biol Drug Des.* 2010;76:361–366.
17. Palner M, McCormick P, Gillings N, Begtrup M, Wilson AA, Knudsen GM. Radiosynthesis and ex vivo evaluation of (R)-(−)-2-chloro-N-[1-11C-propyl]n-propylnorapomorphine. *Nucl Med Biol.* 2010;37:35–40.
18. Kornum BR, Lind NM, Gillings N, Marner L, Andersen F, Knudsen GM. Evaluation of the novel 5-HT4 receptor PET ligand [11C]SB207145 in the Gottingen minipig. *J Cereb Blood Flow Metab.* 2009;29:186–196.
19. Gillings N. A restricted access material for rapid analysis of [11C]-labeled radiopharmaceuticals and their metabolites in plasma. *Nucl Med Biol.* 2009;36:961–965.
20. Watanabe H, Andersen F, Simonsen CZ, Evans SM, Gjedde A, Cumming P. MR-based statistical atlas of the Gottingen minipig brain. *Neuroimage.* 2001;14:1089–1096.
21. Innis RB, Cunningham VJ, Delforge J, et al. Consensus nomenclature for in vivo imaging of reversibly binding radioligands. *J Cereb Blood Flow Metab.* 2007;27:1533–1539.
22. Lammertsma AA, Hume SP. Simplified reference tissue model for PET receptor studies. *Neuroimage.* 1996;4:153–158.
23. Kristiansen H, Elfving B, Plenge P, Pinborg LH, Gillings N, Knudsen GM. Binding characteristics of the 5-HT2A receptor antagonists altanserin and MDL 100907. *Synapse.* 2005;58:249–257.
24. Marazziti D, Rossi A, Giannaccini G, et al. Distribution and characterization of [3H]mesulergine binding in human brain postmortem. *Eur Neuropsychopharmacol.* 1999;10:21–26.
25. Syvanen S, Lindhe O, Palner M, et al. Species differences in blood-brain barrier transport of three positron emission tomography radioligands with emphasis on P-glycoprotein transport. *Drug Metab Dispos.* 2009;37:635–643.
26. Adams KH, Pinborg LH, Svarer C, et al. A database of [18F]-altanserin binding to 5-HT$_{2A}$ receptors in normal volunteers: normative data and relationship to physiological and demographic variables. *Neuroimage.* 2004;21:1105–1113.
27. Ewald AH, Fritschi G, Maurer HH. Metabolism and toxicological detection of the designer drug 4-iodo-2,5-dimethoxy-amphetamine (DOI) in rat urine using gas chromatography-mass spectrometry. *J Chromatogr B Analyt Technol Biomed Life Sci.* 2007;857:170–174.
28. Laruelle M. Imaging synaptic neurotransmission with in vivo binding competition techniques: a critical review. *J Cereb Blood Flow Metab.* 2000;20:423–451.

Supplemental Data

Chemical synthesis of labeling precursor

Dry tetrahydrofuran (THF) was distilled from Na/benzophenone, methanol was distilled from $Mg(OCH_3)_2$. Solvents used for flash chromatography were commercial HPLC-grade. Thin-layer chromatography (TLC) was performed using aluminum plates pre-coated with silica gel (Merck c-60 F_{254}) and visualized using UV-light (254 nm) or heating after dipping in Ninhydrin (0.3 g ninhydrin, 3 mL glacial acetic acid in 100 mL n-butanol). Flash chromatography was performed on silica gel (35-70 μm). Melting points were determined using a Meltemp apparatus and are uncorrected. NMR spectra were performed using Varian Mercury 300BB or Gemini 2000 spectrometers. Me_4Si ($\delta_H = 0.00$) or $CHCl_3$ ($\delta_H = 7.26$) was used as reference for ^{1}H-NMR while $CDCl_3$ ($\delta_C = 77.16$) was used as reference for ^{13}C-NMR.

N-(2-(tert-butyldimethylsilyloxy)benzyl)-2-(4-iodo-2,5-dimethoxyphenyl)ethanamine (**1**): To a solution of 2-(4-iodo-2,5-dimethoxyphenyl)ethanamine (165 mg, 0.54 mmol) in dry methanol (5 mL) was added 2-(*tert*-butyldimethylsilyloxy)benzaldehyde (133 mg, 0.56 mmol) and 5 pieces of 3Å molecular sieves. The mixture was stirred for 4 h before adding $NaBH_4$ (41 mg, 1.08 mmol), the reaction was stirred for a further 30 min, filtered through a plug of Celite and concentrated in vacuo. The residue was purified by flash chromatography (ethyl acetate/heptane 1:4 + 1% triethylamine) to give 149 mg (53%) of **1** as a colorless oil.

Elemental analysis calculated for $C_{23}H_{24}INO_3Si$: C 52.37; H 6.50; N 2.66. Found: C 51.88; H 6.06; N 2.56.

^{1}H-NMR (300 MHz, $CDCl_3$): δ 7.24-7.20 (1H, m), 7.18 (1H, s), 7.16-7.08 (1H, m), 6.94-6.87 (1H, m), 6.80-6.76 (1H, m), 6.65 (1H, s), 3.79 (3H, s), 3.78 (2H, s), 3.72 (3H, s), 2.82 (4H, s), 1.69 (1H, bs), 0.92 (9H, s), 0.22 (6H, s).

^{13}C-NMR (75 MHz, $CDCl_3$): δ 153.6, 152.2, 130.5, 129.9, 127.8, 121.5, 120.9, 118.3, 113.5, 82.3, 57.0, 56.1, 49.6, 48.8, 31.4, 25.8 (3C), 18.2, -3.9.

*tert-butyl 2-(*tert-*butyldimethylsilyloxy)benzyl(4-iodo-2,5-dimethoxyphenethyl)carbamate* (**2**):
1 (121 mg, 0.23 mmol) was dissolved in THF (5 mL), di-*tert*-butyl dicarbonate (100 mg,

0.46 mmol) was added, and the mixture was stirred for 3 h. The reaction mixture was concentrated

in vacuo and purified by flash chromatography (ethyl acetate/heptane 1:20) to yield 291 mg (90%)

of **2** as a clear oil.

Elemental analysis calculated for $C_{28}H_{42}INO_5Si$: C 53.58; H 6.75; N 2.23. Found: C 52.92; H 6.35;

N 2.52.

^{1}H-NMR (300 MHz, CDCl$_3$): δ 7.2-7.0 (3H, m), 6.91 (1H, t, J = 7.4 Hz), 6.78 (1H, d, J = 7.9 Hz),

6.67(rot$_a$)/6.50(rot$_b$) (1H, s), 4.45(rot$_a$)/4.31(rot$_b$) (2H, s), 3.81(rot$_a$)/3.79(rot$_b$) (3H, s), 3.72 (3H, s),

3.46(rot$_a$)/3.34(rot$_b$) (2H, t, J = 7.0 Hz), 2.87(rot$_a$)/2.77(rot$_b$) (2H, t, J = 7.2 Hz),

1.47(rot$_a$)/1.41(rot$_b$) (9H, s), 1.02 (9H, s), 0.24 (6H, s).

^{13}C-NMR (75 MHz, CDCl$_3$): δ 155.7, 153.2, 152.2, 152.1, 129.0, 128.9, 128.4, 128.0, 127.5, 127.2,

126.7, 121.1, 118.2, 113.7, 82.5, 79.4, 79.2, 57.0, 55.9, 47.2, 46.9, 46.6, 45.2, 29.8, 29.2, 28.4, 25.8,

18.3, -4.1.

tert-butyl 2-hydroxybenzyl(4-iodo-2,5-dimethoxyphenethyl)carbamate (**3**): To a solution of **2** (229

mg, 0.36 mmol) in THF (5 mL) was added 1 M solution of tetra-*n*-butylammonium fluoride in THF

(1.1 ml, 1.1 mmol) and saturated aqueous NH$_4$Cl (0.1 mL). The reaction was stirred for 22 h at

room temperature and the THF removed in vacuo. H$_2$O (20 mL) was added and the mixture

extracted with ethyl acetate (3 × 20 mL). The combined organic phases were washed with brine (30

mL), dried over MgSO$_4$, concentrated in vacuo, and purified by flash chromatography (ethyl

acetate/heptane 1:20) to yield 150 mg (81%) of **3** as a clear oil solidifying over time.

Elemental analysis calculated for $C_{22}H_{28}INO_5$: C, 51.47; H, 5.50; N, 2.73. Found: C, 51.37; H,

5.47; N, 2.67. Melting point: 155.2-155.5°C.

^{1}H-NMR (300 MHz, CDCl$_3$): δ 9.37 (1H, s), 7.20 (1H, dt, J = 8.0, 1.6 Hz), 7.15 (1H, s), 7.05 (1H,

dd, J = 7.4, 1.7 Hz), 6.89 (1H, dd, J = 8.1, 1.1 Hz), 6.77 (1H, dt, J = 7.3, 1.2 Hz), 6.37 (1H, s), 4.29

(2H, s), 3.78 (3H, s), 3.67 (3H, s), 3.42 (2H, t, J = 6.9 Hz), 2.74 (2H, t, J = 6.9 Hz), 1.36 (9H, s).

^{13}C-NMR (75 MHz, CDCl$_3$): δ 202.8, 156.1, 152.2, 131.2, 129.9, 128.4, 123.0, 121.1, 119.1, 117.3,

113.7, 57.0, 55.9, 48.5, 47.3, 29.7, 28.2.
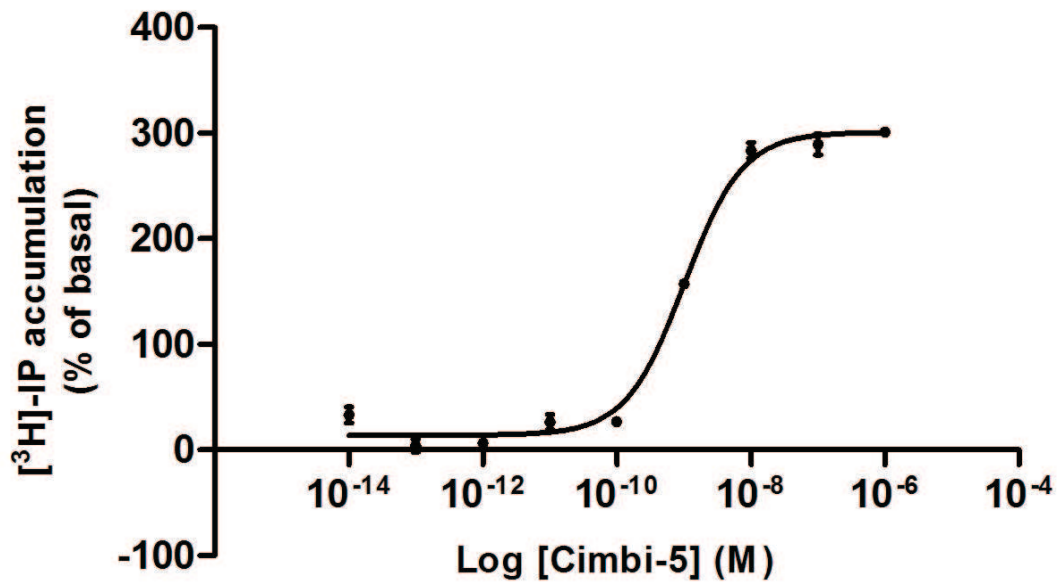
Supplemental figure 1. CIMBI-5 dose-response curve for ^{3}H-PI formation. The EC$_{50}$ of CIMBI-5 for 5-HT$_{2A}$ receptor activation was calculated to 1.02 ± 0.17 nM using non-linear regression analysis. Values, expressed as percentages of basal values, are the means ± SEM (n=4 for all data points).
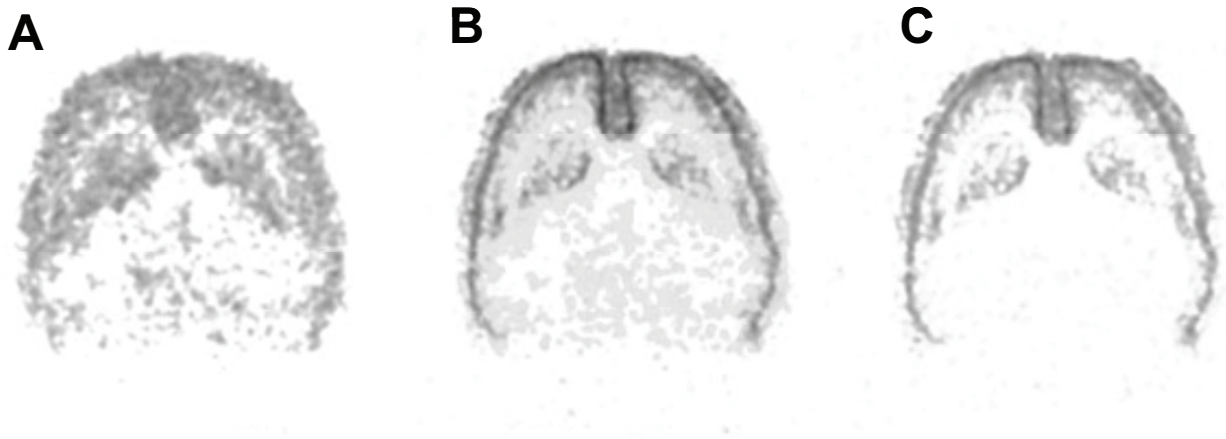
Supplemental figure 2. In vitro receptor autoradiography of ^{11}C-CIMBI-5 and ^{3}H-MDL100907. 20 μm horizontal rat brain sections were incubated with 0.2 nM ^{11}C-CIMBI-5 and 0.2 nM ^{3}H-MDL100907 in a TRIS buffer solution. Non-specific binding was determined in adjacent sections by adding 10 μM ketanserin to the incubation mixture. Sections were washed for 2 x 10 min in ice-cold buffer followed by a quick dip in ice-cold water, quickly air dried and exposed to Fuji-Film IP-MS plates overnight. The sections were then fixed in paraformaldehyde vapor overnight and dried completely before exposure to Fuji-Film IP-TR for 10 days. Total binding of ^{11}C-CIMBI-5 (A) and ^{3}H-MDL100907 (C) is shown in the same section. Similar distribution pattern is shown in the overlay (B) of the two images. Very low binding of both ^{11}C-CIMBI-5 and ^{3}H-MDL100907 is observed in the cerebellum.

Supplemental Table 1. Regional modeling results for ^{11}C-CIMBI-5 PET scanning in the pig brain

Region:	Simplified reference tissue model				Non-invasive logan linearisation				1-tissue compartment model						2-tissue compartment model					
	baseline (n=5)		ketanserin (n=3)		baseline (n=5)		ketanserin (n=3)		baseline (n=1)			ketanserin (n=1)			baseline (n=1)			ketanserin (n=1)		
	BP_{ND}	AIC	BP_{ND}	AIC	DVR	Start Lin.	DVR	Start Lin.	V_T	BP_{ND}	AIC	V_T	BP_{ND}	AIC	V_T	BP_{ND}	AIC	V_T	BP_{ND}	AIC
Cortex	0.46 ± 0.12	136.2 ± 25.4	0.11 ± 0.06 **	117.7 ± 25.1	1.47 ± 0.13	28.3 ± 10.5	1.13 ± 0.06 **	6.6 ± 9.2	3.19	0.57	197.4	2.61	0.13	165.0	4.64	0.61	176.0	3.18	0.11	121.2
Hippocampus	0.40 ± 0.20	205.3 ± 18.5	DNF	DNF	1.22 ± 0.26	72.0 ± 46.2	1.05 ± 0.07	34.8 ± 25.0	2.60	0.28	241.3	2.45	0.06	218.0	4.15	0.44	233.0	3.15	0.10	209.2
Caudate Nucleus	0.16 ± 0.12	215.7 ± 37.2	0.14 ± 0.07	201.0 ± 28.9	1.13 ± 0.11	24.3 ± 21.5	1.15 ± 0.02	21.0 ± 27.8	2.88	0.42	211.3	3.04	0.32	182.0	3.80	0.32	212.2	3.70	0.29	181.5
Putamen	0.31 ± 0.11	220.4 ± 14.1	0.12 ± 0.08	224.5 ± 15.3	1.27 ± 0.16	27.4 ± 34.4	1.17 ± 0.01	9.2 ± 10.5	2.80	0.38	242.5	2.97	0.29	207.7	3.99	0.39	240.3	3.59	0.26	203.3
Lateral Thalamus	0.26 ± 0.08	214.1 ± 9.9	0.22 ± 0.04	195.9 ± 33.5	1.34 ± 0.09	10.7 ± 9.7	1.22 ± 0.03	6.4 ± 2.1	3.00	0.48	231.8	3.13	0.35	183.1	4.32	0.50	225.7		DNF	
Medial Thalamus	0.30 ± 0.08	203.9 ± 20.8	0.18 ± 0.06	206.3 ± 13.9	1.30 ± 0.14	11.4 ± 10.8	1.20 ± 0.07	43.5 ± 41.0	2.81	0.38	217.3	2.98	0.29	203.1	3.88	0.35	209.9	4.97	0.74	194.7
Cerebellum									2.03		197.1	2.31		186.9	2.88		175.0	2.86		133.5

Kinetic modeling outcome at baseline and following ketanserin blockade is shown. For the simplified reference tissue model and non-invasive logan linearisation models, mean values ± SD are given.

BP_{ND}: Non-displacable binding potential, AIC: Akaike information criteria, DVR: distribution volume ratio, DNF: Did not fit.

**p<0.01: Unpaired, two-tailed Student's t-test vs. Baseline.

Paper III

Ettrup A, Hansen M, Santini MA, Paine J, Gillings N, Palner M, Lehel S, Herth MM, Madsen J, Kristensen J, Begtrup M, Knudsen GM.

Radiosynthesis and in vivo evaluation of a series of substituted ^{11}C-phenethylamines as 5-HT$_{2A}$ agonist PET tracers.

Radiosynthesis and in vivo evaluation of a series of substituted ^{11}C-phenethylamines as 5-HT$_{2A}$ agonist PET tracers

Anders Ettrup[1,4*], Martin Hansen[3,4], Martin A. Santini[1,4], James Paine[3,4], Nic Gillings[2,4], Mikael Palner[1,4], Szabolcs Lehel[2], Matthias M. Herth[2,4], Jacob Madsen[2,4], Jesper Kristensen[3,4], Mikael Begtrup[3,4], and Gitte M. Knudsen[1,4]

[1]*Neurobiology Research Unit, Copenhagen University Hospital, Rigshospitalet, Copenhagen, Denmark*

[2]*PET and Cyclotron Unit, Copenhagen University Hospital, Rigshospitalet, Copenhagen, Denmark*

[3]*Department of Medicinal Chemistry, Faculty of Pharmaceutical Sciences, University of Copenhagen, Copenhagen, Denmark*

[4]*Center for Integrated Molecular Brain Imaging (Cimbi), Copenhagen University Hospital, Rigshospitalet, Copenhagen, Denmark*

[*] Corresponding Author:

MD, DMSc, Professor Gitte Moos Knudsen

Neurobiology Research Unit

Blegdamsvej 9

Rigshospitalet, building 9201

DK-2100 Copenhagen, Denmark

Phone (+45) 3545 6720 / Fax: (+45) 3545 6713

Email: gmk@nru.dk

Running title: 5-HT$_{2A}$ receptor agonist PET tracers

ABSTRACT

Purpose Positron emission tomography (PET) imaging of serotonin 2A (5-HT$_{2A}$) receptors with agonist tracers hold promise to selectively label 5-HT$_{2A}$ receptors in their high affinity state. We have previously validated [^{11}C]Cimbi-5 and found that it is an 5-HT$_{2A}$ receptor agonist PET tracer. In an attempt to further optimize the target-to-background binding ratio, we modified the chemical structure of the phenethylamine backbone and ^{11}C-labeling site of [^{11}C]Cimbi-5 in different ways. Here, we present the in vivo validation of nine novel 5-HT$_{2A}$ agonist PET tracers in the pig brain.

Methods Each radiotracer was injected intravenously in anaesthetized Danish Landrace pigs, and the pigs were subsequently scanned for 90 minutes in a high resolution research tomography (HRRT) scanner. To evaluate 5-HT$_{2A}$ receptor binding, cortical non-displaceable binding potentials (BP$_{ND}$) were calculated using the simplified reference tissue model with cerebellum as a reference region.

Results After intravenous injection, all compounds entered the brain and distributed preferentially in the cortical areas, in accordance with the known 5-HT$_{2A}$ receptor distribution. The largest target-to-background binding ratio was found for [^{11}C]Cimbi-36 which also had a high brain uptake compared to its analogues. The cortical binding of [^{11}C]Cimbi-36 was decreased by pre-treatment with ketanserin supporting 5-HT$_{2A}$ receptor selectivity in vivo. [^{11}C]Cimbi-82 and [^{11}C]Cimbi-21 showed lower cortical BP$_{ND}$, while [^{11}C]Cimbi-27, [^{11}C]Cimbi-29, [^{11}C]Cimbi-31, and [^{11}C]Cimbi-88 gave rise to similar cortical BP$_{ND}$ compared to [^{11}C]Cimbi-5.

Conclusion [^{11}C]Cimbi-36 is currently the most promising candidate for investigation of 5-HT$_{2A}$ agonist binding in the living human brain with PET.

Keywords: PET tracer development, 5-HT2A, agonist, porcine, serotonin receptors, [11C]Cimbi-36.

INTRODUCTION

The serotonin 2A (5-HT$_{2A}$) receptors are implicated in the pathophysiology of human diseases such as depression and schizophrenia, and 5-HT$_{2A}$ receptor stimulation exerts the hallucinogenic effects of recreational drugs such as lysergic acid diethylamide (LSD) and 1-(2,5-dimethoxy-4-iodophenyl)-2-aminopropane (DOI) [1], whilst the therapeutic effects of atypical antipsychotics are attributed to the antagonistic effects on these receptors [2]. Positron emission tomography (PET) imaging of cerebral 5-HT$_{2A}$ receptors is used to characterize the serotonergic receptor system in disease states, and PET imaging can also be used to measure receptor occupancy by therapeutic drugs, e.g. antipsychotics.

Currently, only antagonistic PET ligands such as [^{18}F]altanserin [3] and [^{11}C]MDL100907 [4] are available to selectively map and quantify 5-HT$_{2A}$ receptor binding in the human brain. However, whereas 5-HT$_{2A}$ receptor antagonists bind to the total pool of receptors, 5-HT$_{2A}$ receptor agonists selectively bind to receptors in their the high-affinity state [5,6]. Thus, a 5-HT$_{2A}$ receptor agonist PET tracer would ideally bind only to 5-HT$_{2A}$ receptors in their functional state. Alterations in agonist binding measured in vivo with PET may be more relevant for assessing dysfunction in the 5-HT$_{2A}$ receptors in specific patient or population groups. Furthermore, since a large fraction of the 5-HT$_{2A}$ receptors are intracellularly localized [7,8], combining measurements with antagonist and agonist PET tracers would enable in vivo determination of the ratio of the high-affinity, membrane bound and active receptors to the low-affinity, inactive, and intracellular receptors [9]. Thus, quantification of functionally active 5-HT$_{2A}$ receptors in vivo using an agonist PET tracer is hypothesized to be superior to antagonist measurements of total pool of 5-HT$_{2A}$ receptors for studying alterations in receptor function in human diseases such as depression.

In terms of chemical structure, 5-HT$_{2A}$ receptor agonists fall into three classes: Tryptamines, ergolines, and phenetylamines. Recently, several *N*-benzyl-substituted phenethylamines were described as superpotent and selective 5-HT$_{2A}$ receptor agonists with EC$_{50}$ values up to 27-fold lower than 5-HT itself [10]. One of these compounds, 2-(4-iodo-2,5-dimethoxyphenyl)-N-(2-methoxybenzyl)ethanamine (25I-NBOMe, Cimbi-5), was recently tritiated [11], and we have also evaluated [^{11}C]Cimbi-5 as a 5-HT$_{2A}$ receptor agonist PET tracer [12].

Dopamine D$_2$ receptor agonist radiotracers are superior to antagonist radiotracers for measuring dopamine release in vivo in humans [13], monkeys [14], and mice [9], and since several studies have failed to demonstrate that 5-HT$_{2A}$ receptor antagonist PET tracers are displaceable by elevated levels of endogenous 5-HT [15] it may well be that 5-HT$_{2A}$ receptor agonists would be

more prone to displacement by competition with endogenously released 5-HT. Monitoring the release of endogenous 5-HT is highly relevant in relation to human diseases such as depression and Alzheimer's disease which involve dysfunction of the 5-HT system.

Here, we present the synthesis and evaluation a series of carbon-11 labelled substituted phenethylamines structurally related to the previous validated lead compound [11C]Cimbi-5. The agonistic properties of the compounds were ascertained in vitro by phosphoinositide (PI) hydrolysis assays and binding assays. To test the suitability of the compounds as PET tracers in vivo, all substituted phenethylamines were labelled with carbon-11, and cerebral uptake, distribution, and displacement were investigated after intravenous PET tracer injection in pigs.

MATERIALS AND METHODS

Chemical synthesis

Synthesis of precursors and radiochemical labelling are summarized in Fig. 1, bold numbers refer to this figure. Experimental conditions, synthesis routes for the precursors, and NMR data for previously unpublished intermediates is found in the supplementary material. The precursors for the radiolabelling were, with the exception of **14**, synthesized in two steps from their parent phenethylamines. Reductive amination with the appropriate aldehydes followed by selective Boc-protection of the secondary amines gave the labelling precursors. The syntheses of the parent phenethylamines **1** [16], **2** [16], **3** [17], and **4** [18] have been described elsewhere. **5** was synthesized in four steps from 1,4-diiodo-2,5-dimethoxybenzene, and **14** was synthesized in 3 steps from 2-(2-isopropoxy-5-methoxyphenyl)ethanamine [11] as described in the supplementary material. The synthesis of reference compounds except Cimbi-82 have been reported elsewhere [10,16]. The synthesis of Cimbi-82 is described in the supplementary material. The lipophilicity of all PET tracers (cLogD$_{7.4}$) was calculated using CSLogD™ (ChemSilico LLC).

Radiochemical synthesis of ^{11}C-labeled phenethylamines

Radiochemical labelling of all PET tracers is summarized in Fig.1. All radiolabelled compounds except [11C]Cimbi-88 were prepared as follows: [11C]methyl triflate was collected in a solution of 0.3-0.4 mg labelling precursor (see Fig. 1) in a mixture of acetonitrile (200 µl) and acetone (100 µl) containing 2 µl 2 M NaOH at room temperature, and the solution was subsequently heated for 30

seconds at 40ºC. Subsequently 250 µl TFA/CH₃CN (1:1) was added and the mixture heated at 80ºC for 5 min. After neutralization with 750 µl 2 M NaOH and dilution with ca. 4 ml citrate buffer (25 mM, pH 4.7), the reaction mixture was purified by HPLC (Phenomenex Luna C18(2), 250 x 10 mm; 40/60 acetonitrile/25 mM citrate buffer pH 4.7, flow rate 6 ml/min).

The fraction from HPLC containing the product was collected in a flask containing 50ml 0.1% ascorbic acid (aq.). This solution was then passed through a C18 SepPac light column which had been preconditioned with 10 ml ethanol followed by 20 ml 0.1% ascorbic acid. The SepPac was first flushed with 3 ml sterile water, then the trapped activity eluted from the SepPac with 3 ml ethanol followed by 3 ml 0.1% ascorbic acid (aq) into a 20 ml vial containing 9 ml phosphate buffer (100 mM, pH 7) giving a 15 ml solution of the labelled product. The total synthesis time was 40-50 min. Analysis to determine radiochemical purity and specific radioactivity was performed using HPLC with online UV and radiodetection (column: Luna C18(2) 4.6 x 150 mm; eluent: 40/60 acetonitrile/25 mM citrate buffer pH 4.7; flow rate: 2ml/min, wavelength: 300 nm).

[^{11}C]Cimbi-88 was synthesized in an analogous manner to above except that the deprotection step was performed by addition of hyrdrazine monohydrate (300 µl) and heating at 120ºC for 3 min. The solution was neutralised with 2 ml 3 M HCl, diluted with 2.5 ml citrate buffer (25 mM, pH 4.7) and purified as described above. Radiochemical purity of all radiolabelled compounds was >95% and specific activities at end of synthesis varied from 14 - 605 GBq/µmol.

In vitro binding

Competition binding experiments against [^{3}H]MDL100907 were performed on a NIH-3T3 cell line (GF62) stably transfected with the rat 5-HT$_{2A}$ receptor as previously described [19] using 0.2 nM [^{3}H]MDL100907 as the radioactive competitor. Eight different concentrations of test ligand (1 µM - 1 pM) in a total of 1 mL buffer (50 mM Tris-HCl, 150 mM NaCl, 5 mM KCl, 1 mM CaCl$_2$, 1 mM MgCl$_2$, 0.01% Ascorbic Acid, pH 7.4) including cell homogenate. Non-specific binding was determined with 1 µM ketanserin. The incubation was terminated after 1 h by filtration using a 24-channel cell harvester (Brandel), 300 mL/24 channels Tris-HCl buffer was used for washing, and the samples filtered through a Whatman GF/B filter. The filters were soaked with 1% polyethylenimine (PEI) prior to filtration in order to reduce and stabilize non-specific binding to the filters. Radioactive concentrations were determined with a scintillation counter (Packard Instruments), and the K$_i$ values calculated based on %-binding inhibition of the radioactive ligand. Furthermore, K$_i$ determinations against various neuroreceptors were provided by the Psychoactive

Drug Screening Program (PDSP). For experimental details refer to the PDSP web site http://pdsp.med.unc.edu/.

PI hydrolysis assay

GF62 cells (1.5×10^6 cells/mL) were cultured overnight in Dulbecco's modified Eagle's medium (DMEM) supplemented with 10% fetal bovine serum (FBS), 1 mM sodium pyruvate (Sigma), penicillin (P: 100 units/mL), and streptomycin (S: 100 µg/mL) at 37°C and 5% CO_2. Subsequently, cells were incubated overnight with 4 µCi/well of myo-(1,2)-[^{3}H]-inositol (Amersham) in labelling medium (inositol-free DMEM containing 10% dFBS and P/S). The cells were then washed once with incubation buffer (20 mM HEPES, pH 7.4; 20 µM LiCl, 1 mM $MgCl_2$, 1 mM $CaCl_2$) and incubated at 37°C in the same buffer for 30 min, in the presence or absence of 1 µM ketanserin. The solutions were removed and test compounds (10 µM-0.1 pM) or 5-HT (10 µM) were added to the wells for 30 min at 37°C. The formed inositol phosphates were then extracted with 10 mM ice-cold formic acid for 30 min at 4°C. The supernatants were transferred to AG 1-X8 anion exchange resin columns (Bio-Rad) and eluted into Ultima-FLO AF scintillation liquid (Packard) with 2 M ammonium formate/0.1 M formic acid. Accumulated [^{3}H]inositol phosphates were measured with a Tri-Carb 2900TR liquid scintillation counter (Packard Instruments) after 1 h incubation at room temperature.

Animal procedures

A total of ten female Danish Landrace pigs were used, mean weight was 20.1 ± 3.8 kg. After arrival, animals were housed under standard conditions and were allowed to acclimatize for one week before scanning. To minimize stress, the animals were provided with straw bedding and environment enrichment, in the form of plastic balls and metal chains. On the scanning day, pigs were tranquilized by intramuscular (i.m.) injection of 0.5 mg/kg midazolam. Anaesthesia was induced by i.m. injection of a Zoletil veterinary mixture (1.25 mg/kg tiletamin, 1.25 mg/kg zolazepam, and 0.5 mg/kg midazolam; Virbac Animal Health). Following induction, anesthesia was maintained by intravenous (i.v.) infusion of 10 mg/kg/h propofol (B. Braun Melsugen AG). During anaesthesia, animals were endotracheally intubated and ventilated (volume 250 mL, frequency 15 per min). Venous access was granted through two venflons (Becton Dickinson) in the peripheral milk veins, and an arterial line for blood sampling was inserted in the femoral artery after a minor

incision. Vital signs including blood pressure, temperature, and heart rate were monitored throughout the duration of the PET scanning. Immediately after scanning, animals were sacrificed by i.v. injection of pentobarbital/lidocain. All animal procedures were approved by the Danish Council for Animal Ethics (Journal No. 2006/561-1155).

PET scanning protocol

All PET tracers were evaluated with a single PET scan. On the basis of the pharmacokinetic properties, the best candidate was selected for further investigation including a blocking study in vivo and an examination of metabolites in pig brain tissue. All PET tracers were given as an i.v. bolus injection, and the pigs were subsequently scanned for 90 min in list mode with a high resolution research tomography (HRRT) scanner (Siemens AG). Scanning was started at the time of injection (t=0). The injected radioactivity and specific radioactivity at the time of injection is given in Table 2. In all pigs, arterial whole blood samples were taken throughout the entire scan. During the first 15 min after injection, radioactivity in whole blood was continuously measured using an Allogg ABSS autosampler (Allogg Technology) counting coincidences in a lead-shielded detector. Concurrently, blood samples were manually drawn at 2.5, 5, 10, 20, 30, 50, 70, and 90 min and radioactivity in whole blood and plasma was measured using a well counter (Cobra 5003, Packard Instruments) that was cross-calibrated to the HRRT and to the autosampler. Also, radiolabelled parent compound and metabolites were measured in plasma as described below.

To test the displacability of [11C]Cimbi-36 by a known 5-HT$_{2A}$ receptor antagonist in vivo, ketanserin tartrate (10 mg/kg i.v., Sigma No. S006) was given after a [11C]Cimbi-36 baseline scan 30 min prior to a second scan using the same PET protocol. In these two scans, injected radioactivity was 553 MBq and 590 MBq in the baseline and blocked scan, whereas the specific radioactivity at the time of injection was 175.4 GBq/µmol and 257.0 GBq/µmol.

Quantification of PET data

Ninety minutes HRRT list mode PET data were reconstructed using a standard iterative method as previously reported [20] (OSEM3D-OP with point spread function (PSF), 10 iterations, and 16 subsets) into 38 dynamic frames of increasing length (6 x 10, 6 x 20, 4 x 30, 9 x 60, 3 x 120, 6 x 300, 4 x 600 s). Images consisted of 207 planes of 256 x 256 voxels of 1.22 x 1.22 x 1.22 mm^3. A summed image of all counts in the 90 minute scan time for each pig was reconstructed and used for

co-registration to a standardized MRI-based statistical atlas of the Danish Landrace pig brain, similar to that previously reported for the Göttingen minipig [21] using the program Register as previously described [22]. Hereafter, the activity in volumes of interest (VOI), including cerebellum, cortex (defined in the MRI-based atlas as entire cortical grey matter), hippocampus, caudate putamen, putamen, dorsal and ventral thalamus, and lateral ventricle. Activity in all VOIs was calculated as the average of radioactive concentration (Bq/cc) in left and right hemisphere. Radioactive concentration in VOI (in kBq/cm^3) in the time-activity curves was normalized to the injected dose (ID) corrected for animal weight, in kBq/g, thus yielding the unit g/cm^3 and approximating standardized uptake values (SUV) in quantity.

Arterial input measurements were obtained for all PET tracers, expect for [^{11}C]Cimbi-88 where full radiometabolite information was not available, and distribution volumes (V_T) for VOIs were calculated based on the two tissue compartments model (2TC) using parent compound corrected plasma input function as arterial input function (table 2). Assuming the specific 5-HT$_{2A}$ receptor binding in cerebellum is negligible [3], the non-displaceable binding potential (BP$_{ND}$) for all PET tracers was calculated applying the simplified reference tissue model (SRTM) [23]. Kinetic modelling was done in PMOD version 3.0 (PMOD Technologies Inc.). Goodness-of-fit was evaluated using the Akaike Information Criterion (AIC).

HPLC analysis of pig plasma and pig brain tissue

Whole blood samples (10 mL) drawn during PET scanning were centrifuged (1500 × g, 7 min at ambient temperature), and the plasma was filtered through a 0.45 µm filter (13 mm or 25 mm PVDF syringe filter, Whatman GD/X) before HPLC analysis with online radioactivity detection, as previously described [24].

Additionally, the presence of radioactive metabolites of [^{11}C]Cimbi-36 in the brain was investigated in two pigs. Twenty five and sixty min after i.v. injection of ~500 MBq [^{11}C]Cimbi-36, the pigs were sacrificed by i.v. injection of pentobarbital and the brains were removed. Within 30 min of pentobarbital injection, brain tissue was homogenized in 0.1 N perchloric acid (Bie and Bentsen) saturated with sodium-EDTA (Sigma) for 2 × 30 s using a polytron. After centrifugation (1500 × g, 7 min at ambient temperature), the supernatant was neutralized using phosphate buffer, filtered (0.45 µm), and analyzed by HPLC as described above. A plasma sample from blood taken at the time of decapitation was also analysed.

Statistical analysis

All statistical tests were performed using Prism version 5.0 (GraphPad software). p-values below 0.05 were considered statistically significant. Results are expressed in mean +/- standard deviation (SD) unless otherwise stated.

RESULTS

In vitro binding characterization

Affinities of the test compounds towards the 5-HT_{2A} receptor were measured against 0.2 nM [^{3}H]MDL100907 on GF62 cells stably transfected with the rat 5-HT_{2A} receptor, and the K_i of the test compounds are given in Table 1. All tested compounds showed nanomolar affinity towards the 5-HT_{2A} receptor. Highest affinity for the 5-HT_{2A} receptor was found for Cimbi-31 and Cimbi-138, while Cimbi-21 and Cimbi-29 had the lowest affinities of the tested compounds. PDSP screening results were obtained to test if the compounds had significant affinities for other neuroreceptors. The PDSP data showed that K_i for Cimbi-36 against human 5-HT_{2A} receptors was 0.5 ± 0.1 nM. Thus, Cimbi-36 was 3-fold selective over 5-HT_{2C} (K_i: 1.7 ± 0.1 nM). At other targets tested by PDSP, Cimbi-36 was at least 600-fold selective for 5-HT_{2A} receptors. The third highest affinity of Cimbi-36 was at Sigma 1 receptors (K_i: 310.2 ± 62.17 nM). The full PDSP screening results are given in Table S1 in the supplementary material.

In vitro functional characterization

The functional properties of the compounds at the 5-HT_{2A} receptor were assessed by measuring its effect on PI hydrolysis in GF62 cells overexpressing the 5-HT_{2A} receptor. All investigated compounds were found to be highly potent agonists at the 5-HT_{2A} receptor with EC_{50}-values in nanomolar range (0.19 nM - 50.7 nM). For compounds previously tested, EC_{50}-values are in agreement with reported data [10]. For all compounds, pre-treatment with 1 µM ketanserin completely inhibited the induced PI hydrolysis (data not shown). Furthermore, the degree of 5-HT_{2A} receptor activation achieved by the compounds was compared to the maximum effect of 5-HT (10 µM) in the same assays and reported as percentage of intrinsic activation. All compounds acted as full or nearly full agonists at the 5-HT_{2A} receptor, giving rise to 83-99% of the activation evoked by 10 µM 5-HT. The full results of in vitro activation are given in Table S2 in the supplementary material.

In vivo biodistribution in the pig brain

All ^{11}C-labelled phenethylamines showed significant uptake in the pig brain as demonstrated in Fig. 3, and for all PET tracers, time-activity curves showed higher cortical uptake compared to cerebellum (Fig. 2). The peak cortical uptake varied among the tracers; the highest cortical uptake was observed for [^{11}C]Cimbi-36 and [^{11}C]Cimbi-31 with a peak cortical uptake around 2.2 SUV, while the tracers [^{11}C]Cimbi-5-2 and [^{11}C]Cimbi-21 only showed an uptake around 0.8 SUV. The cortex-to- cerebellum uptake ratios, as measured by cortical SRTM BP_{ND}, are given in Table 2. The lowest cortex-to-cerebellum ratios of the nine tested PET tracers were found for [^{11}C]Cimbi-21 and [^{11}C]Cimbi-88 with cortical SRTM BP_{ND} of 0.17. PET scanning with [^{11}C]Cimbi-5-2, [^{11}C]Cimbi-27, [^{11}C]Cimbi-31, and [^{11}C]Cimbi-82 gave cortical SRTM BP_{ND} similar to that found with [^{11}C]Cimbi-5 (0.46 ± 0.11). The highest cortical-to-cerebellum uptake ratios were found with [^{11}C]Cimbi-36, and [^{11}C]Cimbi-138 yielding cortical SRTM BP_{ND} of 0.60 and 0.82 indicative of high target-to-background ratios with these tracers. For all regional time-activity curves, peak radioactivity concentration was 10-20 min post-injection and hereafter they declined, implying that binding is reversible over the 90 min scan time. The time-activity curves showed that regional activity in the pig brain of [^{11}C]Cimbi5-2 and [^{11}C]Cimbi-88 declined at a slower rate compared to the other PET tracers. [^{11}C]Cimbi-21, [^{11}C]Cimbi-31, [^{11}C]Cimbi-36, and [^{11}C]Cimbi-82 showed more rapid decline in regional brain radioactivity indicating faster kinetics with these tracers. V_T was calculated using the 2TC model with metabolite corrected arterial plasma radioactivity as input function and given in Table 2. Due to missing radiometabolite data, 2TC V_T could not be calculated for [^{11}C]Cimbi-82, while the 2TC model did not fit data with [^{11}C]Cimbi-31.

Ketanserin blockade of [^{11}C]Cimbi-36 in vivo

In a single pig, the effect of ketanserin pre-treatment on [^{11}C]Cimbi-36 binding was examined. In this baseline scan, the cortical SRTM BP_{ND} of [^{11}C]Cimbi-36 was 0.70. Following 10 mg/kg ketanserin administered i.v. 30 minutes prior to a second scan, the binding potential was decreased to 0.26. Also, the time-activity curves are indicative of a decreased cortical [^{11}C]Cimbi-36 binding by ketanserin pre-treatment (Fig. 5). However, the ketanserin blockade was not complete as indicated by the persistent difference between the cortical and cerebellar radioactive concentration in the blocked time-activity curves (Fig. 5).

Radiolabelled metabolites

For all compounds with full metabolite data, the relative amount of parent compound in plasma declined exponentially at similar rates, and 5-9% remained in plasma 90 min post injection (see Fig. 6 for an example). In the radio-HPLC chromatograms of pig plasma taken 30 min after i.v. injection of the PET tracers, a distinct peak was found for most of the PET tracers, eluting prior to the parent compound (Fig. 4). This lipophilic radiolabelled metabolite reached a maximum in plasma at around 20-40 min post-injection and then dropped off slightly up to 90 min (see Fig. 6 for an example). In the HPLC analysis of homogenized pig brain tissue taken 20 min after [11C]Cimbi-36 injection, only negligible amounts of this metabolite were found in frontal cortex tissue compared to plasma obtained at the same time (Fig. 7). The brain tissue obtained 60 min after i.v. injection of [11C]Cimbi-36 contained insufficient radioactivity for reliable HPLC analysis.

DISCUSSION

We here present the radiosynthesis and biological evaluation of a series of substituted phenethylamines as 5-HT$_{2A}$ agonist PET tracers. Based on an in vivo screening approach conducting a HRRT PET scan with each tracer, we identified [11C]Cimbi-36 as the most promising candidate and conducted further studies with this compound. [11C]Cimbi-36 had a higher brain uptake and improved target-to-background binding ratios over the previously validated candidate [11C]Cimbi-5 (cortical SRTM BP$_{ND}$: 0.46 ± 0.11) [12]. We used SRTM BP$_{ND}$ to evaluate the target-to-background binding ratios of the PET tracers since cerebellum generally is a valid reference region for quantification of 5-HT$_{2A}$ receptor binding [3,25]. Time-activity curves from [11C]Cimbi-36 showed the highest brain uptake (peak cortical SUV 2.2), and the greatest separation between cortical and cerebellar uptake (cortical SRTM BP$_{ND}$ 0.82) of the nine tested compounds, thus the target-to-background ratio of [11C]Cimbi-36 it is the highest of [11C]Cimbi-5 and the eight other currently tested compounds. Although, [11C]Cimbi-138 also displayed promising PET tracer properties with a SRTM BP$_{ND}$ of 0.60 and a peak cortical uptake of 1.4, [11C]Cimbi-36 was superior to [11C]Cimbi-138 in both outcome measures. 5-HT$_{2A}$ receptor blocking with ketanserin resulted in a reduction in the cortical SRTM BP$_{ND}$ from 0.70 to 0.26, supporting that [11C]Cimbi-36 binding in the pig cortex represent 5-HT$_{2A}$ receptor binding.

PET tracers such as [11C]Cimbi-21 and [11C]Cimbi-88 were discarded for further studies based on their low target-to-background binding ratio in the screening procedure. The cortical SRTM BP_{ND} of these PET tracers were lower in the pig brain compared to the previously validated candidate [11C]Cimbi-5. It should be noted that the [11C]Cimbi-21 scan was conducted with lower specific radioactivity than the other compounds and target-to-background binding ratios, however, it is unlikely that improving specific radioactivity in a repeat scan with this tracer would improve cortical BP_{ND} to the level of [11C]Cimbi-36. [11C]Cimbi-5-2, [11C]Cimbi-27, [11C]Cimbi-29, [11C]Cimbi-31, and [11C]Cimbi-82 showed roughly similar brain uptake and cortical SRTM BP_{ND} as the previously labelled candidate PET tracer. Given the close structural resemblance of these compounds it is perhaps not surprising that these PET tracers showed similar properties in vivo in the pig brain.

The regional time-activity curves for [11C]Cimbi-36 clearly declined over the 90 min scanning time meaning that [11C]Cimbi-36 shows reversible binding to 5-HT$_{2A}$ receptor during the PET-scan. The time-activity of [11C]Cimbi-36 also seemed more reversible than e.g. [11C]Cimbi-5-2, [11C]Cimbi-27, and [11C]Cimbi-138. Reversible binding kinetics is advantageous for quantification [26], and the faster kinetics of [11C]Cimbi-36 may prove important when moving into clinical studies in humans where kinetics usually are slower.

The in vitro binding results confirmed that all compounds tested as PET tracers had high-affinity for the 5-HT$_{2A}$ receptor and that all compound, as expected based on their phenethylamine structure, activated 5-HT$_{2A}$ receptors with EC_{50} values in the nanomolar range, and thus indeed are 5-HT$_{2A}$ receptors agonists. This is in agreement with previous data describing Cimbi-5, Cimbi-27, Cimbi-29, Cimbi-36 as selective and high-affinity agonists [10]. Cimbi-31 and Cimbi-88 had the lowest 5-HT$_{2A}$ receptor affinity and lower EC_{50} values than most other tested compounds, and they also showed the lowest target-to-background binding ratios in the in vivo studies. Since the binding potential of a PET tracer is proportional to the affinity of the tracer [26], it is not surprising that the compounds with the lowest affinity also gave lowest cortical SRTM BP_{ND}. However, Cimbi-31 showed the highest 5-HT$_{2A}$ receptor affinity, and in this respect, it is perhaps somewhat surprising that [11C]Cimbi-31 did not seem to bind receptors more irreversibly as compared to some of the other tracers as observed by rate of wash-out from the cortical region. However, this testifies to the complexity of the binding in vivo in the living brain when comparing to affinity constants measured in vitro. The in vivo properties of a PET tracer are influenced by several factors, including brain uptake and transport, binding kinetics, and very prominently non-

specific binding. We here report roughly similar in vitro binding and activation properties of Cimbi-36, Cimbi-5, Cimbi-27, Cimbi-29, and Cimbi-82, yet [11C]Cimbi-36 was a markedly better PET tracer with higher target-to-background ratios compared to all these compound. Thus, in this test of a series of substituted ^{11}C-labelled phenethylamines we have demonstrated that minor structural changes may alter the PET tracer properties of a compound without greatly changing its in vitro properties. With these nine tested PET tracers there was no apparent relationship between calculated LogD values and non-specific uptake as determined by cerebellum V_T. This supports that the non-specific binding for phenethylamine PET tracers is dependent on other factors other than just lipophilicity, and that lipophilicity alone is not even a solid predictor for the level of non-specific binding of a PET tracer in vivo, which also has been suggested previously [27].

Most of the tested *N*-benzyl substituted ^{11}C-phenethylamines gave rise to a distinct lipophilic radiolabelled metabolite. We were unable to determine the identity of these labelled metabolites in pig plasma based on the retention time on the radiochromatograms alone. It is proposed that they result from an *O*-demethylation at the 2- or 5-methoxy position in the phenethylamine-moiety. Several lines of evidence support this speculation. Firstly, DOI has been shown to be metabolized through demethylation at either or both methoxy groups [28]. Further, the radiochromatograms for [11C]Cimbi-31 (which has no methoxy groups in the phenethylamine-moiety) only show small amounts of lipophilic metabolites. Also, the demethylation products of [11C]Cimbi-88 would be rather polar and therefore expected to elute with polar metabolites, as was the case. For Cimbi-88, the metabolism has also been described to involve demethylation at both at the 2- or 5-methoxy positions [29]. Changing the 4-substituent from iodine to bromine, chlorine or trifluromethyl in the phenethylamine-moiety had a considerable effect on the amount of radiolabelled metabolite in plasma. Since the plasma parent compound in plasma declined similarly over time for all compounds ([11C]Cimbi-5-2, [11C]Cimbi-36, [11C]Cimbi-82, and [11C]Cimbi-138), this difference is expected to be caused by variation in the rate of further metabolism of the lipophilic metabolites. However, further studies would be needed to uniquely identify the in vivo metabolic route of these substituted phenethylamines.

Given that a radiolabelled metabolite of [11C]Cimbi-36 was present in pig plasma, we investigated the eventual presence of the metabolite in the pig brain. Although substantial amounts of radiometabolite was present in plasma 20 min after i.v. injection of [11C]Cimbi-36, the radiometabolite was barely detectable in frontal cortex tissue from the same pig (Fig. 7). This suggests that the radiometabolite of [11C]Cimbi-36 does not enter the brain to any extent that would

interfere with the [^{11}C]Cimbi-36 signal or decrease the binding potential in vivo. Based on our data, however, we can not firmly dismiss the presence of some radiometabolites in the pig brain since some small peaks were observed in the radiochromatogram which concurrently were noisy due to the dilution of the tissue needed for homogenization. In contrast, plasma is loaded directly to the HPLC without dilution, thus this chromatogram is less noisy. Although the present results can not rule out the presence of radiolabelled metabolites in the pig brain, a much lower fraction was clearly present in brain compared to plasma, and the small amounts in brain implied by the tissue radiochromatogram may derive from blood present in the vascular compartments of the brain tissue.

All the *N*-benzyl substituted ^{11}C-labelled phenethylamines had a low free fraction in the pig plasma (0.4%-1.5%); a low free plasma fraction should theoretically impair brain uptake. However, since many of these compounds with similar free fraction showed different degree of brain uptake as measured by peak SUV, it seems that the level of brain uptake is not markedly influenced by fraction of free tracer in plasma. The only non-*N*-benzyl substituted compound, [^{11}C]Cimbi-88, had a higher free fraction in pig plasma (6.5%) which is in accordance with this compound being less lipophilic than the *N*-benzyl substituted tracers. However, brain uptake of [^{11}C]Cimbi-88 was lower than both [^{11}C]Cimbi-36, [^{11}C]Cimbi-27, and [^{11}C]Cimbi-31.

Two PET scans were performed with [^{11}C]Cimbi-36 and [^{11}C]Cimbi-82 at relatively low specific radioactivities (6.9 and 9.0 GBq/μmol, respectively, data not shown). In these scans, lower cortical BP_{ND} were found for both tracers, suggesting that tracer doses for 5-HT$_{2A}$ receptor agonist binding were exceeded. Thus, future PET studies with [^{11}C]Cimbi-36 should be conducted with an injected mass of <10 μg cold dose.

CONCLUSION

Our in vivo screening of phenethylamine 5-HT$_{2A}$ receptor agonist PET tracer led to the identification of [^{11}C]Cimbi-36 as the most promising PET tracer for further investigations. [^{11}C]Cimbi-36 showed the highest target-to-background binding ratio of all compounds tested, and it was also displaceable by ketanserin in vivo supporting its 5-HT$_{2A}$ receptor selectivity. No radiolabelled metabolites of [^{11}C]Cimbi-36 were found in the pig brain. In vitro studies confirmed that [^{11}C]Cimbi-36 is a highly potent, high-affinity and selective 5-HT$_{2A}$ receptor agonist. Thus, [^{11}C]Cimbi-36 is currently the most promising PET tracer for imaging cerebral 5-HT$_{2A}$ receptor agonist binding in the living brain.

ACKNOWLEDGEMENTS

CONFLICT OF INTEREST

The authors declare that they have no conflict of interest.

REFERENCES

1. Gonzalez-Maeso J, Weisstaub NV, Zhou M et al. Hallucinogens recruit specific cortical 5-HT(2A) receptor-mediated signaling pathways to affect behavior. Neuron. 2007;53:439-52.

2. Abbas A, Roth BL. Pimavanserin tartrate: a 5-HT2A inverse agonist with potential for treating various neuropsychiatric disorders. Expert Opin Pharmacother. 2008;9:3251-3259.

3. Pinborg LH, Adams KH, Svarer C et al. Quantification of 5-HT2A receptors in the human brain using [18F]altanserin-PET and the bolus/infusion approach. J Cereb Blood Flow Metab. 2003;23:985-996.

4. Ito H, Nyberg S, Halldin C, Lundkvist C, Farde L. PET imaging of central 5-HT2A receptors with carbon-11-MDL 100,907. J Nucl Med. 1998;39:208-214.

5. Fitzgerald LW, Conklin DS, Krause CM et al. High-affinity agonist binding correlates with efficacy (intrinsic activity) at the human serotonin 5-HT2A and 5-HT2C receptors: evidence favoring the ternary complex and two-state models of agonist action. J Neurochem. 1999;72:2127-2134.

6. Song J, Hanniford D, Doucette C et al. Development of homogeneous high-affinity agonist binding assays for 5-HT2 receptor subtypes. Assay Drug Dev Technol. 2005;3:649-659.

7. Cornea-Hebert V, Watkins KC, Roth BL et al. Similar ultrastructural distribution of the 5-HT(2A) serotonin receptor and microtubule-associated protein MAP1A in cortical dendrites of adult rat. Neuroscience. 2002;113:23-35.

8. Peddie CJ, Davies HA, Colyer FM, Stewart MG, Rodriguez JJ. Colocalisation of serotonin2A receptors with the glutamate receptor subunits NR1 and GluR2 in the dentate gyrus: an ultrastructural study of a modulatory role. Exp Neurol. 2008;211:561-573.

9. Cumming P, Wong DF, Gillings N, Hilton J, Scheffel U, Gjedde A. Specific binding of [(11)C]raclopride and N-[(3)H]propyl-norapomorphine to dopamine receptors in living mouse striatum: occupancy by endogenous dopamine and guanosine triphosphate-free G protein. J Cereb Blood Flow Metab. 2002;22:596-604.

10. Braden MR, Parrish JC, Naylor JC, Nichols DE. Molecular interaction of serotonin 5-HT2A receptor residues Phe339(6.51) and Phe340(6.52) with superpotent N-benzyl phenethylamine agonists. Mol Pharmacol. 2006;70:1956-1964.

11. Nichols DE, Frescas SP, Chemel BR, Rehder KS, Zhong D, Lewin AH. High specific activity tritium-labeled N-(2-methoxybenzyl)-2,5-dimethoxy-4-iodophenethylamine (INBMeO): a high-affinity 5-HT2A receptor-selective agonist radioligand. Bioorg Med Chem. 2008;16:6116-6123.

12. Ettrup A, Palner M, Gillings N et al. Radiosynthesis and evaluation of [11C]Cimbi-5 as a 5-HT2A receptor agonist radioligand for positron emission tomography. J Nucl Med. In press.

13. Narendran R, Mason NS, Laymon CM et al. A comparative evaluation of the dopamine D(2/3) agonist radiotracer [11C](-)-N-propyl-norapomorphine and antagonist [11C]raclopride to measure amphetamine-induced dopamine release in the human striatum. J Pharmacol Exp Ther. 2010;333:533-539.

14. Narendran R, Hwang DR, Slifstein M et al. In vivo vulnerability to competition by endogenous dopamine: comparison of the D2 receptor agonist radiotracer (-)-N-[11C]propyl-norapomorphine ([11C]NPA) with the D2 receptor antagonist radiotracer [11C]-raclopride. Synapse. 2004;52:188-208.

15. Paterson LM, Tyacke RJ, Nutt DJ, Knudsen GM. Measuring endogenous 5-HT release by emission tomography: promises and pitfalls. J Cereb Blood Flow Metab. 2010.

16. Shulgin A, Shulgin A. *PIHKAL, A Chemical Love Story*. Berkeley, CA: Transform Press; 1991:1-978.

17. Nichols DE, Frescas S, Marona-Lewicka D et al. 1-(2,5-Dimethoxy-4-(trifluoromethyl)phenyl)-2-aminopropane: a potent serotonin 5-HT2A/2C agonist. J Med Chem. 1994;37:4346-4351.

18. Monte AP, Marona-Lewicka D, Parker MA, Wainscott DB, Nelson DL, Nichols DE. Dihydrobenzofuran analogues of hallucinogens. 3. Models of 4-substituted (2,5-dimethoxyphenyl)alkylamine derivatives with rigidified methoxy groups. J Med Chem. 1996;39:2953-2961.

19. Herth MM, Kramer V, Piel M et al. Synthesis and in vitro affinities of various MDL 100907 derivatives as potential 18F-radioligands for 5-HT2A receptor imaging with PET. Bioorg Med Chem. 2009;17:2989-3002.

20. Sureau FC, Reader AJ, Comtat C et al. Impact of image-space resolution modeling for studies with the high-resolution research tomograph. J Nucl Med. 2008;49:1000-1008.

21. Watanabe H, Andersen F, Simonsen CZ, Evans SM, Gjedde A, Cumming P. MR-based statistical atlas of the Gottingen minipig brain. Neuroimage. 2001;14:1089-96.

22. Kornum BR, Lind NM, Gillings N, Marner L, Andersen F, Knudsen GM. Evaluation of the novel 5-HT4 receptor PET ligand [11C]SB207145 in the Gottingen minipig. J Cereb Blood Flow Metab. 2009;29:186-196.

23. Lammertsma AA, Hume SP. Simplified reference tissue model for PET receptor studies. Neuroimage. 1996;4:153-158.

24. Gillings N. A restricted access material for rapid analysis of [11C]-labeled radiopharmaceuticals and their metabolites in plasma. Nucl Med Biol. 2009;36:961-965.

25. Meyer PT, Bhagwagar Z, Cowen PJ, Cunningham VJ, Grasby PM, Hinz R. Simplified quantification of 5-HT2A receptors in the human brain with [11C]MDL 100,907 PET and non-invasive kinetic analyses. Neuroimage. 2010;50:984-993.

26. Innis RB, Cunningham VJ, Delforge J et al. Consensus nomenclature for in vivo imaging of reversibly binding radioligands. J Cereb Blood Flow Metab. 2007;27:1533-1539.

27. Guo Q, Brady M, Gunn RN. A biomathematical modeling approach to central nervous system radioligand discovery and development. J Nucl Med. 2009;50:1715-1723.

28. Ewald AH, Fritschi G, Maurer HH. Metabolism and toxicological detection of the designer drug 4-iodo-2,5-dimethoxy-amphetamine (DOI) in rat urine using gas chromatography-mass spectrometry. J Chromatogr B Analyt Technol Biomed Life Sci. 2007;857:170-174.

29. Theobald DS, Putz M, Schneider E, Maurer HH. New designer drug 4-iodo-2,5-dimethoxy-beta-phenethylamine (2C-I): studies on its metabolism and toxicological detection in rat urine using gas chromatographic/mass spectrometric and capillary electrophoretic/mass spectrometric techniques. J Mass Spectrom. 2006;41:872-886.

FIGURE LEGENDS

Fig. 1 Chemical synthesis of precursor compounds and radiochemical preparation of PET tracers. For synthesis specifications, refer to the supplementary material.

Fig. 2 Regional time-activity curves of ^{11}C-labelled phenethylamines in the pig brain. Circles connected by black line indicate cortex while squares connected by gray line indicate cerebellum. Standardized uptake values (SUV) in pig brain are shown for each tracer.

Fig. 3 Colour coded PET images showing the distribution of radioactivity in the pig brain after i.v. injection of tracers. Sagittal average images of activity from 10 to 90 minutes are shown. Right insert shows corresponding sagittal view of the MRI-based average atlas of the pig brain with structures labelled: fcx, frontal cortex; cx, cerebral cortex; tha, thalamus; cere, cerebellum; str, striatum.

Fig. 4 HPLC radiochromatograms of pig plasma 30 min post-injection (10 min for [^{11}C]Cimbi-88). Black arrows indicate parent compounds. Eluent compositions were adjusted so that each parent compound eluted at 5-7 min retention time.

Fig. 5 Cortical and cerebellar time-activity curves of [^{11}C]Cimbi-36 from one pig brain at baseline (black line) and following 10 mg/mg ketanserin pre-treatment (gray line). Standardized uptake values (SUV) normalized to injected dose per body weight is shown. Cortical SRTM BP$_{ND}$ of [^{11}C]Cimbi-36 was 0.70 baseline and 0.26 after ketanserin pre-treatment.

Fig. 6 HPLC analysis of radioactive metabolites in pig plasma after i.v. injection of [^{11}C]Cimbi-36. Parent compound (circles), lipophilic metabolite (squares), and polar metabolites (triangles) as percent of total radioactivity are given.

Fig. 7 HPLC analysis of plasma (A) and frontal cortex extract (B) 20 min after injection of [^{11}C]Cimbi-36. Peaks; 1: polar metabolites, 2: lipophilic metabolites, 3: parent compound.

Fig. 1

Table 1 In vitro 5-HT$_{2A}$ competitive binding affinities of PET tracer compounds

Compound	5-HT$_{2A}$ antagonist binding[a]
Cimbi-5	1.49 ± 0.35
Cimbi-21	12.5 ± 3.11
Cimbi-27	1.12 ± 0.08
Cimbi-29	1.36 ± 0.37
Cimbi-31	0.16 ± 0.04
Cimbi-36	1.01 ± 0.17
Cimbi-82	2.89 ± 1.05
Cimbi-88	47.2 ± 16.3
Cimbi-138	0.35 ± 0.05

[a] K$_i$ (nM ± SEM) measured against [^{3}H]MDL100907 at GF-62 cells overexpressing rat 5-HT$_{2A}$ receptors

Table 2 PET tracers in the pig brain: Injection data, cLogD values, free fraction, and in vivo biodistribution as calculated by kinetic modelling

| PET tracer | ID / MBq | A_s / GBq/µmol | cLogD[a] | Plasma free fraction / % | 2TC distribution volumes | | SRTM |
					Cortex	Cerebellum	Cortical BP_{ND}
[^{11}C]Cimbi-5-2	682	122.7	3.33	0.4	10.93	6.88	0.32
[^{11}C]Cimbi-21	627	9.6	3.86	0.8	7.24	5.73	0.17
[^{11}C]Cimbi-27	434	21.6	2.94	0.7	16.79	11.00	0.45
[^{11}C]Cimbi-29	710	45.2	3.35	0.4	5.15	3.57	0.32
[^{11}C]Cimbi-31	390	36.3	2.87	1.0	dnf	dnf	0.43
[^{11}C]Cimbi-36	506	210.4	3.42	1.1	13.42	6.76	0.82
[^{11}C]Cimbi-82	578	445.5	3.49	0.7	4.51	2.82	0.49
[^{11}C]Cimbi-88	462	231.2	-0.24	6.5	n.d.	n.d.	0.17
[^{11}C]Cimbi-138	589	455.6	4.40	1.2	13.85	6.19	0.60

[a] LogD calculated using CSLogD (ChemSilico)
ID; injected activity at time of injection. A_s; specific activity at time of injection. 2TC; 2 tissue compartment model. SRTM ; simplified reference tissue model. BP_{ND}; non-displaceable binding potential. dnf; did not fit kinetic model. n.d.; not determined

Fig. 2
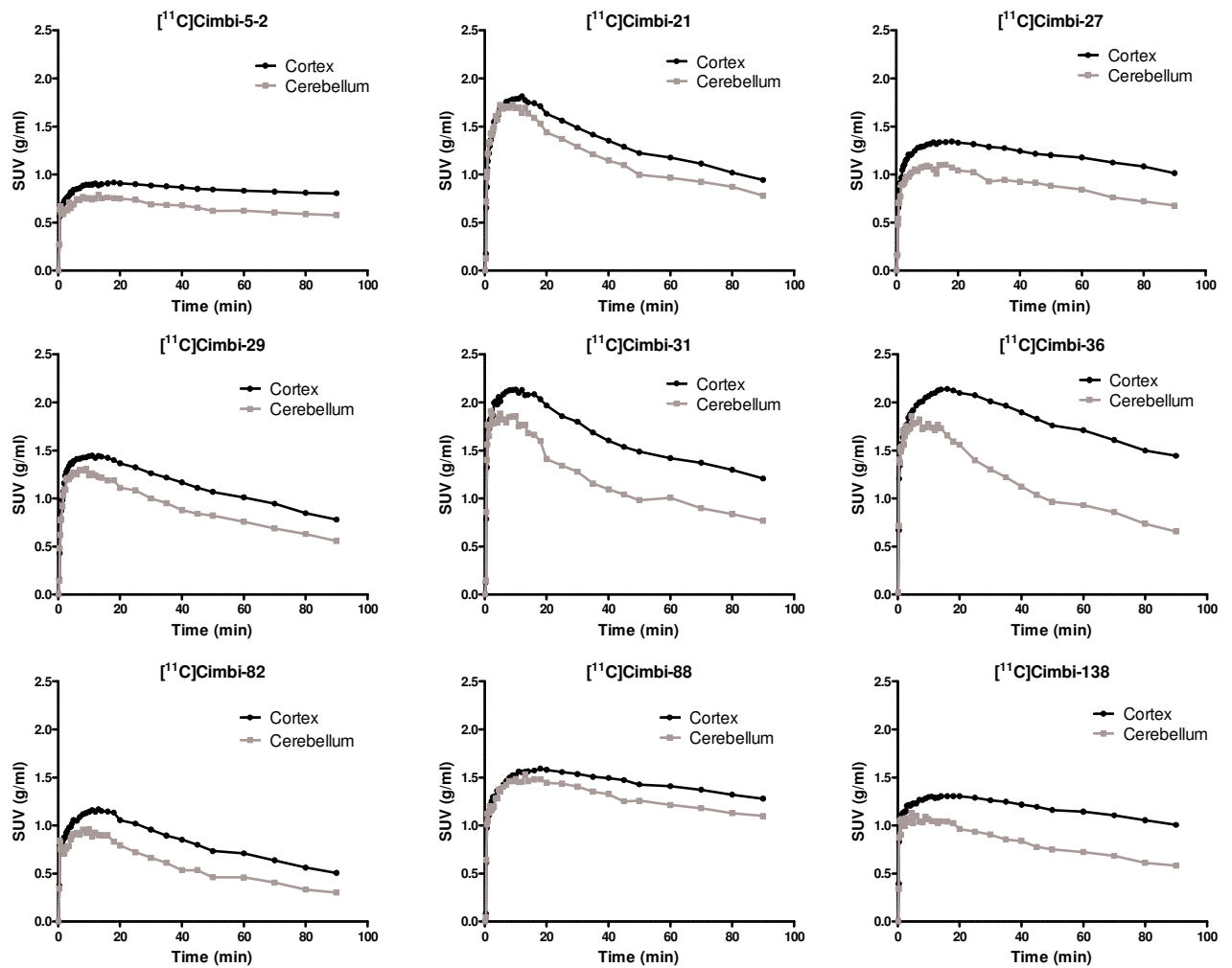
Fig. 3
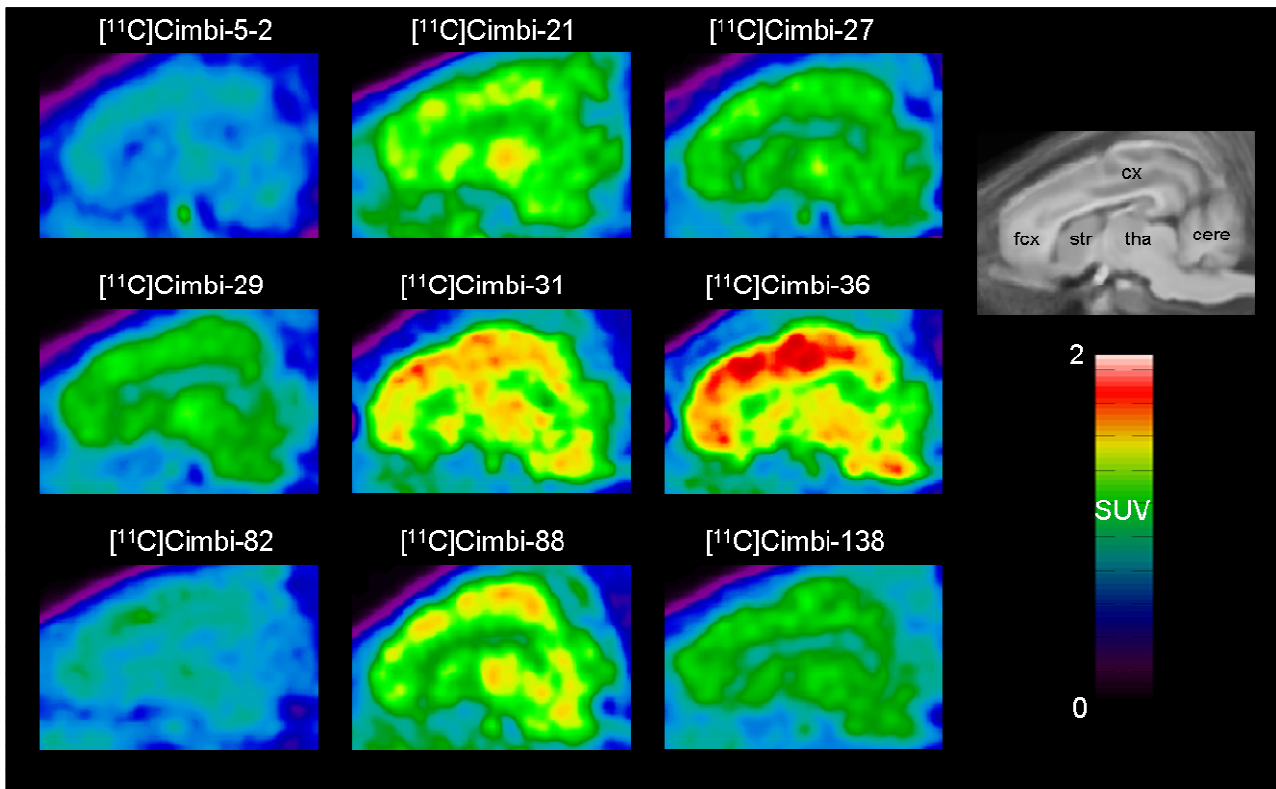
Fig. 4
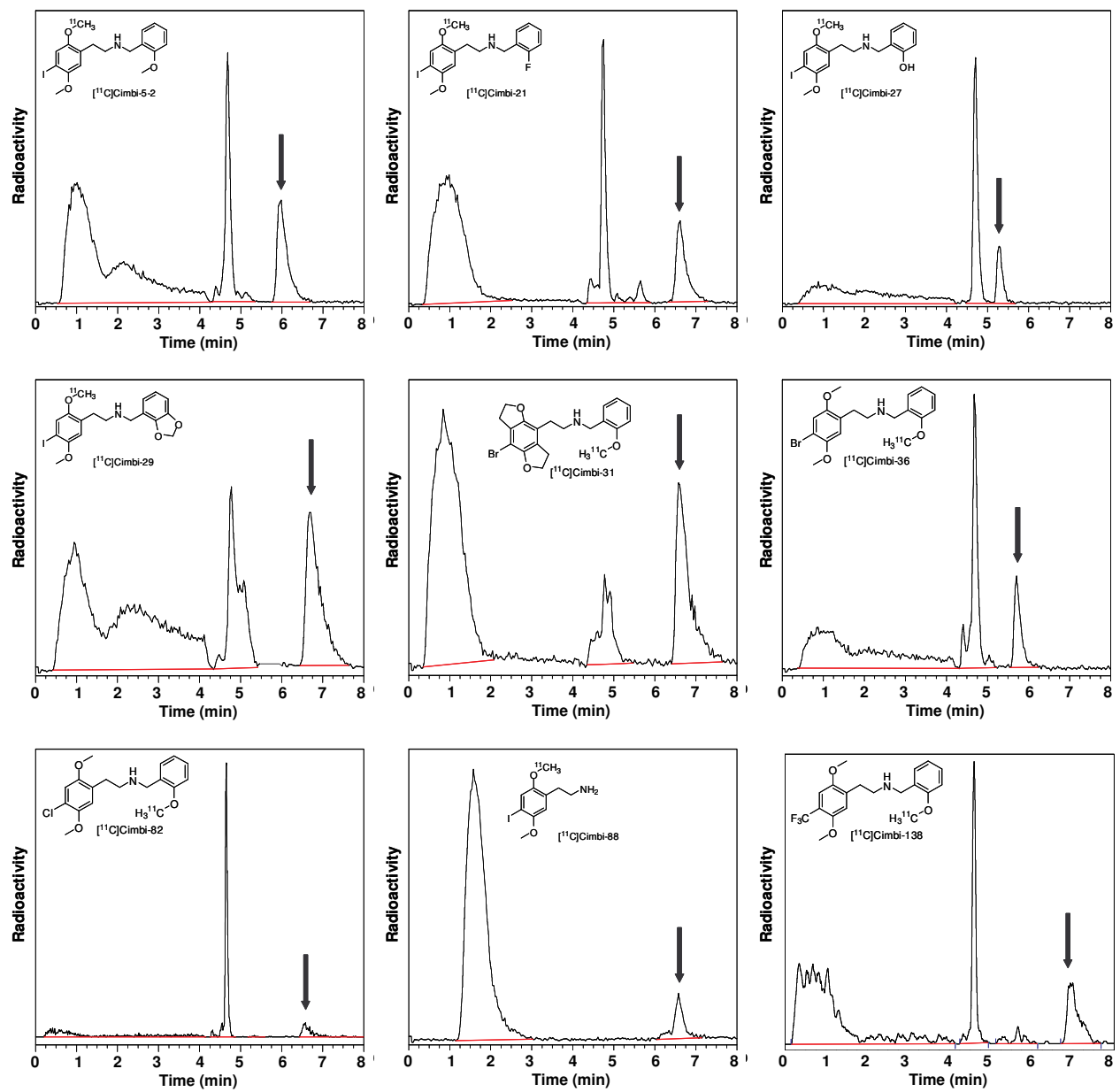
Fig. 5
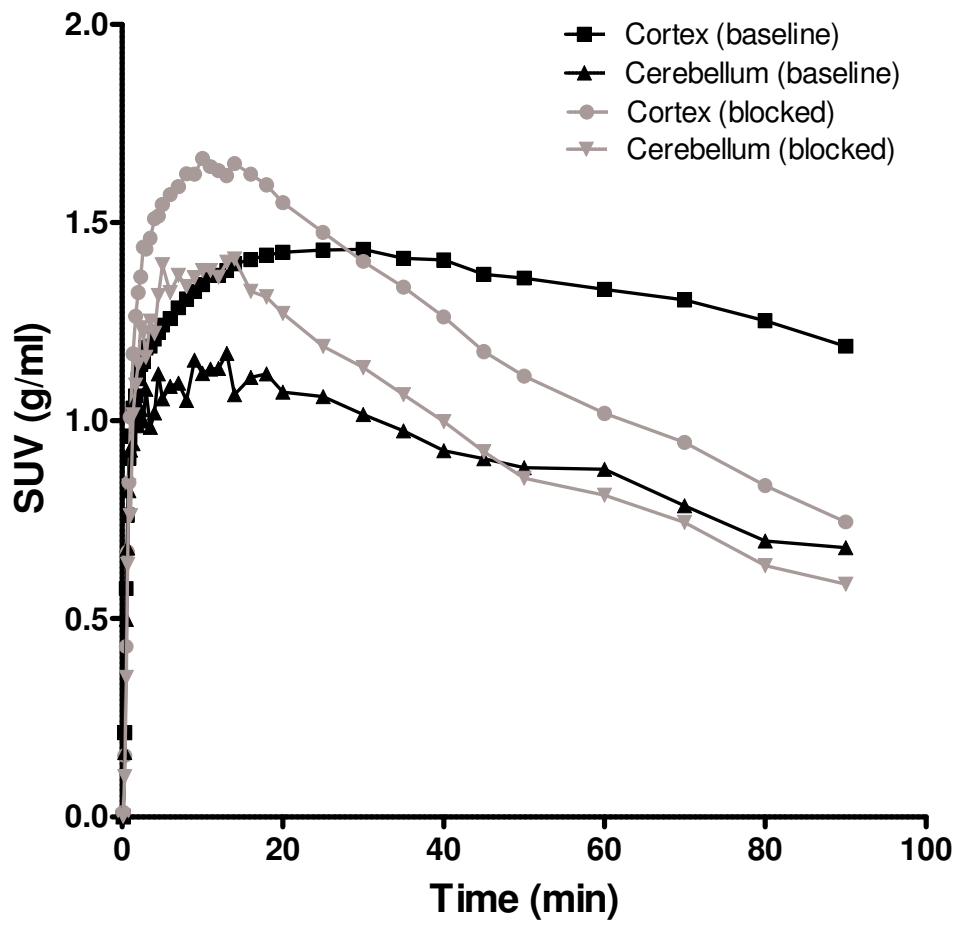
Fig. 6
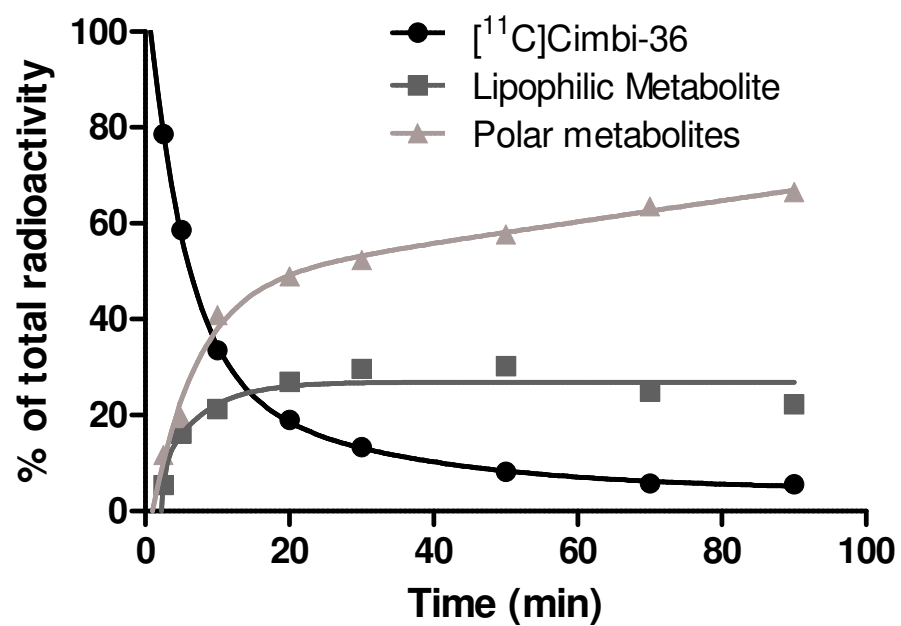
Fig. 7
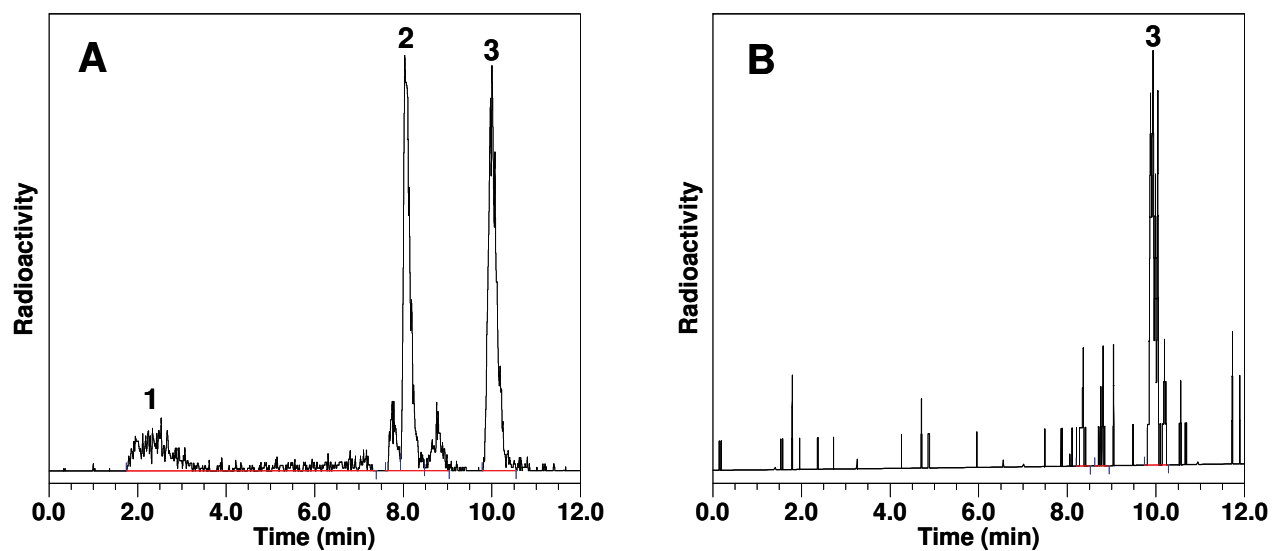
Supplementary Materials

Chemical synthesis

Tetrahydrofuran (THF) was freshly distilled from Na-benzophenone ketyl. Et_2O was dried over a Na-wire. All other solvents were commercial HPLC grade dried over 3Å molecular sieves. Unless otherwise stated, all reactions were performed under anhydrous conditions using N_2 as inert atmosphere.

Melting points (mp) were determined using an Optimelt apparatus and are uncorrected. NMR spectra were determined using a Varian Mercury 300 MHz or Varian Gemini 2000, 300 MHz spectrometer. δ_H is given in ppm relative to tetramethylsilane (TMS) or solvent residual peaks. δ_C is given in ppm relative to solvent residual peaks. Flash chromatography was performed on silica gel 40-63 μm (230-400 mesh). Radial chromatography was performed on a Harrison Research Chromatotron model 7924T. All compounds were of >95% purity.

Synthesis of 2-desmethyl-2C-I

Synthesis of 2-(2-aminoethyl)-5-iodo-4-methoxyphenol (2-desmethyl-2C-I), **5**.
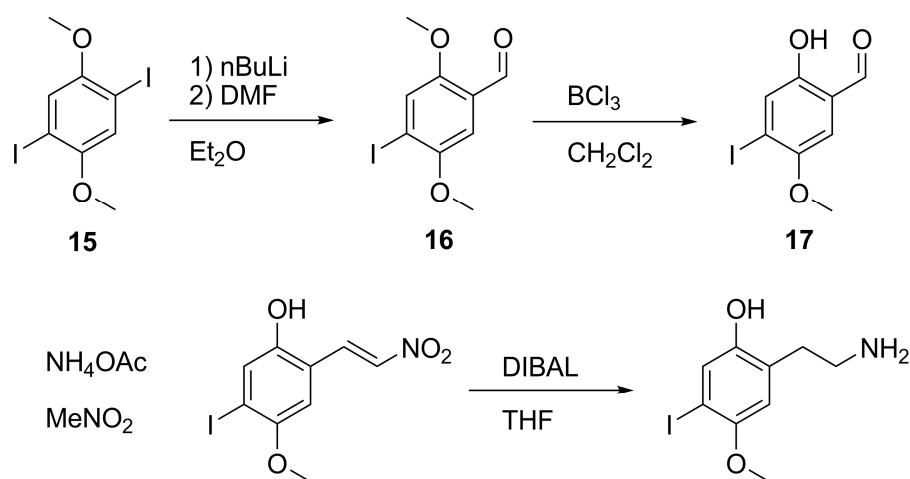
4-iodo-2,5-dimethoxybenzaldehyde, **16**.

To a cooled (0ºC) solution of **15** (7.797 g, 20 mmol) in dry Et_2O (250 mL) was added *n*-butyllithium (20 mmol) over a period of 5 min. The reaction was stirred at 0ºC for 10 min and DMF (3.1 mL, 40 mmol) was added. The cooling was removed, and the reaction was stirred for 2 h and then quenched by the addition of water (100 mL). The organic layer was isolated and the aqueous layer was extracted with Et_2O (2 × 50 mL). The combined organic layers were dried ($MgSO_4$),

filtered and evaporated to give a yellow solid. The product was purified by flash chromatography (petroleum ether/dichloromethane, 6:1 → 1:1) to give **16** (73%) as white crystals. mp: 140-142°C.

^{1}H-NMR (CDCl$_3$, 300 MHz): δ 3.88 (s, 3H), 3.90 (s, 3H), 7.21 (s, 1H), 7.46 (s, 1H), 10.38 (s, 1H).

^{13}C-NMR (CDCl$_3$, 75 MHz): δ 56.5, 57.1, 99.0, 108.0, 123.7, 125.0, 152.7, 156.1, 189.0.

2-hydroxy-4-iodo-5-methoxybenzaldehyde, **17**.

To a solution of **16** (1.51 g, 5.15 mmol) in dry dichloromethane (40 mL) was added 1.0 M BCl$_3$ in dichloromethane (20.60 mmol), and the reaction was stirred overnight at room temperature. The reaction was quenched by the addition of water (40 mL) and saturated aqueous NaHCO$_3$ until neutral pH. The organic layer was isolated and the aqueous layer was extracted with CH$_2$Cl$_2$ (2 × 50 mL). The combined organic layers were dried (MgSO$_4$), filtered and evaporated *in vacuo*. The residue was purified by flash chromatography (petroleum ether/ethyl acetate, 9:1) and the collected fraction were evaporated, and the solid was recrystallized from *i*Pr$_2$O to give **17** (85%) as bright yellow crystals. mp: 107-108°C.

^{1}H-NMR (CDCl$_3$, 300 MHz): δ 3.88 (s, 1H), 6.85 (s, 1H), 7.51 (s, 1H), 9.81 (s, 1H), 10.61 (s, 1H)

^{13}C-NMR (CDCl$_3$, 75 MHz): δ 57.1, 99.0, 112.2, 120.1, 129.1, 151.7, 155.5, 195.5.

(*E*)-5-iodo-4-methoxy-2-(2-nitrovinyl)phenol, **18**.

To a solution of **17** (2.500 g, 8.992 mmol) in MeNO$_2$ (30 mL), was added NH$_4$OAc (0.693 g, 8.992 mmol) and the reaction was stirred at reflux until TLC indicated full conversion (60-80 min). Excess MeNO$_2$ was removed *in vacuo* and the residue was dissolved in Et$_2$O (100 mL). The organic layer was washed with water (2 × 50 mL), dried (MgSO$_4$), filtered and evaporated *in vacuo*. The residue was purified by flash chromatography (petroleum ether/acetone, 9:1), and the collected fractions were evaporated to give **18** (65%) as deep orange crystals. mp: 146°C.

^{1}H-NMR (DMSO-d_6, 300 MHz): δ 3.78 (s, 3H), 7.29 (s, 1H), 7.38 (s, 1H), 8.13 (d, J = 13.5 Hz, 1H), 8.25 (d, J = 13.5 Hz), 10.64 (s, 1H). ^{13}C-NMR (DMSO-d_6, 75 MHz): δ 56.9, 93.4, 111.6, 117.1, 126.4, 134.6, 137.6, 151.1, 152.5.

2-(2-aminoethyl)-5-iodo-4-methoxyphenol (2-desmethyl-2C-I), **5**.

To a solution of *i*Bu$_2$AlH (4.58 mL, 25.68 mmol) in dry THF (40 mL) was added a solution of **18** (1.178 g, 3.669 mmol) in dry THF (20 mL). The reaction was stirred at 60°C for 2 h and then cooled to 0°C. The reaction mixture was diluted with Et$_2$O (60 mL), and there was added in the following order water (1.05 mL), 15% aqueous NaOH (1.05 mL) and water (2.6 mL). The mixture was stirred at room temperature for 30 min, anhydrous Na$_2$SO$_4$ (10 g) was added, and stirring was

continued for 10 min. The mixture was filtered and the filtrate was evaporated *in vacuo*. The residue was purified by flash chromatography (CH₂Cl₂/MeOH/NH₃, 95:5:0.05), and the collected fractions were evaporated *in vacuo* to give **5** (0.809 g, 95%) as a pale yellow solid. mp: 173-174°C.

^{1}H-NMR (DMSO-d_6, 300 MHz): δ 2.61 (t, J = 5.6 Hz, 2H), 2.78 (t, J = 5.6 Hz, 2H), 3.69 (s, 1H), 5.70 (br s, 3H), 6.68 (s, 1H), 7.04 (s, 1H). ^{13}C-NMR (DMSO-d_6, 75 MHz): δ 35.4, 41.4, 56.8, 82.9, 114.2, 125.8, 128.8, 150.0, 151.9.

General procedure for reductive amination

Amine (1 mmol) and aldehyde (1.2 mmol) was dissolved in EtOH or MeOH (10 mL) and stirred until TLC showed full conversion to the imine (1-3 h). NaBH₄ was added in one portion, and the reaction was stirred for 1 h. The reaction was concentrated *in vacuo* and the residue was partitioned between water (20 mL) and CH₂Cl₂ (20 mL). The organic layer was isolated, and the aqueous layer was extracted with CH₂Cl₂ (2 × 15 mL). The combined extracts were dried (Na₂SO₄), filtered and evaporated. The residue was purified by flash chromatography (petrol/EtOAc 1:1 → 1:4) to give the secondary amine.

2-((4-bromo-2,5-dimethoxyphenethylamino)methyl)phenol, **19**.

Obtained from **1** and salicylaldehyde in 82% yield.

^{1}H-NMR (CDCl₃, 300 MHz): δ 2.76-2.82 (m, 2H), 2.84-2.91 (m, 2H), 3.74 (s, 3H), 3.81 (s, 3H), 3.95 (s, 2H), 6.69 (s, 1H), 6.73 (ddd, J = 1.2, 7.4, 7.4 Hz, 1H), (dd, J = 1.2, 8.1 Hz, 1H), 6.93 (dd, J = 1.7, 7.4 Hz), 7.12 (ddd, J = 1.7, 7.4, 8.1 Hz, 1H), 7.00 (s, 1H). ^{13}C-NMR (CDCl₃, 75 MHz): δ 30.7, 48.3, 52.6, 56.1, 57.0, 109.3, 114.8, 115.8, 116.3, 118.9, 122.5, 127.7, 128.2, 128.6, 149.8, 151.8, 158.2.

2-((4-chloro-2,5-dimethoxyphenethylamino)methyl)phenol, **20**.

Obtained from **2** and salicylaldehyde in 64% yield. mp: 164-167°C (HCl salt).

^{1}H-NMR (HCl salt, CD₃OD, 300 MHz): δ 2.98-3.07 (m, 2H), 3.18-3.27 (m, 2H), 3.78 (s, 3H), 3.83 (s, 3H), 4.23 (s, 2H), 6.84-6.93 (m, 2H), 6.98 (s, 1H), 7.00 (s, 1H), 7.23-7.34 (m, 2H). ^{13}C-NMR (HCl salt, CD₃OD, 75 MHz): δ 28.3, 47.8, 48.2, 56.6, 57.3, 114.1, 116.1, 116.3, 118.5, 120.8, 122.5, 125.1, 132.2, 132.5, 150.4, 152.7, 157.2.

2-((2,5-dimethoxy-4-(trifluoromethyl)phenethylamino)methyl)phenol, **21**.

Obtained from **3** and salicylaldehyde in 79% yield

^{1}H-NMR (HCl salt, DMSO-d_6, 300 MHz): δ 3.07 (br s, 4H), 3.79 (s, 3H), 3.84 (s, 3H), 4.09 (m, 2H), 6.82 (ddd, J = 1.0, 7.4, 7.5 Hz, 1H), 6.99 (dd, J = 1.0, 8.1 Hz, 1H), 7.11 (s, 1H), 7.16 (s, 1H), 7.21 (ddd, J = 1.7, 7.5, 8.1 Hz), 7.41 (dd, J = 1.7, 7.5 Hz, 1H), 9.24 (br s, 2H), 10.32 (s, 1H). ^{13}C-NMR (HCl salt, DMSO-d_6, 75 MHz): δ 26.5, 44.9, 45.5, 56.1, 56.5, 109.0 (q, $^3J_{CF}$ = 5.0 Hz), 115.3, 115.4 (q, $^2J_{CF}$ = 30.5 Hz), 115.5, 117.9, 118.9, 123.5 (q, $^1J_{CF}$ = 272 Hz), 130.2, 131.1, 131.5, 150.3, 150.6 (m), 155.9.

2-((2-(8-bromo-2,3,6,7-tetrahydrobenzofuro[5,6-b]furan-4-yl)ethylamino)methyl)phenol, **22**. Obtained from **4** and salicylaldehyde in 75% yield. mp: 230-231°C (HCl salt).
^{1}H-NMR (HCl salt, DMSO-d_6, 300 MHz): δ 2.81-3.04 (m, 4H), 3.08 (t, J = 8.5 Hz, 2H), 3.22 (t, J = 8.5 Hz, 2H), 4.07 (m, 2H), 4.52 (t, J = 8.5 Hz, 2H), 4.55 (t, J = 8.5 Hz, 2H), 6.81 (dt, J = 1.0, 7.4 Hz, 1H), 6.99 (dd, J = 0.9, 8.1 Hz, 1H), 7.17-7.24 (m, 1H), 7.40 (dd, J = 1.5, 7.4 Hz, 1H), 9.28 (br s, 2H), 10.31 (s, 1H). ^{13}C-NMR (HCl salt, DMSO-d_6, 75 MHz): δ 24.1, 29.5, 31.2, 44.7, 44.9, 70.9, 71.5, 97.0, 114.3, 115.3, 117.9, 118.8, 126.1, 127.0, 130.2, 131.5, 150.4, 151.9, 155.9.

5-iodo-4-methoxy-2-(2-(2-methoxybenzylamino)ethyl)phenol, **23**.
Obtained from **5** and 2-methoxybenzaldehyde in 56% yield.
^{1}H-NMR (CDCl$_3$, 300 MHz): δ 2.70-2.77 (m, 2H), 2.81-2.88 (m, 2H), 3.76 (s, 3H), 3.83 (s, 5H), 6.46 (s, 1H), 6.83-6.93 (m, 2H), 7.13-7.17 (m, 1H), 7.22-7.30 (m, 1H), 7.27 (s, 1H). ^{13}C-NMR (CDCl$_3$, 75 MHz): δ 34.2, 48.9, 49.1, 55.4, 57.3, 83.9, 110.4, 113.9, 120.6, 125.6, 128.0, 128.6, 129.2, 130.5, 151.0, 152.2, 157.6.

2-(2-(2-fluorobenzylamino)ethyl)-5-iodo-4-methoxyphenol, **24**.
Obtained from **5** and 2-fluorobenzaldehyde in 62% yield.
^{1}H-NMR (CDCl$_3$, 300 MHz): δ 2.71-2.76 (m, 2H), 2.90-2.96 (m, 2H), 3.75 (s, 3H), 3.88 (s, 2H), 6.45 (s, 1H), 6.99-7.13 (m, 2H), 7.22-7.30 (m, 2H), 7.28 (s, 1H). ^{13}C-NMR (CDCl$_3$, 75 MHz): δ 34.1, 47.0, 49.3, 83.9, 113.8, 115.5 (d, $^2J_{CF}$ = 21.6 Hz), 124.5 (d, $^4J_{CF}$ = 3.6 Hz), 124.6 (d, $^2J_{CF}$ = 15.0 Hz), 127.9, 128.4, 129.7 (d, $^3J_{CF}$ = 8.2 Hz), 130.7 (d, $^3J_{CF}$ = 4.4 Hz), 151.2, 151.7, 161.1 (d, $^1J_{CF}$ = 245.4 Hz).

2-(2-(benzo[*d*][1,3]dioxol-4-ylmethylamino)ethyl)-5-iodo-4-methoxyphenol, **25**. Obtained from **5** and 2,3-methylenedioxybenzaldehyde in 72% yield.

^{1}H-NMR (CDCl$_3$, 300 MHz): δ 2.74-2.78 (m, 2H), 2.93-2.98 (m, 2H), 3.78 (s, 3H), 3.85 (s, 2H), 5.96 (s, 2H), 6.48 (s, 1H), 6.72-6.84 (m, 3H), 7.30 (s, 1H). ^{13}C-NMR (CDCl$_3$, 75 MHz) δ 34.2, 47.6, 49.3, 57.3, 83.9, 101.0, 108.2, 113.8, 119.2, 121.9, 122.3, 128.0, 128.4, 145.6, 147.3, 151.2, 151.8.

2-(2-(2-(*tert*-butyldimethylsilyloxy)benzylamino)ethyl)-5-iodo-4-methoxyphenol, **26**.
Obtained from **5** and 2-(*tert*-butyldimethylsilyloxy)benzaldehyde in 47% yield.
^{1}H-NMR (CDCl$_3$, 300 MHz): δ 0.02 (s, 6H), 0.76 (s, 9H), 2.47-2.53 (m, 2H), 2.62-2,67 (m, 2H), 3.53 (s, 3H), 3.57 (s, 2H), 6.22 (s, 1H), 6.53-6.58 (m, 1H), 6.63-6.71 (m, 1H), 6.86-7.01 (m, 2H), 7.04 (s, 1H). ^{13}C-NMR (CDCl$_3$, 75 MHz): δ -3.8 (2C), 18.4, 26.0 (3C), 34.2, 49.1, 49.2, 57.3, 83.9, 113.8, 118.5, 121.4, 127.9, 128.1, 128.5, 128.9, 130.7, 151.1, 152.1, 153.9.

General procedure for Boc-protection of secondary amines

A solution of the secondary amine (1 equiv.) and Boc$_2$O (1.1 equiv) in THF (10 mL/mmol) was stirred until TLC showed full conversion. The reaction was concentrated *in vacuo* and purified by flash chromatography or radial chromatography.

tert-butyl 4-bromo-2,5-dimethoxyphenethyl(2-hydroxybenzyl)carbamate, **6**.
Yield: 77%.
^{1}H-NMR (CDCl$_3$, 300 MHz): δ 1.27 (s, 9H), 2.65, (t, *J* = 6.9 Hz, 2H), 3.33 (t, *J* = 6.9 Hz, 2H), 3.68 (s, 6H), 4.20 (s, 2H), 6.36 (s, 1H), 6.68 (ddd, *J* =1.2, 7.4, 7.4 Hz, 1H), 6.80 (dd, *J* = 1.2, 8.1 Hz, 1H), 6.87 (s, 1H), 6.96 (dd, *J* = 1.7, 7.4 Hz, 1H), 7.10 (ddd, 1.7, 7.4, 8.1 Hz, 1H), 9.28 (br s, 1H).
^{13}C-NMR (CDCl$_3$, 75 MHz): δ 28.7 (3C), 30.0, 47.8, 49.0, 56.4, 57.3, 81.8, 109.7, 115.4, 115.9, 117.8, 119.6, 123.5, 127.8, 130.4, 131,.7, 150.2, 152.3, 156.6, 158.2.

tert-butyl 4-chloro-2,5-dimethoxyphenethyl(2-hydroxybenzyl)carbamate, **7**.
Yield: 92%.
^{1}H-NMR (CDCl$_3$, 300 MHz): δ 1.37 (s, 9H), 2.75 (t, *J* = 6.9 Hz, 2H), 3.42 (t, *J* = 6.9 Hz, 2H), 3.78 (s, 3H), 3.79 (s, 3H), 4.29 (s, 2H), 6.47 (s, 1H), 6.77 (dt, *J* = 1.2, 7.4 Hz, 1H), 6.82 (s, 1H), 6.89 (dd, *J* = 1.1, 8.1 Hz, 1H), 7.05 (dd, *J* = 1.7, 7.4 Hz, 1H), 7.16-7.23 (m, 1H), 9.38 (br. s, 1H). ^{13}C-NMR (CDCl$_3$, 75 MHz): δ 28.3, 29.6, 47.5, 48.6, 56.1, 56.9, 81.4, 112.7, 115.2, 117.4, 119.2, 120.4, 123.1, 126.6, 130.0, 131.3, 148.8, 151.6, 156.2, 157.8.

tert-butyl 2,5-dimethoxy-4-(trifluoromethyl)phenethyl(2-hydroxybenzyl)carbamate, **8**.

Yield: 86%.

^{1}H-NMR (CDCl$_3$, 300 MHz): δ 1.33 (s, 9H), 2.79 (t, *J* = 6.8 Hz, 2H), 3.47 (t, *J* = 6.8 Hz, 2H), 3.78 (s, 3H), 3.81 (s, 3H), 4.32 (s, 2H), 6.50 (s, 1H), 6.78 (ddd, *J* = 1.1, 7.4, 7.4 Hz, 1H), 6.90 (dd, *J* = 1.1, 8.1 Hz, 1H), 6.96 (s, 1H), 7.07 (dd, *J* = 1.7, 7.4 Hz, 1H), 7.20 (ddd, *J* = 1.7, 7.4, 8.1 Hz, 1H), 9.36 (br s, 1H). ^{13}C-NMR (CDCl$_3$, 75 MHz): δ 28.3 (3C), 29.9, 47.5, 48.8, 56.0, 56.7, 81.6, 108.8 (q, $^3J_{CF}$ = 5.4 Hz), 115.5, 117.5, 119.3, 123.1, 123.6 (q, $^1J_{CF}$ = 272 Hz), 130.2, 131.4, 132.6, 150.9, 151.3 (m), 156.3. The quaternary aromatic carbon bearing the CF$_3$-group was not discernible or coinciding with other peaks

tert-butyl 2-(8-bromo-2,3,6,7-tetrahydrobenzofuro[5,6-*b*]furan-4-yl)ethyl(2-hydroxybenzyl)carbamate, **9**.

Yield: 99%. mp: 140-142°C.

^{1}H-NMR (CDCl$_3$, 300 MHz): δ 1.42 (s, 9H), 2.68 (t, *J* = 7.0 Hz, 2H), 3.11 (t, *J* = 8.6 Hz, 2H), 3.14 (t, *J* = 8.6 Hz, 2H), 3.36 (t, *J* = 7.0 Hz, 2H), 4.26 (s, 2H), 4.58 (t, *J* = 8.6 Hz, 2H), 4.60 (t, *J* = 8.6 Hz, 2H), 6.71-6.78 (m, 1H), 6.86-6.91 (m, 1H), 7.01 (dd, *J* = 1.5, 7.4 Hz, 1H), 7.15-7.22 (m, 1H), 9.27 (br s, 1H). ^{13}C-NMR (CDCl$_3$, 75 MHz): δ 26.7, 28.4, 30.0, 31.9, 46.0, 48.2, 71.2, 71.8, 81.6, 97.5, 116.4, 117.4, 119.2, 122.9, 126.2, 126.3, 130.0, 131.2, 150.8, 152.9, 156.2, 157.8

tert-butyl 2-hydroxy-4-iodo-5-methoxyphenethyl(2-methoxybenzyl)carbamate, **10**.

Yield: 72%.

^{1}H-NMR (CDCl$_3$, 300 MHz): δ 1.47 (s, 9H), 2.68-2.75 (m, 2H), 3.25-3.33 (m, 2H), 3.74 (s, 3H), 3.83 (s, 3H), 4.46 (s, 2H), 6.39 (s, 1H), 6.86 (d, *J* = 8.2 Hz, 1H), 6.92 (t, 7.4 Hz, 1H), 7.13 (d, *J* = 7.2Hz), 7.21-7.30 (m, 1H), 7.24 (s, 1H), 8.25 (br s, 1H).

^{13}C-NMR (CDCl$_3$, 75 MHz): δ 28.6 (3C), 31.0, 47.3, 48.2, 55.4, 57.2, 81.1, 83.9, 110.3, 112.9, 120.5, 125.4, 126.0, 128.6, 128.7, 150.5, 151.6, 157.0, 157.2

tert-butyl 2-fluorobenzyl(2-hydroxy-4-iodo-5-methoxyphenethyl)carbamate, **11**.

Yield: 89%.

^{1}H-NMR (CDCl$_3$, 300 MHz): δ 1.46 (s, 9H), 2.75 (t, *J* = 7.4 Hz, 2H), 3.34 (t, *J* = 7.4 Hz, 2H), 3.75 (s, 3H), 4.48 (s, 2H), 6.43 (s, 1H), 6.97-7.13 (m, 2H), 7.18-7.29 (m, 3H), 7.97 (br s, 1H). ^{13}C-NMR (CDCl$_3$, 75 MHz): δ 28.5 (3C), 30.8, 46.0, 48.1, 57.2, 81.5, 83.8, 113.0, 115.4 (d, $^2J_{CF}$ = 21.6 Hz), 124.3 (d, $^4J_{CF}$ = 3.6 Hz), 125.0 (d, $^2J_{CF}$ = 14.7 Hz), 125.3, 126.9, 129.2 (d, $^3J_{CF}$ = 8.0 Hz), 129.6, 150.2, 151.7, 156.5, 160.8 (d, $^1J_{CF}$ = 245.6 Hz).

tert-butyl benzo[*d*][1,3]dioxol-4-ylmethyl(2-hydroxy-4-iodo-5-methoxyphenethyl)carbamate, **12**.

Yield: 72%.

^{1}H-NMR (CDCl$_3$, 300 MHz): δ 1.49 (s, 9H), 2.73-2.80 (m, 2H), 3.31-3.40 (m, 2H), 3.77 (s, 3H), 4.43 (s, 2H), 5.95 (s, 2H), 6.45 (s, 1H), 6.70-6.84 (m, 3H), 7.29 (s, 1H), 8.05 (br s, 1H). ^{13}C-NMR (CDCl$_3$, 75 MHz): δ 28.6 (3C), 30.8, 46.7, 48.1, 57.2, 81.4, 83.9, 100.9, 107.9, 113.0, 119.5, 121.5, 121.7, 125.3, 126.4, 145.4, 147.3, 150.3, 151.6, 156.5.

tert-butyl 2-(tert-butyldimethylsilyloxy)benzyl(2-hydroxy-4-iodo-5-methoxyphenethyl)carbamate, **13**.

Yield: 62%.

^{1}H-NMR (CDCl$_3$, 300 MHz): δ 0.26 (s, 6H), 1.03 (s, 9H), 1.47 (s, 9H), 2.71-2.78 (m, 2H), 3.25-3.33 (m, 2H), 3.73 (s, 3H), 4.47 (s, 2H), 6.80 (d, *J* = 7.9 Hz, 1H), 6.92 (t, *J* = 7.4 Hz, 1H), 7.08-7.16 (m, 2H), 7.29 (s, 1H), 8.16 (br s, 1H). ^{13}C-NMR (CDCl$_3$, 75 MHz): δ -3.8 (2C), 18.6, 26.1 (3C), 28.6 (3C), 31.2, 46.9, 48.2, 81.3, 83.9, 112.7, 118.6, 121.5, 125.2, 127.1, 128.2 (2C), 128.3, 150.5, 151.6, 153.1, 153.2, 157.0.

Synthesis of [^{11}C]Cimbi-88 labelling precursor

2-(2-hydroxy-4-iodo-5-methoxyphenethyl)isoindoline-1,3-dione, **14**.
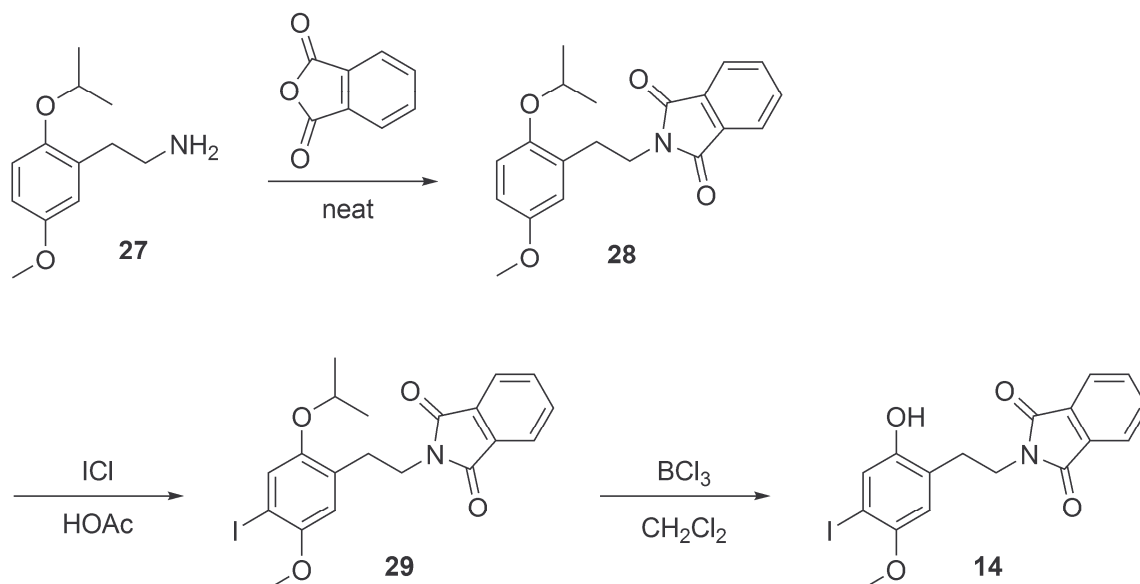
2-(2-isopropoxy-5-methoxyphenethyl)isoindoline-1,3-dione, **28**.

2-(2-isopropoxy-5-methoxyphenyl)ethanamine, **27** (synthesis previously described [11]) (608 mg, 2.9 mmol) and phthalic anhydride (431 mg, 2.9 mmol) were heated with an open flame until a clear

liquid phase was formed. This was allowed to cool and crystallised from EtOH to give **28** (743 mg, 75%) as a colourless solid. mp. 79-80°C.

^{1}H-NMR (CDCl$_3$, 300 MHz): δ 2.95 (t, J = 7.4 Hz, 2H), 3.68 (s, 3H), 3.92 (t, J = 7.4 Hz, 2H), 4.41 (septet, J = 6.0 Hz, 1H), 6.71-6.64 (m, 2H), 6.74 (d, J = 8.6 Hz, 1H), 7.70-7.62 (m, 2H), 7.81-7.74 (m, 2H). ^{13}C-NMR (CDCl$_3$, 75 MHz): δ 22.2 (2C), 30.0, 38.0, 55.6, 70.7, 112.4, 114.2, 116.1, 122.9 (2C), 128.7, 132.1, 133.5 (2C), 149.9, 153.0, 168.0 (2C).

2-(4-iodo-2-isopropoxy-5-methoxyphenethyl)isoindoline-1,3-dione, **29**.

ICl (0.11 mL, 2.2 mmol, 1.2 equiv.) was added to a solution of phthalimide **28** (612 mg, 1.8 mmol) in AcOH (10 mL). The reaction was stirred at room temperature for 24 h then quenched with saturated aqueous Na$_2$S$_2$O$_3$ and diluted with water (30 mL). The precipitated product was collected by filtration, washed with water and crystallised from aqueous EtOH to give **29** (596 mg, 71%) as a yellow solid. mp. 134-136°C.

^{1}H-NMR (CDCl$_3$, 300 MHz): δ 1.30 (d, J = 6.0 Hz, 6H), 2.95 (t, J = 7.4 Hz, 2H), 3.71 (s, 3H), 3.92 (t, J = 7.4 Hz, 2H), 4.40 (septet, J = 6.0 Hz, 1H), 6.62 (s, 1H), 7.19 (s, 1H), 7.72-7.64 (m, 2H), 7.83-7.76 (m, 2H). ^{13}C-NMR (CDCl$_3$, 75 MHz): δ 22.1 (2C), 30.0, 37.7, 56.9, 71.2, 83.2, 113.3, 123.0 (2C), 124.3, 128.8, 132.0, 133.7 (2C), 150.6, 152.0, 168.0 (2C).

2-(2-hydroxy-4-iodo-5-methoxyphenethyl)isoindoline-1,3-dione, **14**.

BCl$_3$ (0.93 mL, 1 M in hexanes, 1.2 equiv.) was added dropwise to a cooled (-78°C) solution of phthalimide **29** (359 mg, 0.77 mmol) in CH$_2$Cl$_2$ (20 mL). The reaction was allowed to warm to room temperature and stirred for a further 1 h before pouring into water (100 mL). The organic layer was separated and the aqueous phase extracted with CH$_2$Cl$_2$ (2 × 25 mL). The combined organic extracts were washed with brine, dried over Na$_2$SO$_4$ and concentrated under reduced pressure. The residue was crystallized from EtOAc/petroleum ether to give, **14** (205 mg, 63%) as a light yellow solid. mp: 209-210°C

^{1}H-NMR (DMSO-d_6, 300 MHz): δ 2.83 (t, J = 6.5 Hz, 2H), 3.55 (s, 3H), 3.80 (t, J = 6.5 Hz, 2H), 6.63 (s, 1H), 7.08 (s, 1H), 7.75-7.83 (m, 4H), 9.20 (s, 1H). ^{13}C-NMR (DMSO-d_6, 75 MHz): δ 28.8, 37.3, 56.6, 83.1, 113.6, 122.8, 124.4, 125.8, 131.4, 134.1, 150.1, 150.6, 167.5.

Synthesis of reference compounds: Cimbi-82 was synthesized using the general procedure for reductive amination. Yield: 60% mp: 179-180°C (HCl salt).

^{1}H-NMR (HCl salt, CD$_3$OD, 300 MHz): δ 2.99-3.07 (m, 2H), 3.17-3.25 (m, 2H), 3.77 (s, 3H), 3.82 (s, 3H), 3.88 (s, 3H), 4.24 (s, 2H), 6.97-7.03 (m, 3H), 7.07 (d, J = 8.3 Hz, 1H), 7.36-7.46 (m, 2H).

^{13}C-NMR (HCl salt, CD$_3$OD, 75 MHz): δ 28.2, 47.8, 47.9, 56.2, 56.6, 57.3, 111.9, 114.1, 116.4, 120.1, 121.9, 122.5, 125.1, 132.6, 150.4, 152.8, 159.1.

Table S1 PDSP[a] binding data of PET tracer compounds

	Cimbi-5	Cimbi-21	Cimbi-27	Cimbi-29	Cimbi-31	Cimbi-36	Cimbi-82	Cimbi-88
5-HT$_{1A}$	85	3627	>10000	1351	1439	1255	2353	107
5-HT$_{1B}$	3742	>10000	2446	>10000	6573	>10000	2372	56
5-HT$_{1D}$	-	3505	1277	752	1837	1472	1024	40
5-HT$_{1E}$	-	>10000	>10000	>10000	>10000	>10000	5776	131
5-HT$_{2A}$[b]	2.2	2.8	-	0.6	-	0.5	1.6	-
5-HT$_{2A}$[c]	-	-	0.7	1.0	1.3	0.8	0.9	7.2
5-HT$_{2B}$	2.3	19	2.8	1.3	0.4	0.5	1.1	9.3
5-HT$_{2C}$	7.0	21	1.4	22	2.1	1.7	5.4	9.3
5-HT$_3$	>10000	>10000	>10000	>10000	>10000	>10000	>10000	>10000
5-HT$_{5A}$	2.200	4954	965	1858	3537	4087	4796	>10000
5-HT$_6$	58.1	469	-	474	-	-	36.2	-
5-HT$_7$	1670	>10000	3472	4243	4168	4720	1729	1316
D1	3718	>10000	-	>10000	>10000	>10000	>10000	>10000
D2	1600	4827	>10000	6898	604	>10000	7508	1013
D3	117	-	678	389	693	718	878	989
D4	647	502	844	318	1399	2253	>10000	2788
D5	7847	>10000	>10000	>10000	>10000	>10000	>10000	>10000
Beta1	-	2229	1088	-	4750	6719	-	4512
Beta2	-	1002	-	-	>10000	>10000	-	>10000
H1	-	669	-	-	-	-	-	-
H2	-	1016	-	-	-	-	-	>10000
H3	-	>10000	>10000	-	>10000	>10000	-	>10000
Sigma 1	-	-	160	761	4125	310	441	>10000
Sigma 2	-	-	264	16	117	64	41	5470
Alpha 1A	-	496	3924	853	207	1256	2319	>10000
Alpha 1B	-	>10000	>10000	1104	4975	6180	>10000	>10000
Alpha 1D	-	2897	>10000	920	1391	2253	>10000	>10000
Alpha 2A	1106	-	2257	2369	3596	3551	3175	305
Alpha 2B	-	-	3043	>10000	1293	1264	224	608
Alpha 2C	348	-	1003	406	513	646	185	315
DAT	5031	-	-	>10000	8464	>10000	>10000	>10000
SERT	1009	2522	1155	>10000	540	388	>10000	2510
NET	4574	3662	-	2286	>10000	1718	>10000	>10000
MOR	-	-	47.2	-	>10000	>10000	-	2522
KOR	-	-	328	-	327	642	-	>10000
M1	>10000	>10000	>10000	>10000	>10000	>10000	>10000	>10000
M2	>10000	>10000	>10000	>10000	1991	>10000	>10000	1429
M3	>10000	>10000	>10000	>10000	-	>10000	>10000	950
M4	>10000	>10000	>10000	8439	-	>10000	5410	1129
M5	1381	>10000	>10000	6280	3293	5241	>10000	2151

K_i values in nM are based on the means of 4 experiments; -, not determined. K_i >10000 indicate that compounds did not show affinity for the target in the primary binding assay.

[a] See http://pdsp.med.unc.edu/ for experimental details.

[b] Measured against [³H]ketanserin

[c] Measured against [³H]LSD

Table S2 In vitro activation of 5-HT$_{2A}$ receptors by PET tracer compounds

Compound	PI hydrolysis assay	
	5-HT$_{2A}$ activation[a]	% of intrinsic activity[b]
Cimbi-5	1.02 ± 0.08	91
Cimbi-21	50.7 ± 12.3	86
Cimbi-27	0.19 ± 0.03	99
Cimbi-29	29.7 ± 2.82	93
Cimbi-31	1.06 ± 0.19	83
Cimbi-36	0.51 ± 0.19	87
Cimbi-82	2.31 ± 0.11	88
Cimbi-88	6.39 ± 0.97	84
Cimbi-138	0.96 ± 0.18	92

[a] ED$_{50}$ values (nM $\pm$ SEM) for 5-HT$_{2A}$ activation at GF-62 cells.
[b] Mean maximal activation by test compound compared to 10 μM 5-HT.